INSTITUTO TECNOLOGICO Y DE ESTUDIOS SUPERIORES DE MONTERREY
CAMPUS MONTERREY

PROGRAMA DE GRADUADOS DE LA DIVISION DE TECNOLOGIAS DE INFORMACION Y ELECTRONICA

Interference and Capacity Analysis of CDMA Ad-Hoc Network Using Multibeam Smart Antennas

THESIS

Presented as a partial fulfillment of the requirements for the degree of

Master of Science in Electronic Engineering
Major in Telecommunications

Ing. Antonio Ramos García

Monterrey, N.L. November 2005

Instituto Tecnológico y de Estudios Superiores de Monterrey

Campus Monterrey

División de Tecnologías de Información y Electrónica

Programa de Graduados

Interference and Capacity Analysis of CDMA Ad-Hoc Network Using Multibeam Smart Antennas

THESIS

Presented as a partial fulfillment of the requirements for the degree of

Master of Science in Electronic Engineering
Major in Telecommunications

Ing. Antonio Ramos García

Monterrey, N.L. November 2005

Instituto Tecnológico y de Estudios Superiores de Monterrey

Campus Monterrey

División de Tecnologías de Información y Electrónica

Programa de Graduados

The members of the thesis committee recommended the acceptance of the thesis of Antonio Ramos García as a partial fulfillment of the requirements for the degree of Master of Science in:

Electronic Engineering

Major in Telecommunications

THESIS COMMITTEE

_____

David Muñoz Rodríguez, Ph.D.
Advisor

_____

César Vargas Rosales, Ph.D.
Synodal

_____

José Ramón Rodríguez Cruz, Ph.D.
Synodal

Approved

_____

David Garza Salazar, Ph.D.
Director of the Graduate Program

November 2005

This work is dedicated to God my Lord for all his blessings and faithful love, for giving me the chance of this living, and for supporting me in all I do, he is always with me. Thank You Lord.

My work is dedicated
To my parents Juan and Martha for your love and unconditional support,
To my brothers Lenin and Jasson and to my sister Génesis for your love, support and friendship,
To all my family, friends and partners,
To Margarita for your support, understand and all your love.

Blessed is the man who finds wisdom, the man who gains understanding, for she is more profitable than silver and yields better returns than gold. She is more precious than rubies; nothing you desire can compare with her.
Proverbs 3:13-15

Este trabajo está dedicado a Dios mi Señor por todas sus bendiciones y maravillas que ha hecho en mi vida, por todo su amor y por la vida que me da cada día, y por su apoyo incondicional en todas las cosas que hago, siempre está conmigo. Gracias Dios.

Dedico mi trabajo
A mis padres Juan y Martha por su amor y apoyo incondicional,
A mis hermanos Lenin, Jasson y a mi hermana Génesis por todo su amor, apoyo y amistad,
A toda mi familia, amigos y compañeros,
A Margarita por tu apoyo, comprensión y por todo tu amor.

Bienaventurado el hombre que halla la sabiduría, y que obtiene la inteligencia; por que su ganancia es mejor que la ganancia de la plata, y sus frutos más que el oro fino. Más preciosa es que las piedras preciosas; y todo lo que puedes desear, no se puede comparar a ella..
Proverbio 3:13-15

Contents

List of Figures

List of Tables

Table of Acronyms

BS	Base Station
AC	Access Point
MSC	Mobile Switching Center
MTSO	Mobile Telephony Switching Office
HLR	Home Location Register
CDMA	Code Division Multiple Access
f_c	Carrier Frequency
SNR	Signal-to-noise Ratio
DS	Direct Sequence
FH	Frequency Hop
CIR	Carrier-to-Interference-Ratio
SNR	Signal-to-Noise-Ratio
E_b/N_0	Energy per bit noise density
HPBW	Half-power beamwidth
EIRP	Effective Isotropic Radiated Power
DOA	Direction-Of-Arrival
BFN	Beam Forming Network
MMSE	Minimum Mean Square Error
SIR	Signal-to-Interference Ratio
MVDR	Minimum Variance Distortionless Response
LMS	Least-Mean-Square Algorithm
DMI	Direct Matrix Inversion
NDRP	Not Desired Radiation Pattern

Acknowledgments

I want to express my gratitude to Francisco Olivares, my Track & Field Coach, for giving me the chance and opportunity to carry out all my studies in the ITESM, always believing in me.

To my thesis advisor David Muñoz Rodríguez, Ph. D., for all the support and guide granted to finish this work.

To Cesar Vargas Rosales, Ph. D. and José Ramón Rodríguez Cruz, Ph. D., members of this thesis committee, for their advising, comments and observations that helped to improve this work.

Thanks to my parents Juan and Martha because all I am and all I have, have been possible with their love and support, to my brother Jasson and my sister Génesis for their love and frienship, to my brother Lenin and his wife Rosa and their son Jeshua, because they are one bless more in our lives, and to all my family.

To all my friends from the CET and to all my friends from the Track & Field team, for their support and friendship.

I want to thank to Rafaela for your help typing this work

To my girlfriend Maggie, thank you for always being with me, for your support and all your love, and for all the moment we spent together during this thesis time.

Antonio Ramos García

Instituto Tecnológico y de Estudios Superiores de Monterrey
November 2005

Interference and Capacity Analysis of CDMA Ad-Hoc Network Using Multibeam Smart Antennas

Ing. Antonio Ramos García
Instituto Tecnológico y de Estudios Superiores de Monterrey, 2005

Abstract

Mobile hosts such as a mobile computers, featuring powerful CPUs, large main memories, hundreds of megabytes of disk space, multimedia sound capabilities, and color displays, are now easily affordable and becoming quite common in every day business and personal life. At the same time, network connectivity options for use with mobile hosts have increased dramatically, including support for a growing number of wireless networking products based on radio and infrared.

The ad-hoc networks are being developed to satisfy this demand of mobile and faster services. Smart antennas offer a broad range of ways to improve wireless system performance. In general, smart antennas have the potential to provide enhanced range and reduce infrastructure costs in early deployments, enhanced link performance as the system is built-out, and increased long-term system capacity. Code Division Multiple Access (CDMA) seems to be the future wireless interface and, because of its characteristics, it could play an important role in future communications systems. Both smart antenna technology and CDMA promise to revolutionize the field of wireless communications.

This work will focus on CDMA as the access method, and due that this access technique is just interference limited, we will determine the interference levels caused in the network that can support a great number of users (network capacity) within a faster service, always taking care to guarantee the QoS necessarily to be commercially competitive in the market.

Chapter 1

Introduction

Since the beginning of the times the need to communicate always has been carried out no matter the time, the natural conditions or the distance between two points. The distance, as a special consideration, has made the science to grow in telecommunications area. During the past ten years, the mobile radio communications industry has grown by orders of magnitude, fueled by digital and RF circuit fabrication improvements, new large-scale circuit integration, and other miniaturization technologies which make portable radio equipment smaller, cheaper, and more reliable [1].

Advances in wireless technology and portable computing along with demands for greater user mobility and bandwidth have provided a major impetus toward development of an emerging class of self-organizing, rapidly deployable network architecture referred as ad-hoc networks [2]. Ad-Hoc wireless networks are systems of mobiles nodes without a fixed structure, where users can communicate with each other by intermediate nodes as relays.

Joining advances in wireless ad-hoc networks, recently, there has been intensive research on smart antennas in mobile communications for exploiting the spatial domain, like null steering for insolating co-channel users, suppressing interference and beam steering for focusing energy toward desired users. Then allowing multiple radio subscribers to share the same frequency band at the same time by assigning each user a unique code we have the Code Division Multiple Access (CDMA). The CDMA technology makes very efficient use of limited spectral resources and allows robust communications over time-varying radio channels. Both smart antenna technology and CDMA promise to revolutionize the field of wireless communications. [3].

1.1 Objective

The objective of this thesis is to evaluate the interference, using CDMA as a Medium Access Control (MAC), by simulating an Ad-Hoc wireless network through out a spatial point process, in which each node is supplied by a multibeam smart antenna. For this, we design a smart antenna that can form simultaneous beams toward different targets at the same time, (multibeam smart antenna). Finally, we shall present the results of interference and capacity of the CDMA Ad-Hoc network using different adaptive arrays (Linear and Circular, as the smart antenna in each node) against the omni directional case.

1.2 Justification

Due to the rapid growth of technologies along wireless systems, the demand on mobility and the increase of the number of users in a network has increased too. Due to this we need to develop systems that can support a great number of users than the conventional does, with a faster service as an addition, always taking care to guarantee the QoS necessarily to be commercially competitive in the market. Due to the CDMA systems are interference limited, we focus on calculating and reducing the interference as the principal target. This work apply realistic radiation pattern of the smart antennas, considering all the side lobes, and simulating realistic scenarios like spatial point process, instead of ideal radiation pattern and ideal scenarios, to obtain values nearest to the reality.

1.3 Organization

This thesis is organized as follows. The chapter 2 is a basic introduction of ad-hoc wireless networks and CDMA systems. Concepts that are used through the thesis, such as clustering, CDMA interference, perfect power control and capacity, are explained. The chapter 3 shows the basic antenna array parameters used in this thesis, differences between switched and adaptive systems, and an introduction to the criteria for the optimal weights and linear array and circular array calculation parameters are explained. Finally in this chapter is shown the calculation for the optimal weights for a multibeam smart antenna. Chapter 4 introduces to the model used in this thesis as the simulation scenario. Finally in chapter 5 interference and capacity analysis are shown. The conclusion and the future work are presented here.

Chapter 2

Ad-Hoc Wireless Networks

Mobile hosts such as a mobile computers, featuring powerful CPUs, large main memories, hundreds of megabytes of disk space, multimedia sound capabilities, and color displays, are now easily affordable and becoming quite common in every day business and personal life. At the same time, network connectivity options for use with mobile hosts have increased dramatically, including support for a growing number of wireless networking products based on radio and infrared. The purpose of this chapter is to present the fundamental aspects of the ad-hoc wireless networks, such as their characteristics.

2.1 Basic Concepts of Ad-Hoc Wireless Networks

Most of the mobile computing applications today require single hop wireless connectivity to the wired network. This is the traditional cellular network model, which support the current mobile computing needs by installing BSs and APs, as shown in the Figure 2.1. In such networks, communications between two mobile hosts rely on the backbone and fixed BSs. A mobile host is only one hope away from a BS.

At times, however, no wired backbone infrastructure may be available for use by a group of mobile hosts. Also, there may be situations in which setting up fixed access points is not viable solution due to cost, convenience, and performance consideration. Still, the group of users may be need to communicate with each other and share information between them. In such situations, an ad-hoc wireless network can be formed.

An ad-hoc wireless network is a temporary network operating without the aid of any established infrastructure of centralized administration or standard support services regularly available on the wide area network to which the hosts may normally be connected [5]. Applications of ad-hoc wireless networks include military tactical communication, emergency relief operations, and commercial and educational use in, for

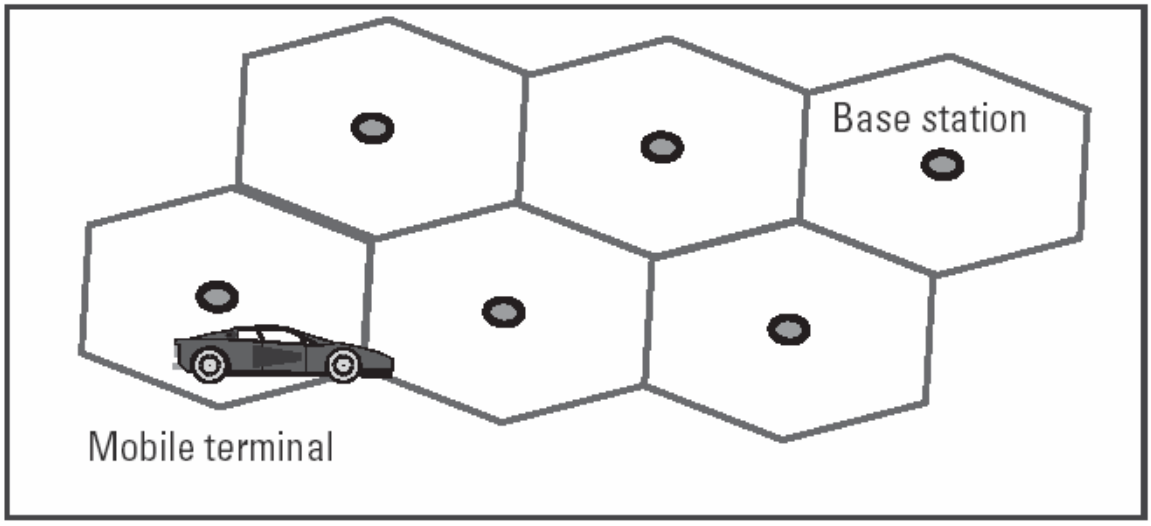

Figure 2.1: A cellular network (infrastructured network).

example remote areas or meetings where the networking is mission-oriented or community based.

Ad-hoc wireless networks are envisioned [5,6] as infrastructureless networks where each node is a mobile router equipped with a wireless transceiver. A message transfer in an ad-hoc wireless network environment would take place either between two nodes that are within the transmission range of each other or nodes that are indirectly connected via multiple hops through some other intermediate nodes. This is shown in the Figure 2.2. Node *C* and node *F* are outside the wireless transmission range of each other but are still able to communicate via the intermediate node *D* in multiple hops.

There has been a growing interest in ad-hoc wireless networks in recent years [4,7]. The basic assumption in an ad-hoc wireless network is that two nodes willing to communicate may be outside the wireless transmission range of each other, but they are still able to communicate if other nodes in the network are willing and capable of forwarding packets from them. The successful operation of an ad-hoc wireless network will be interrupted, however, if an intermediate node, participating in a communication between two nodes, either moves out of the range suddenly or switches itself off in between message transfer. The situation is worse if there is no alternative path available between those two nodes. Thus, the dynamics of these two networks, as a consequence of mobility and disconnection of mobile hosts, pose a number of problems in designing schemes for effective messages communications between any source and destination.

2.1.1 Characteristics of an Ad-Hoc Wireless Network

The Ad-Hoc wireless networks have several salient characteristics, some of them are the following [4]:

- **Dynamic topologies**
  Because the possibility rapid and unpredictable movement of the node and fast-changing propagation condition, network information, such as link state, becomes

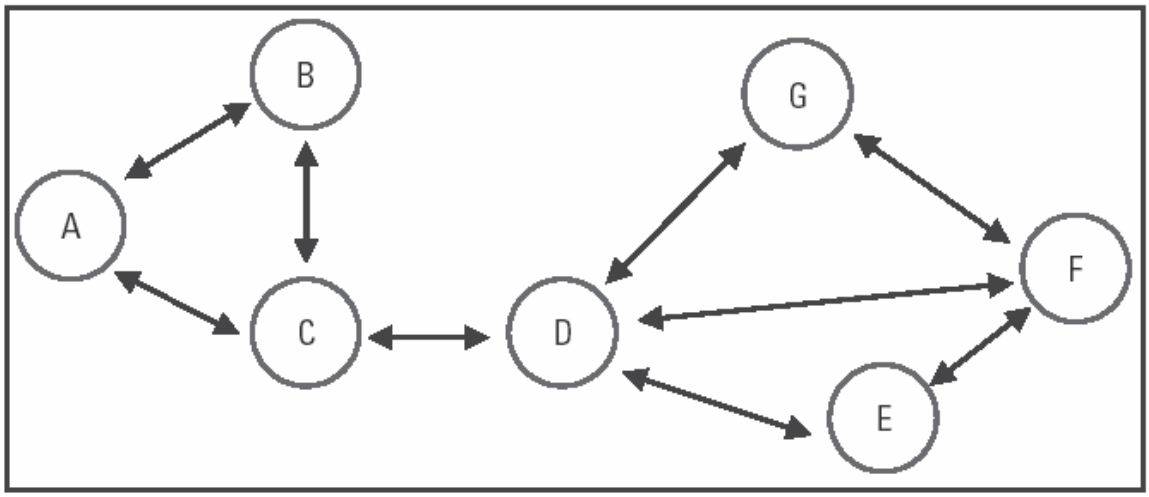

Figure 2.2: Basic structure of an ad-hoc wireless network.

quickly obsolete. This leads to frequent network reconfiguration and frequent exchanges of control information over the wireless medium.

- **Multihop Communication**
  Each node in an ad-hoc wireless network will act as a transmitter, a receiver, or a relay station. So, packets from a transmitter node (source) may reach the receiver node (destination) in multiple hops through several intermediate relay nodes. However the successful operation of an ad-hoc wireless network will be hampered if an intermediate node, participating in a communication between a source-destination pair, moves out of range suddenly or switches it self off in between message transfer. The situation is worse if there is no other path between those two nodes. In Figure 2.2, if *D* moves out of range disconnecting the link between *C* and *D*, or if *D* switches itself off, the communication between *C* and *F* would be interrupted. The absence of *D* creates two disconnected components: {*A*,*B*,*C*} and {*E*,*F*,*G*}.

- **Decentralized operation**
  Ad-hoc wireless networks are network architectures that can be rapidly deployed and that do not need to relay on preexisting infrastructure or centralized control. In cellular wireless networks, there are a number of centralized entities; (e.g, BSs, MSCs and the HLR). In ad-hoc wireless networks, since there is no preexisting infrastructure, these centralized structures do not exist. The centralized entities in the cellular networks perform the function of coordination. Thus, lack of these entities in the ad-hoc wireless networks requires more sophisticated distributed algorithms to perform equivalent functions.

- **Self-organizing**
  An ad-hoc wireless network is self-organizing and adaptive to communication requirements of the moment. This is a fundamental feature of ad-hoc wireless networks. A terminal has to be capable of detecting terminals that are within the range, and it also must learn which other terminals can be reached through these. Autoconfiguration also concerns detecting services available in the networks.

Because of this characteristic, most of the protocols for traditional networks can not easily be adapted to ad-hoc wireless networks.

- **Bandwidth constrained variable-capacity links**
  Wireless links will continue to have significant lower capacity than their hardwired counter part. In addition, the realized throughput of wireless communications is often much less than a radio's maximum transmission rate because of the effects of multiple access, fading, noise, and interference condition, for example. One effect of the relatively low to moderate link capacities is that congestion is typically the norm rater than the exception. Thus, the aggregate application demand will likely approach or exceed network capacity frequently. This demand will continue to increase as multimedia computing and collaborative networking application increase.

- **Energy-constrained operation**
  The mobile nodes in an ad-hoc wireless network rely on batteries or other exhaustible mean for their energy. For these nodes, the most important system design criteria for optimization may be energy conservation. One way of achieving this is to optimize the transmission power of each node.

2.2 Network Architecture

There are several characteristics to define and design a specific ad-hoc wireless network, such as the routing protocol, the medium access control and the network architecture. Here we focus on the architecture of an ad-hoc wireless network.

2.2.1 Flat versus Hierarchical Architecture

The architecture of an ad-hoc wireless network can be classified into hierarchical and flat architecture [8]. In a hierarchical architecture, the network nodes are dynamically partitioned into groups called clusters. Thus, the details of the network topology are concealed by aggregating nodes into clusters, clusters into superclusters, and so on [4]. The membership in each cluster changes over time in response to node mobility and is determined by the criteria specified in the clustering algorithm. Within each cluster, one node is chosen to perform the function of a cluster head [9]. Routing traffic between two nodes that are into two different clusters is normally done through the cluster heads of the source and destination cluster head. However, frequent changes in clusters membership and consequent reselection of cluster head adversely affect routing protocol performance. In order to get rid of this problem, a fully distributed approach for cluster formation and intracluster communication has been proposed [10] that eliminate the requirement for a cluster head together. Even then, in the context of a highly dynamic scenario, the reconfiguration of clusters and the assignments of nodes to cluster do require excessive processing and increase communication overhead. This is depicted in Figure 2.3, where three clusters are shown. Here, nodes marked *C* are cluster heads and nodes marked *N* are clusters members. Another type of node, called gateway node, is introduces here. Nodes marked *G* are gateway nodes for intercluster communications [4].

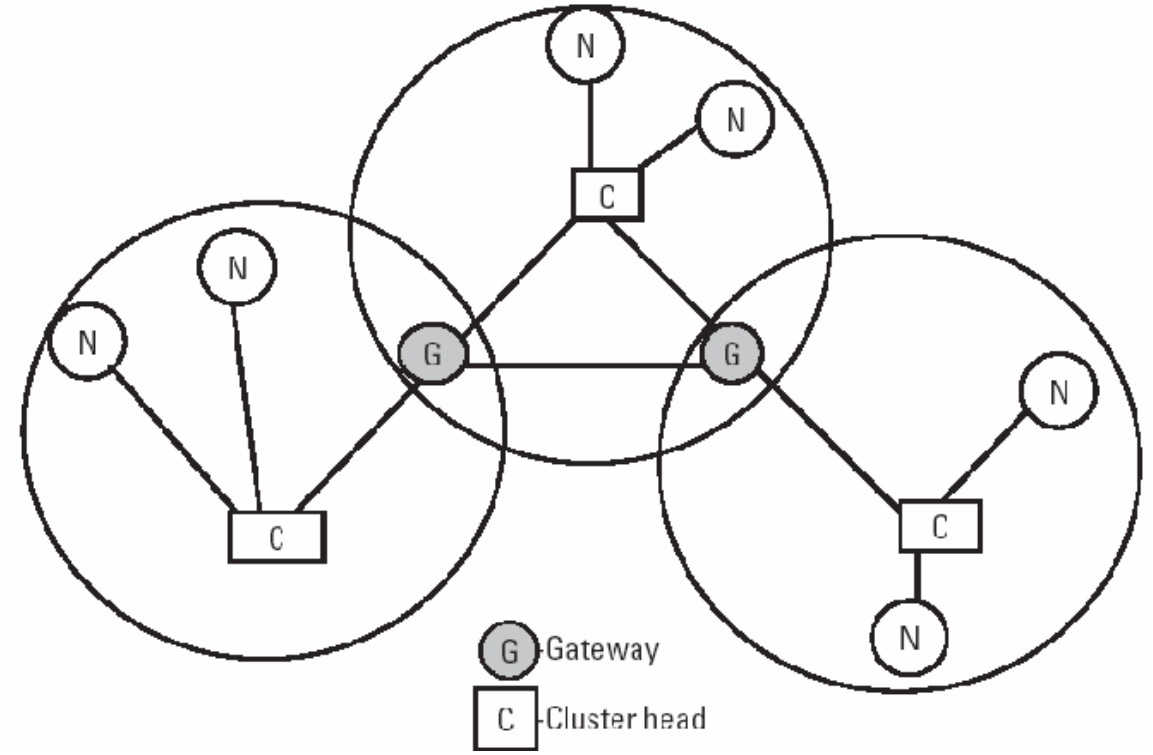

Figure 2.3: Clustered architecture of an ad-hoc wireless network.

Intercluster communications are done through the respective cluster head.

In contrast, in a flat architecture, there are no clusters and the neighboring nodes can communicate directly. It has been argued that the routing in flat architecture is more optimal (close-by nodes do not have to communicate through the hierarchy) [4], and the network tends to better balance the load among the multiple paths, thus reducing the traffic bottleneck that occur at the cluster nodes in the hierarchical approach [8].

In a hierarchical architecture, some nodes, such as cluster head and gateway nodes, have a higher computation and communication burden than others nodes. The network reliability may be affected due to this single point of failure of these critical nodes. However, the routing messages may only have to propagate within a cluster. Thus, the number of globally propagated messages is small. On the contrary, in a flat architecture, all nodes carry the same responsibility, and reliability is not dependent on any single point of failure. However, this flat architecture is not bandwidth efficient because the routing messages have to propagate globally throughout the network. The scalability gets worse when the number of nodes increase [4].

The main advantage of the hierarchical ad-hoc wireless network is the ease of the mobility management process. In order to limit far-reaching impact to topology dynamics, complete routing information is maintained only for intracluster routing. Intercluster routing is achieved by hiding the topology details within a cluster form external nodes and using hierarchical aggregation, reactive routing, or a combination of both techniques. Cluster heads can act as databases that contain the location of the nodes in their own clusters. To determine the existence and the location of a mobile node, a query is broadcasted to all the cluster heads. The cluster under which the node resides, responds to

the query originator. A mobility management scheme needs to be implemented in the flat networks by appropriate routing algorithm, although it would increase the overhead due to control messages propagation throughout the network [8].

2.3 Medium Access

In ad-hoc wireless networks, since the media are shared by multiple mobile had-hoc nodes, access to the common channel must be made in a distributed fashion, through the presence of a MAC protocol. The MAC protocol must contend for the access to the channel while at the same time avoiding possible collision with neighboring nodes. There are three multiple access techniques: FDMA, TDMA and CDMA, as shown in the Figure 2.4.

In the traditional Frequency division Multiple Access (FDMA) scheme [11], Figure 2.4 (a), each individual user is assigned a particular frequency band in which transmission can be carried out. A portion of the frequency spectrum is divided into different channels. Different user's signals are lowpass filtered and modulated onto an assigned carrier frequency f_c of a particular channel. This way, multiple users can simultaneously share the frequency spectrum.

In Time Division Multiple Access (TDMA), Figure 2.4 (b), each user is assigned a different time slot in which to transmit; in this case the division of the users occurs in the time domain.

In CDMA, Figure 2.4 (c), each user's narrowband signal is spread over a wider bandwidth. Each user is assigned a different code, and each of the codes is orthogonal to one other.

While FDMA and TDMA are frequency limited, CDMA is interference limited. This means a capacity limited for the different access techniques, being CDMA the promising highly capacity, just by reducing interference.

2.3.1 CDMA Principles

Traditionally, in radio communication system, the carrier was modulated with user data using techniques that minimize the transmitted bandwidth to conserve spectrum resources [3]. This was because radio systems were designed so that only a single channel occupied a given frequency band, as illustrated in Figure 2.4 (a). If signals are transmitted in multiple non-overlapping frequency bands, they do not interfere with each other and the signals may each be recovered, provided that the power levels are high enough relative to the noise which is always present in the channel. In a spread spectrum system, rather trying to minimize the bandwidth of the modulated signal, the goal is to create a modulated signal that uses a large amount of bandwidth. There are two main types of a spread spectrum system: direct sequence (DS) and frequency hop (FH). The remainder of this text focuses on Direct Sequence rather than Frequency Hop Spread Spectrum.

The Direct Sequence Code Division Multiple Access (DS-CDMA) is a wireless access technique, where signals from different users are assigned a unique *spreading code*. Signals from different users occupy the same spectrum at the same time. The receiver separates signals using their codewords, as in Figure 2.5 [3].

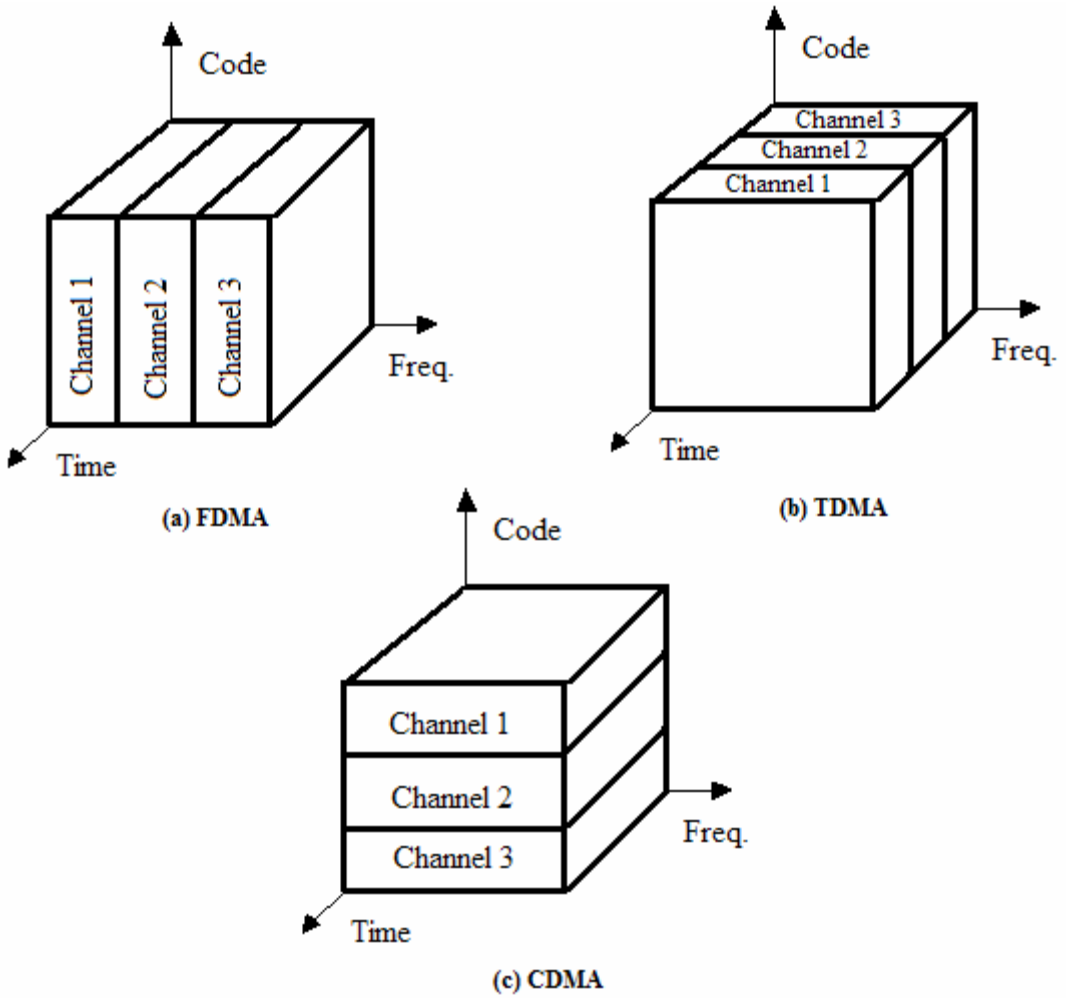

Figure 2.4: Three multiple access schemes: (a) Frequency division Multiple Access (FDMA), in which different channels are assigned to different frequency bands; (b) Time Division Multiple Access (TDMA), where each channel occupies a cyclically repeating time slot; and (c) Code Division Multiple Access (CDMA), in which each channel is assigned a unique signature sequence code .

In DS systems, a narrowband signal, containing a message with bandwidth B_1, is multiplied by a signal with a much larger bandwidth B_2, which is called the spreading signal. Essential features of Direct Sequence Spread Spectrum are that

- The bandwidth of the spreading signal, B_2, is much larger than the bandwidth of the message signal, B_1, and
- The spreading signal is independent of the message signal.

Thus, assuming that the bandwidth of the spreading signal is much larger than the bandwidth of the narrowband information signal, the transmitted signal will have a bandwidth which is essentially equal to the bandwidth of the spreading signal, as shown in the Figure 2.5.

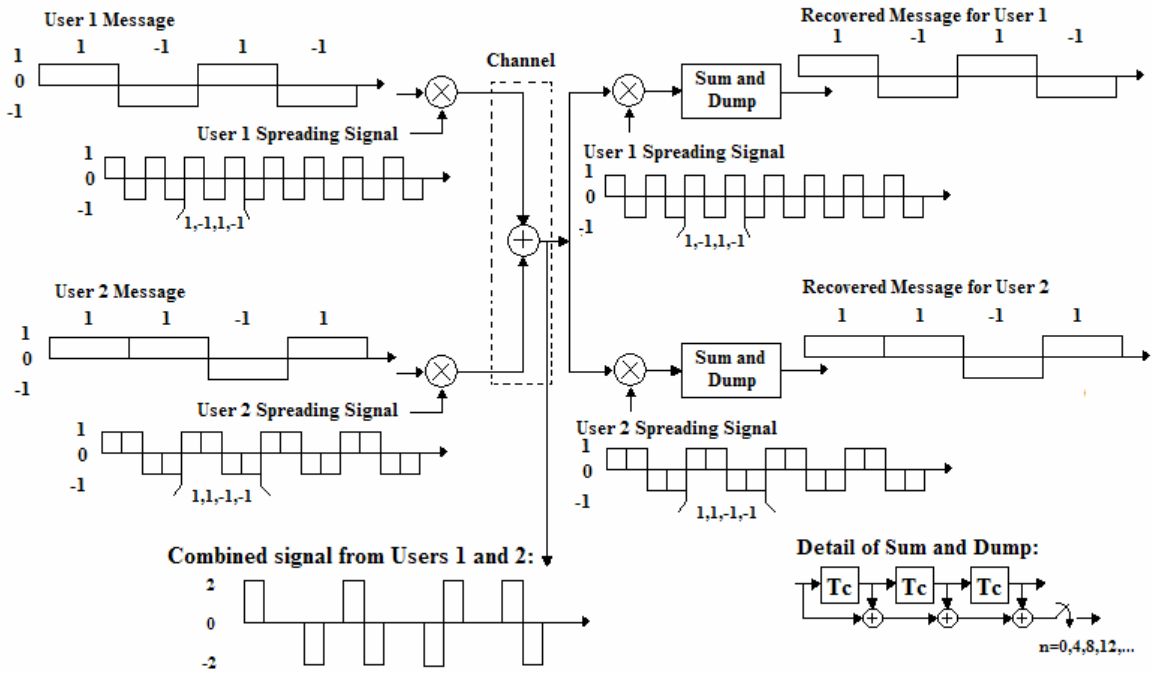

Figure 2.5: A simple Direct Sequence CDMA system. The signals from each user are spread by a spreading code, which is known at the transmitter and receiver. CDMA signals can occupy the same spectrum at the same time.

2.3.2 Power Control

We can consider a single cell CDMA Cellular System, which consists of numerous mobile (or personal) subscribers communicating with one or multiple cell sites (or base stations) which are interconnected with a mobile telephony switching office (MTSO), which also serves as a gateway to the public switched telephone network [12]. Consider the CDMA uplink where subscribers are transmitting signals that are received at a single base station receiver, as shown in the Figure 2.6 [3]. If the BS just listen a subscriber p the *Carrier-to-Interference-Ratio* (CIR) can be represented by γ_p. Letting P_p represent the received power from user p, γ_p is

$$\gamma_p = \frac{P_p}{\sum_{\substack{k=0 \\ k \neq p}}^{K-1} P_k} \tag{2.1}$$

Recall that P_k represents the power received at the base station from a particular subscriber. If every user transmits at the same power level, then the received power from users closer to the base station will tend to be higher that than the received power from subscribers that are farther away from the base station. This leads to a different performance for subscribers links, depending on where the subscribers are located in the cell. More importantly, a few subscribers closest to the base station may contribute so

much Multiple Access Interference that they prevent other uplink signals from being successfully received at the base station [3].

To solve this problem, *power control* is used in CDMA systems. Power control forces all users to transmit the minimum amount of power needed to achieve acceptable signal quality at the base station. Power control typically reduces the power transmitted by subscribers closest to the base station, while increasing the power of subscribers farthest away from the base station. Compared with the case where all users transmit at the same power level, power control reduces the denominator of (2.1), increasing the CIR, and lowering the error rate of all subscribers.

If all subscribers in a system have the same bandwidth, data rate, and other signal characteristics, then one reasonable approach to power control is to set all of the received power levels, P_k, to a constant value, P_c. Then (2.1) [3], can be rewritten as

$$\gamma_p = \frac{1}{(K-1)} \tag{2.2}$$

This is called *perfect power control.* In practice, this sort of perfect power control is not achievable and under many circumstances, despite its name, may not even be desirable. Perfect power control requires exact knowledge of the loss in the radio propagation channel between the subscriber transmitter ad the base station receiver, commonly referred to as *path loss*.

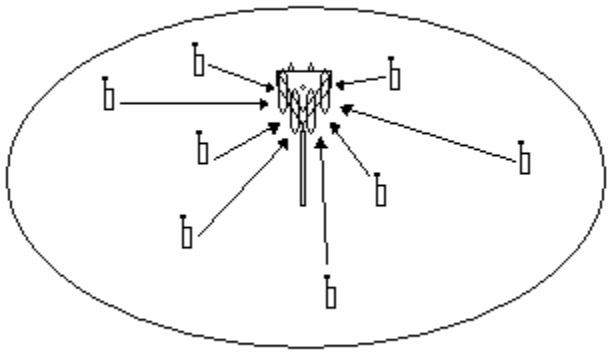

Figure 2.6: A Single Cell Cellular System in reverse-link case.

2.3.3 Capacity and Interference in CDMA Systems

In digital communication, we are primarily interested in a link metric called E_b/N_0, or energy per bit noise density. This quantity can be related to the conventional *signal-to-noise radio* (SNR) by recognizing that energy per bit equates to the average modulating signal power allocated to each bit duration; that is,

$$E_b = ST \tag{2.3}$$

where *S* is the average modulating signal power and *T* is the time duration of each bit. Notice that (2.3) is consistent with dimensional analysis, which states that energy is equivalent to power multiplied by time. We can further manipulate (2.3) by substituting the bit rate *R*, which is the inverse of bit duration *T*:

$$E_b = \frac{S}{R}$$

E_b / N_0 is thus

$$\frac{E_b}{N_0} = \frac{S}{RN_0} \tag{2.4}$$

We further substitute the noise power density N_0, which is the total noise power *N* divided by the bandwidth *W*; that is,

$$N_0 = \frac{N}{W} \tag{2.5}$$

Substituting (2.5) into (2.4) yields

$$\frac{E_b}{N_0} = \frac{S}{N}\frac{W}{R} \tag{2.6}$$

Equation (2.6) relates the energy per bit E_b/N_0 to two factors: the signal-to-noise ratio *S/N* of the link and the ratio of the transmitted bandwidth *W* to bit rate *R*. The ratio *W/R* is also known as the processing gain of the system.

Now, we consider the reverse-link capacity since in CDMA this is often the limiting link in terms of capacity, as shown in the Figure 2.6. Reverse link is the mobile to base station link. For N users, we assume that the system possesses perfect power control, so each user signal is received with power S. Having (N-1) interfering signals each also of power S, the SNR of one user can be written as

$$\frac{S}{N} = \frac{S}{(N-1)S} = \frac{1}{N-1} \tag{2.7}$$

This is so because the total interference power in the band is equal to the sum of powers from individual users. Note that (2.7) also ignores other sources of interferences such as thermal noise.

We proceed to substitute (2.7) into (2.6), and the result is

$$\frac{E_b}{N_0} = \frac{1}{N-1}\frac{W}{R} \tag{2.8}$$

Solving for *(N-1)* yields

$$N - 1 = \frac{(W / R)}{(E_b / N_0)} \tag{2.9}$$

Note that if N is large, then

$$N \approx \frac{(W / R)}{(E_b / N_0)} \tag{2.10}$$

where N is the capacity of users of the system. But in ad-hoc wireless networks, the perfect power control is accomplished by forcing all nodes to transmit the minimum amount of power needed to achieve acceptable signal quality at their neighbors, as shown in the Figure 2.7.

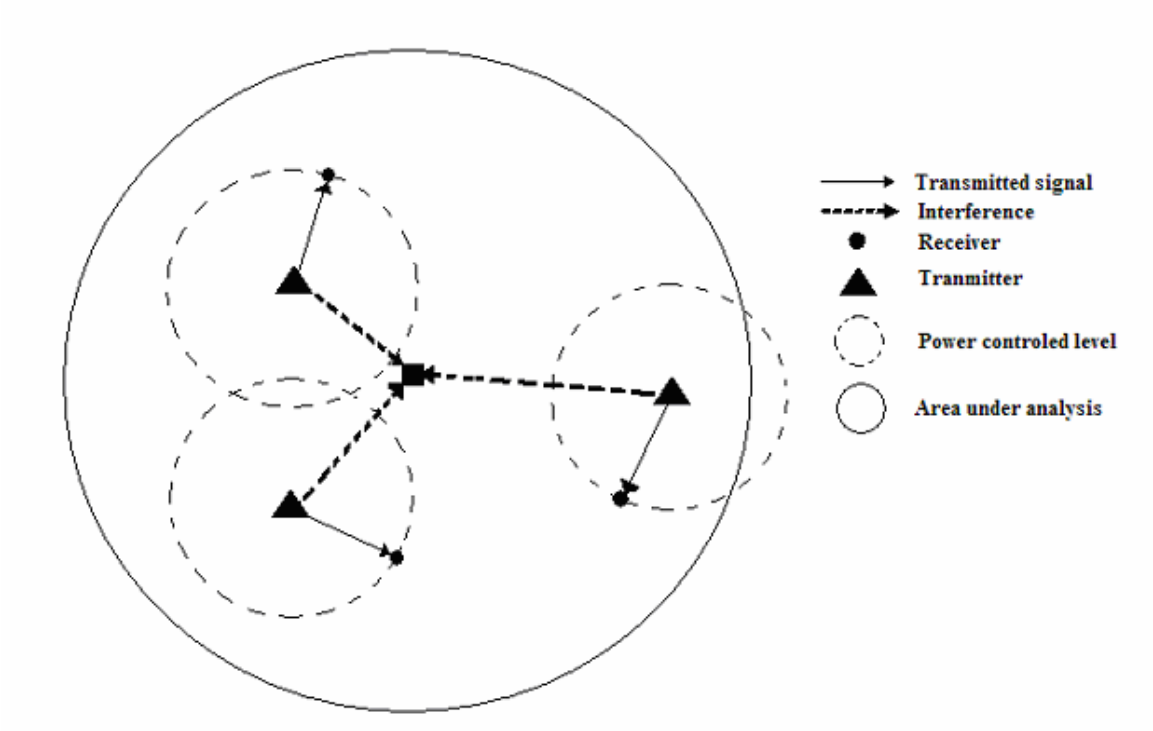

Figure 2.7: Power control scenario in an ad-hoc wireless network.

Here, the interference caused in the center of the area under analysis, is the sum of power of all the interferers in that area, like the denominator of (2.1) (as we will see in chapter 4). The total interference is dependent of the nodes location, the distance and the kind of antenna used in the transmission. Due to this reasons, the power level at the center of the analysis area is not controlled and neither easy to establish the total interference of the wireless ad-hoc network, and for that reason, the capacity of the CDMA wireless ad-hoc network system can vary from one scenario to other.

Chapter 3

Smart Antenna Concepts

Smart antennas offer a broad range of ways to improve wireless system performance. In general, smart antennas, as shown in Figure 3.1, have the potential to provide enhanced range and reduce infrastructure costs in early deployments, enhanced link performance as the system is built-out, and increased long-term system capacity [3].

Radio antennas couple energy from one medium to another. An isotropic antenna radiates or receives energy equally well in all directions. In reality, no antenna is perfectly omnidirectional, but we use this term to represent any antenna that is not intentionally directional. A directional antenna has certain preferred transmission and reception directions, that is, it transmits/receives more energy in one direction compared to the other [14].

Smart antennas can be used [3], in cellular systems, to allow the subscribers and the base station to operate at the same range as a conventional system, but at lower power. This may allow FDMA and TDMA systems to be rechannelized to reuse frequency channels more often than systems using conventional fixed antennas, since the carrier-to-interference ratio is much greater when smart antennas are used. In CDMA systems, if smart antennas are used to allow subscribers to transmit less power for each link, then the Multiple Access Interference is reduced which increases the number of simultaneous subscribers that can be supported in each cell.

In the present chapter we will introduce the smart antenna concepts. First we will see the smart antenna parameters, then two types of arrays used through this work, linear and circular, and two principal types of smart antenna: switched beam and adaptive array. After this, we will present different techniques to calculate the optimal weights necessary to the beamforming process. As a final part, we will demonstrate an optimal weight technique for multiple beams, within the same weight vector.

3.1 Basic Antenna Array Parameters

Here we will provide some of the parameters and definitions that are particularly relevant to issues addresses in this work. Although most of the parameters are defined in terms of transmitting antennas, reciprocity ensures that these definitions are also applicable to receiving antennas [13].

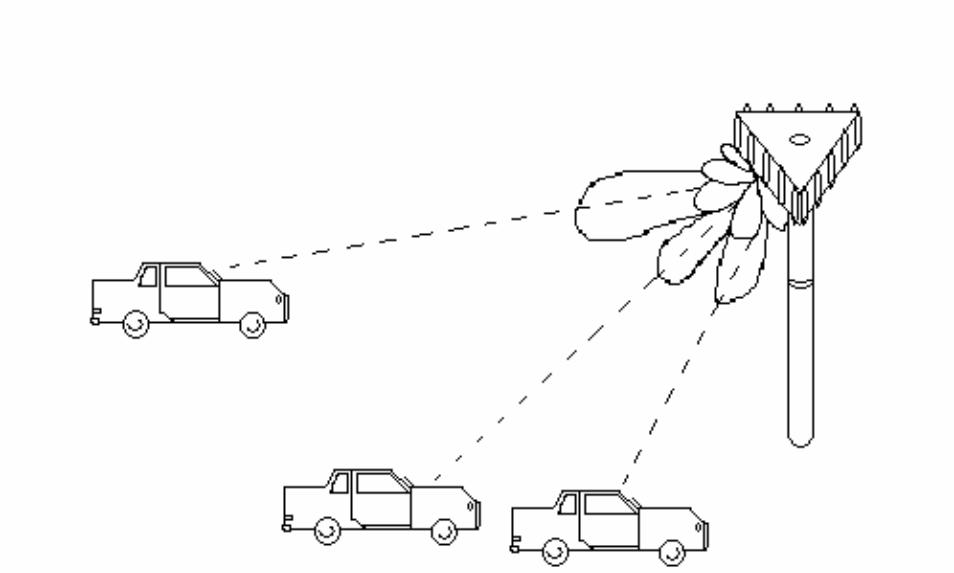

Figure 3.1: Smart antenna systems can form a different beam for each node, minimizing the impact of noise and interference between nodes or mobiles.

Radiation Pattern

The relative distribution of radiation power as a function of direction in space is called the radiation pattern of an antenna, as shown in the Figure 3.2.

Array Factor

The array factor represents the far-field radiation pattern of an array of isotropically radiating elements.

Main Lobe

The main lobe of an antenna radiation pattern is the lobe containing the direction of maximum radiation power.

Sidelobes

Sidelobes are lobes in any direction other than that of the main lobe. For a linear array with uniform weighting, the first sidelobe (i.e., the one nearest the main lobe) in the radiation pattern is about 13 dBi below the peak of the main lobe.

Beamwidth

The beamwidth of an antenna is the angular width of the main lobe in its far-field radiation pattern. Half-power beamwidth (HPBW), or 3 dBi beamwidth, is the angular

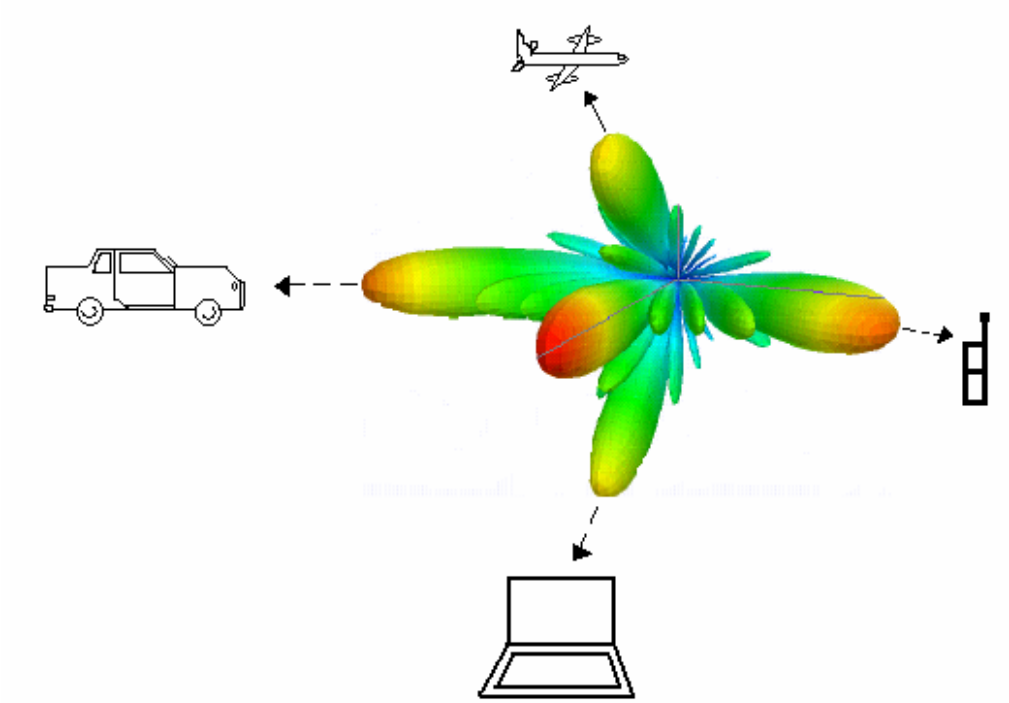

Figure 3.2: Smart antenna radiation pattern.

width measured between the points on the main lobe that are 3 dBi below the peak of the main lobe.

Grating Lobe

In an antenna array, if the element spacing is too large, several main lobes will be formed in visible space on each side of the array plane. The extra main lobes formed with large element spacing are referred to as grating lobes.

Directive Gain

Directive gain is a far-field quantity and defined as the ratio of the radiation density in a particular angular direction in space to the ratio density of the same power radiated isotropically; that is,

$$D(\phi,\theta) = \frac{4\pi \ power\ radiated\ \ perunit\ solid\ angel\ in\ direction\ \varphi,\theta}{Total\ \ power\ radiated\ by\ antenna} \qquad (3.1)$$

Directivity

Directivity is the maximum directivity gain of an antenna; that is, it is the directive gain in the direction of the maximum radiation density.

Antenna Gain

The gain of an antenna is defined as the ratio of the radiation density in a particular angular direction in space to the total input power to the antenna; that is,

$$G(\phi,\theta) = \frac{4\pi \ \ power\ radiated\ \ per\ unit\ solid\ \ angle\ in\ direction\ \phi,\theta}{Total\ \ input\ \ power\ to\ antenna} \qquad (3.2)$$

Effective Isotropic Radiated Power

The effective isotropic radiated power (EIRP) is the product to the input power to the antenna and its maximum gain.

dBi

The term dBi refers to the gain of an antenna, in dB, relative to an isotropic antenna. If an isotropic antenna is loss less, then the Gain of this antenna is $G_{iso} = 1$. Therefore, the gain of an antenna relative to an isotropic antenna is

$$G_{dBi} = 10\log\left(\frac{G}{G_{iso}}\right) = 10\log(G) \qquad (3.3)$$

3.2 Types of Smart Antennas

The simplest way of improving the "intelligence" of antennas is to have multiple elements [14]. The slight physical separation between elements results in signal diversity and can be used to counteract multipath effects. There are two well-known methods. In switched diversity, the system continually switches between elements so as to always use the element with the best signal. Although this reduces the negative effects of multipath fading, there is no increase in gain. In diversity combining, the phase error of multipath signals is corrected and the power combined to both reduce multipath and fading, as well as increase the gain.

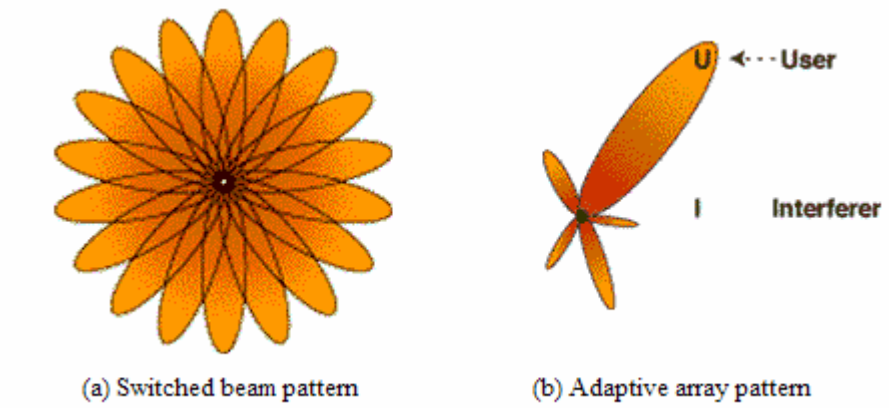

Figure 3.3: Different smart antenna patterns. (a) Switched beam pattern. (b) Adaptive array pattern.

The next step up in sophistication involves incorporating more control in the way the signals from multiple elements (the antenna array) are used to provide increased gain,

more beams, and beam agility. Again, there are two main classes of techniques, as described below [14].

In switched beam systems, multiple fixed beams are formed by shifting the phase of each element's signal by a predetermined amount (this is done by a beamforming network), or simply by switching between several fixed directional antennas, as shown in the Figure 3.3 (a) [15]. The transceiver can then choose between one or more beams/antennas for transmitting or receiving. Although they provide increased spatial reuse, switched beam system cannot track moving nodes, which therefore experience periods of lower gain as they move between beams.

In a steered beam system, the main lobe can be pointed virtually in any direction, often automatically using the received signal from the target and sophisticated "direction-of-arrival" techniques, as shown in the Figure 3.3 (b). One may distinguish between two kinds of steered beam systems: dynamic phased arrays that maximizes the gain toward the target, and adaptive array that additionally minimizes the gain (produce nulls) toward interfering sources. The former allows beam steering, and the latter additionally provides adaptive beamforming.

3.2.1 Switched Beam Systems

In smart antenna systems which use only the fixed Beam Forming Network (BFN) [3], a switch is used to select the best beam to receive a particular signal. The switched system illustrated in the Figure 3.4 is relatively simple to implement, requiring only a beamforming network, an RF switch, and control logic to select a particular beam. By selecting an output, one of the *M* predetermined weight vectors is used. A separate beam selection must be made for each receiver. The mechanism for performing beam selection is highly dependent on whether we are considering an FDMA, TDMA, or CDMA system; however, it is possible to consider switched beam approach to each of these multiple access methods.

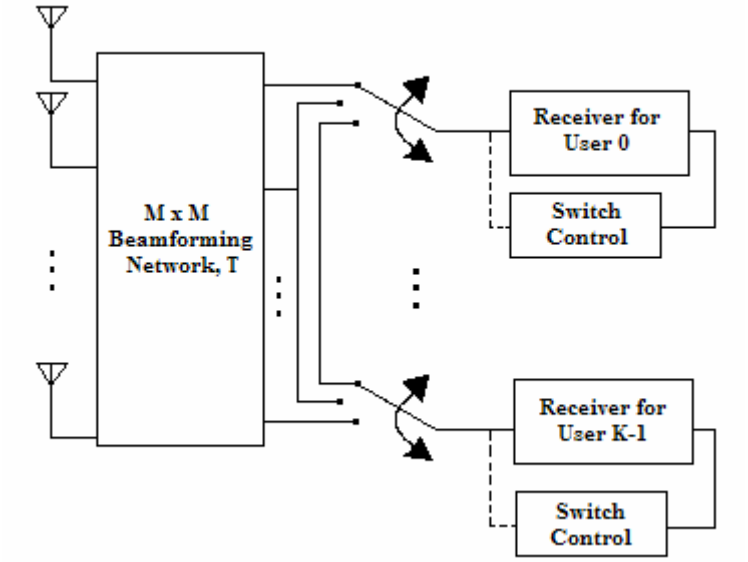

Figure 3.4: A switched beam network uses a beamforming network to form *M* beams from *M* array elements.

Switched beam systems offer many of the advantages of more elaborate smart antenna systems at a fraction of the complexity and expense. There are, however, several limitations to switched beam arrays. First of all, the system is not able to provide any protection from multipath components which arrive with Direction-Of-Arrival (DOA) near that the desired component. A second disadvantage of switched beam systems is that they are typically unable to take advantage of path diversity by combining coherent multipath components. Finally, the received power level from one node fluctuates as a mobile node travels in an arc about the receiver node due to scalloping. Scalloping is the roll-off of the antenna pattern as a function of angle as the DOA varies from the boresight of each beam produced by the BFN. Typically, BFNs provide beams which cross at 4 dB points. Thus a transmitter node's signal strength varies as the node moves from the center of the beam to the edge of the region of a particular beam.

Despite these disadvantages, switched beam systems are popular for several reasons. They provide some of the range extension benefits obtained from more elaborate systems. Depending on the propagation environment, switched beam systems offer some reduction in delay spread, as shown in [16][17], which provides the capability to deploy low tier PCs systems in high-antenna height, high node speed environments. Switched beam systems require only moderate interaction with the receiver node, compared with the adaptive antenna systems, which appeals to manufacturers wishing to supply "bolt-on" solutions. Finally, since this is a relatively low technology approach, the engineering costs associated with implementing these systems may be much lower that those associated with more complicated systems.

3.2.2 Adaptive Antenna Systems

By increasing the complexity of the array signal processing, it is possible to achieve greater performance improvements than are attainable using switched beam systems. In an adaptive array, as shown in the Figure 3.5, the weight vector $\boldsymbol{w}_{k,i}$ is adjusted, or adapted, to maximize the quality of the signal that is available to the demodulator for signal k a time index i.

In optimal beamforming techniques, a weight vector is determined which minimizes a cost function. Typically, this cost function is inversely associated with the quality of the signal at the array output, so that when the cost function is minimized, the quality of the signal is maximized at the array output. One of the most popular techniques which have been applied extensively in communication systems are the Minimum Mean Square Error (MMSE). In this technique, the square of the difference between the array output, $z(t)=\boldsymbol{w}^H{}_k\boldsymbol{u}_i(t)$, and $d_k(t)$, a locally generated estimate of the desired signal for the k^{th} subscriber, is minimized by finding an appropriate weight vector, $\boldsymbol{w}_k$. MMSE solutions are posed in terms of ensemble averages and produce a single weight vector, $\boldsymbol{w}_k$, which is optimal over the ensemble of possible realizations of the stationary environment. This is the approach used in classical Wiener filter theory.

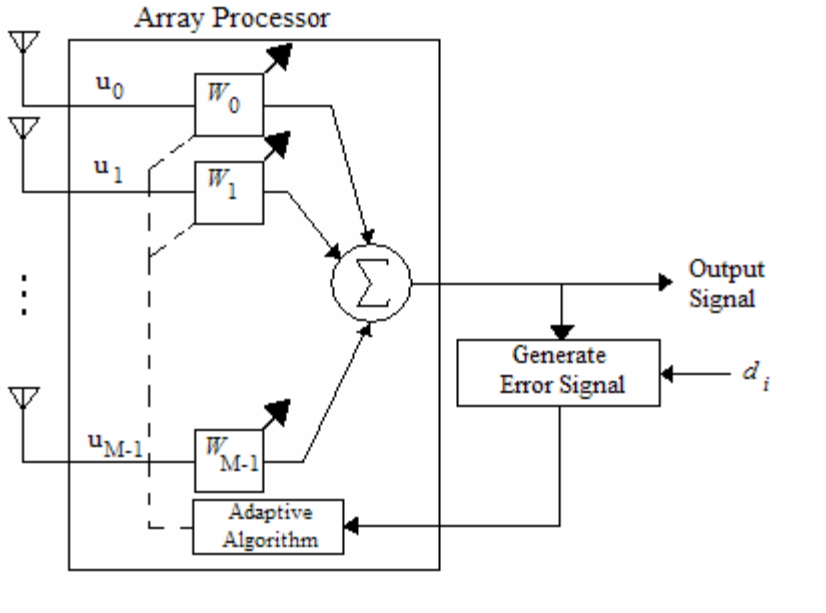

Figure 3.5: An adaptive array basic structure.

3.3 Criteria for Optimal Weight

The following example illustrates the procedure used for steering and modifying an array's beam pattern in order to enhance the reception of a desired signal, while simultaneously suppressing interfering signals through complex weight selection [13]. Consider the array shown in the Figure 3.6, which consists of two omnidirectional antennas with $\lambda_0/2$ spacing. The desired signal *S(t)*, arrives from the boresight direction ($\theta_S=0$), and the interference signal, *I(t)*, arrives from the angle ($\theta_I=\pi/6$) radians. Both signals have the same frequency f_0. The signal from each element is multiplied by a variable complex weight, and the weighted signals are then summed to form the array output. The array output due to the desired signal is

$$y_d = Ae^{j2\pi f_0 t}(w_1 + w_2) \tag{3.4}$$

For $y_d(t)$ to be equal to $S(t)$, it is necessary that

$$\left.\begin{aligned}\Re[w_1] + \Re[w_2] = 1\\ \Im[w_1] + \Im[w_2] = 0\end{aligned}\right\} \tag{3.5}$$

where $\Re[]$ and $\Im[]$ operate on the real and imaginary values, respectively. The incident interference signal arrives at element 2 with a phase lead with respect to element 1 of value of value $2\pi\frac{1}{\lambda_0}d\sin(\pi/6) = \pi/2$. Consequently, the array output due to the interference is

$$y_I(t) = Ne^{j2\pi f_0 t} w_1 + Ne^{j(2\pi f_0 t + \pi/2)} w_2 \tag{3.6}$$

For the array interference response to be zero, it is necessary that

$$\left.\begin{aligned} \Re[w_1] + \Re[w_2] = 0 \\ \Im[w_1] + \Im[w_2] = 0 \end{aligned}\right\} \tag{3.7}$$

Simultaneous solution of (3.5) and (3.7) yields

$$w_1 = \frac{1}{2} - j\frac{1}{2}, w_2 = \frac{1}{2} + j\frac{1}{2}$$

With these weights, the array will accept the desired signal while simultaneously reject the interference. The choice of the weight vector ***w*** is based on the statistics of the signal ***x(t)*** received at the array. Basically, the objective is to optimize the beamformer response with respect to a prescribed criterion, so that the output *y(t)* contains minimal contribution from noise and interference. There are a number of criteria for choosing the optimum weights, which will be discussed in the next sections.

3.3.1 Minimum Mean Square Error

The most widely used method for estimating the weights is the minimum mean square error (MMSE). This method needs a reference signal *r*, and that is the main reason why this criterion is used through this work as the criteria for the calculation of the optimal weights, as we will show in section 3.6.

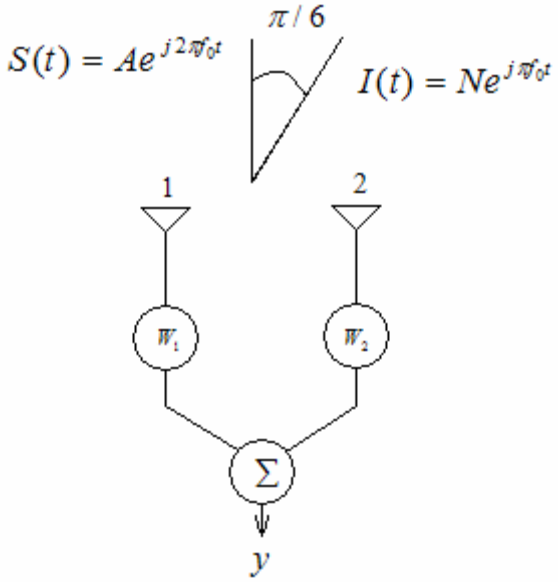

Figure 3.6: Two-element array for interference suppression.

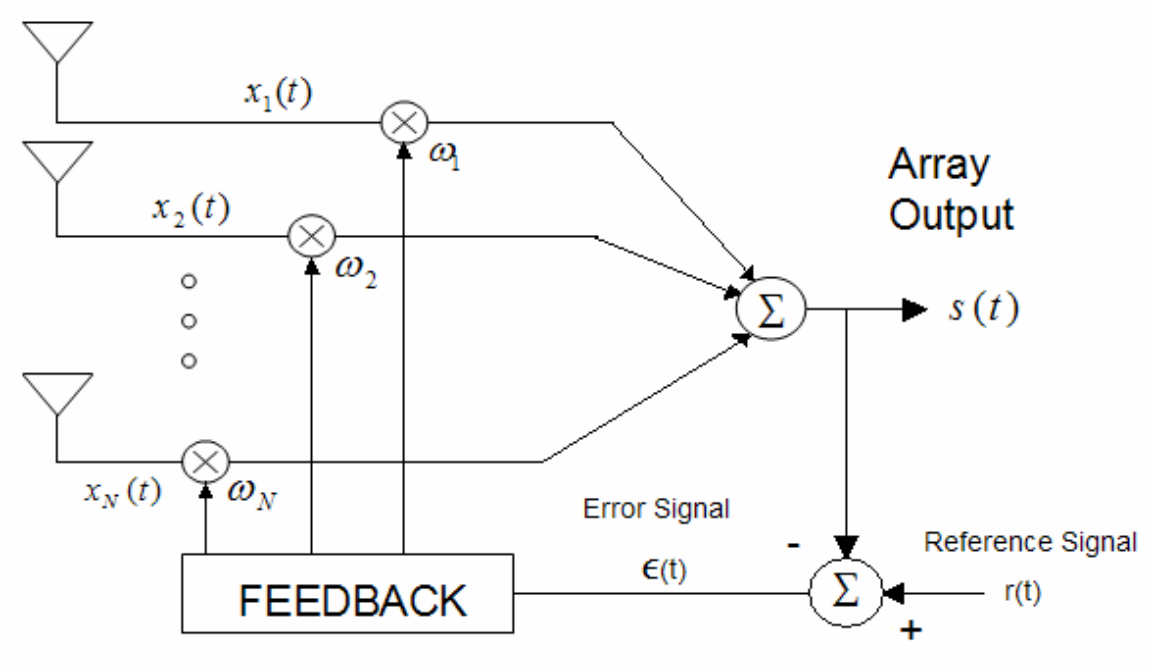

Figure 3.7: Adaptive array structure in the MMSE criterion.

Consider the *N*-element array shown in the Figure 3.7, each element receives a $x_j(t)$ signal. Each of these signals is multiplied by a weight w_j [18]. The weighted signals are then summed to produce the array output signal $s(t)$. To make the array adaptive, a feedback system is used to control the weights as shown in the Fig. 3.7. The feedback system attempts to drive the weights toward their optimal values, which are defined as follows.

The array is based on a minimum mean-square error concept. An error signal ϵ(t) is obtained by subtracting the array output $s(t)$ from another signal called the reference signal $r(t)$. The feedback adjust the weights to minimize $E[\varepsilon^2(t)]$, where $E[\bullet]$ denotes expectation. The details of feedback will be explained below.

First, however, let consider why a minimum mean-square error criterion is useful. Suppose this array is used in a communication system. Assume the array output contains a desired signal, interference, and thermal noise; that is,

$$s(t) = \alpha s_d(t) + \beta s_i(t) + \gamma n(t), \qquad (3.8)$$

where $s_d(t)$ is the desired signal, $s_i(t)$ is the interference, $n(t)$ is the thermal noise, and α, β, and γ are constant representing the combined affect of the weights on these signals. We would like to adjust the weights in the array to maximize the desired signal and minimize the interference and thermal noise at the array output. To do so, suppose we let the reference signal $r(t)$ be a replica of the desired signal:

$$r(t) = s_d(t)$$

Then $\varepsilon(t)$ will be

$$\varepsilon(t) = (1-\alpha)s_d(t) - \beta s_i(t) - \gamma n(t) \tag{3.9}$$

and the mean-square error is

$$E[\varepsilon^2(t)] = E[\{(1-\alpha)s_d(t) - \beta s_i(t) - \gamma n(t)\}^2] \tag{3.10}$$

If the desired signal, interference and thermal noise are *uncorrelated* with each other, then all cross product are zero, then the mean-square error is

$$E[\varepsilon^2(t)] = (\alpha-1)^2 E[s_d^2(t)] - \beta^2 E[s_i^2(t)] - \gamma^2 E[n^2(t)]. \tag{3.11}$$

Now let us determine the weights settings that yield minimum $E[\varepsilon^2(t)]$. For an arbitrary set of weights, the array output [4] is given by

$$s(t) = \sum_{j=1}^{N} w_j x_j(t). \tag{3.12}$$

Therefore, the error signal is

$$\varepsilon(t) = r(t) - \sum_{j=1}^{N} w_j x_j(t) \tag{3.13}$$

and the mean-square error is

$$E[\varepsilon^2(t)] = E\left[r^2(t) - 2r(t)\sum_{j=1}^{N} w_j x_j(t) + \left\{ \sum_{j=1}^{N} w_j x_j(t) \right\}^2 \right] \tag{3.14}$$

$$E[\varepsilon^2(t)] = E[r^2(t)] - 2\sum_{j=1}^{N} w_j E[r(t)x_j(t)] + \sum_{i=1}^{N}\sum_{j=1}^{N} w_i w_j E[x_i(t)x_j(t)] \tag{3.15}$$

This result may be written more simply by using matrix notation:

$$E[\varepsilon^2(t)] = E[r^2(t)] - 2\,\boldsymbol{W}^T\boldsymbol{S} + \boldsymbol{W}^T\boldsymbol{\Phi}\boldsymbol{W}, \tag{3.16}$$

where $\boldsymbol{W}$ and $\boldsymbol{S}$ are column matrices,

$$W = [w_1, w_2, w_3, ..., w_N]^T \tag{3.17}$$

$$\boldsymbol{S} = E\begin{bmatrix} x_1(t)r(t) \\ x_2(t)r(t) \\ \vdots \\ x_N(t)r(t) \end{bmatrix} \tag{3.18}$$

where (3.18) is the reference correlation vector , and $\boldsymbol{\Phi}$ is a N x N matrix,

$$\boldsymbol{\Phi} = E\begin{bmatrix} x_1(t)x_1(t) & x_1(t)x_2(t) & x_1(t)x_3(t) & \cdots & x_1(t)x_N(t) \\ x_2(t)x_1(t) & x_2(t)x_2(t) & x_2(t)x_3(t) & \cdots & x_2(t)x_N(t) \\ \vdots & \vdots & \vdots & \ddots & \vdots \\ x_N(t)x_1(t) & x_N(t)x_2(t) & x_N(t)x_3(t) & \cdots & x_N(t)x_N(t) \end{bmatrix} \tag{3.19}$$

where (3.19) is the covariance matrix. Superscript T denotes the transpose.

The weight vector yielding minimum $E[\varepsilon^2(t)]$, which we denote by $\boldsymbol{W}_{opt}$, may be found by setting

$$\nabla_W \left\{E[\varepsilon^2(t)]\right\} = 0\,, \tag{3.20}$$

where ∇_W denotes the gradient with respect to $\boldsymbol{W}$. Since

$$\nabla_W \left\{E[\varepsilon^2(t)]\right\} = -2\,\boldsymbol{S} + 2\boldsymbol{\Phi}\boldsymbol{W} = 0\,, \tag{3.21}$$

we find

$$\boldsymbol{\Phi}\ \boldsymbol{W}_{opt} = \boldsymbol{S}$$

or

$$\boldsymbol{W}_{opt} = \boldsymbol{\Phi}^{-1}\boldsymbol{S} \tag{3.22}$$

where $\boldsymbol{\Phi}$ is assumed to be nonsingular so its inverse matrix exists. (Nonsingular means whenever the element signals contain thermal noise).

Example 1

Consider an array consisting of two isotropic elements, as shown in the Figure 3.8. A desired signal at frequency ω_d and an interference signal propagates into the array from angle θ_d and θ_i respectively, relative to the broadside. Let the element be one-half wavelength apart at frequency ω_d. Now the element signal are given by

$$x_1(t) = d_1(t) + i_1(t) + n_1(t) \tag{3.23}$$

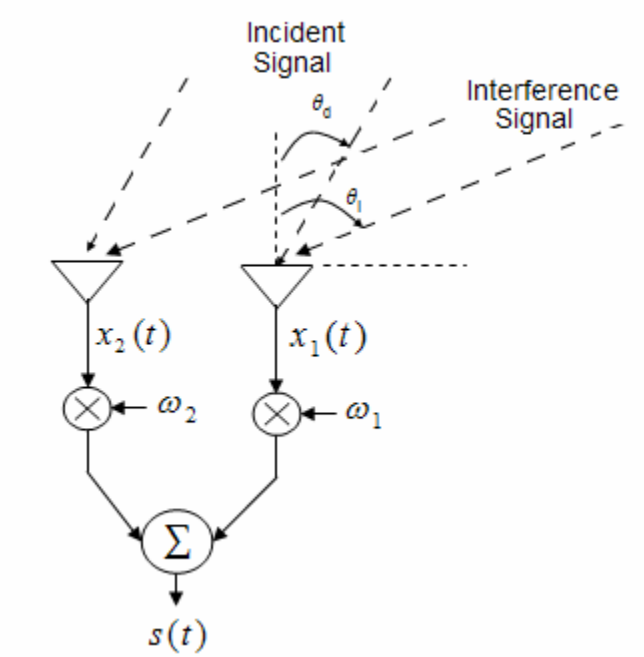

Figure 3.8: A two element array with desired signal and interference signal.

and

$$x_2(t) = d_2(t) + i_2(t) + n_2(t) \tag{3.24}$$

where $d_j(t)$ and $n_j(t)$ are the desired signal and thermal noise components, respectively. For a desired signal, $d_1(t)$ and $d_2(t)$ will be given by

$$d_1 = A_d e^{j\omega_d t} \tag{3.25}$$

and

$$d_2 = A_d e^{j(\omega_d t - \phi_d)}, \tag{3.26}$$

where A_d is the desired signal amplitude and ϕ_d is the interelement phase shift. Since the element spacing is one-half wavelength, ϕ_d is given by

$$\phi_d = \pi \sin\theta_d . \tag{3.27}$$

The interference signals $i_1(t)$ and $i_2(t)$ are assumed to be

$$i_1 = A_i e^{j\omega_d t} \tag{3.28}$$

and

$$i_2 = A_i e^{j(\omega_d t - \phi_i)} \tag{3.29}$$

where A_i is the amplitude, ϕ_i is the interelement phase shift,

$$\phi_i = \pi \sin\theta_i . \tag{3.30}$$

The thermal noises are assumed to be zero-mean random processes, statistically independent of each other and the desired signal, each power σ^2. Thus,

$$E\{n_i^*(t)n_j(t)\} = \sigma^2\delta_{ij}, \tag{3.31}$$

where δ_{ij} is the Kronecker delta,

$$\delta_{ij} = \begin{cases} 1, & i = j \\ 0, & i \neq j, \end{cases} \tag{3.32}$$

and

$$E\{d_i^*(t)n_j(t)\} = 0 . \tag{3.33}$$

Finally we suppose the reference signal is correlated with the desired signal,

$$r(t) = \mathrm{Re}^{j\omega_d t} \tag{3.34}$$

Before proceeding, we note that for the desired signal assumed for d_j and interference signal i_j, the signal power received from each element is A_d^2 and A_i^2 respectively. Furthermore, the noise power on each element is σ^2,

$$E\{n_i^*(t)n_i(t)\} = \sigma^2 \tag{3.35}$$

Thus the input signal-to-noise ratio and interference-to-noise ratio are

$$\xi_d = \frac{A_d^2}{\sigma^2} \tag{3.36}$$

$$\xi_i = \frac{A_i^2}{\sigma^2} \tag{3.37}$$

respectively. The signal vector may be written

$$\mathbf{X} = \mathbf{X}_d + \mathbf{X}_i + \mathbf{X}_n , \tag{3.38}$$

where the desired signal is given by

$$\mathbf{X}_d = \begin{bmatrix} d_1(t) \\ d_2(t) \end{bmatrix} = A_d e^{j\omega_d t} \begin{bmatrix} 1 \\ e^{-j\phi_d} \end{bmatrix} = A_d e^{j\omega_d t}\, \mathbf{U}_d \tag{3.39}$$

and the interference signal given by

$$\mathbf{X}_i = \begin{bmatrix} i_1(t) \\ i_2(t) \end{bmatrix} = A_i e^{j\omega_d t} \begin{bmatrix} 1 \\ e^{-j\phi_i} \end{bmatrix} = A_i e^{j\omega_d t}\ \mathbf{U}_i \tag{3.40}$$

where

$$\mathbf{U}_d = \begin{bmatrix} 1 \\ e^{-j\phi_d} \end{bmatrix} \tag{3.41}$$

and

$$\mathbf{U}_i = \begin{bmatrix} 1 \\ e^{-j\phi_i} \end{bmatrix}. \tag{3.42}$$

Finally we have

$$\mathbf{X}_n = \begin{bmatrix} n_1(t) \\ n_2(t) \end{bmatrix}. \tag{3.43}$$

The covariance matrix, using (3.19), now becomes

$$\mathbf{\Phi} = E\left[\boldsymbol{X}^*(t)\boldsymbol{X}^T(t)\right]$$

$$\mathbf{\Phi} = E(\mathbf{X}_d{}^* \mathbf{X}_d{}^T) + E(\mathbf{X}_i{}^* \mathbf{X}_i{}^T) + E(\mathbf{X}_n{}^* \mathbf{X}_n{}^T). \tag{3.44}$$

We find that

$$E(\mathbf{X}_d{}^* \mathbf{X}_d{}^T) = A_d{}^2\, \mathbf{U}_d{}^* \mathbf{U}_d{}^T = A_d^2 \begin{bmatrix} 1 & e^{-j\phi_d} \\ e^{+j\phi_d} & 1 \end{bmatrix} \tag{3.45}$$

and

$$E(\mathbf{X}_i{}^* \mathbf{X}_i{}^T) = A_i{}^2\, \mathbf{U}_i{}^* \mathbf{U}_i{}^T = A_i^2 \begin{bmatrix} 1 & e^{-j\phi_i} \\ e^{+j\phi_i} & 1 \end{bmatrix} \tag{3.46}$$

and

$$E(\mathbf{X}_n{}^* \mathbf{X}_n{}^T) = \sigma^2\, \mathbf{I} = \begin{bmatrix} \sigma^2 & 0 \\ 0 & \sigma^2 \end{bmatrix} \tag{3.47}$$

Where $\mathbf{I}$ is the identity matrix. Therefore $\mathbf{\Phi}$ is

$$\mathbf{\Phi} = A_d^2\ \mathbf{U}_d{}^* \mathbf{U}_d{}^T + A_i^2\ \mathbf{U}_i{}^* \mathbf{U}_i{}^T + \sigma^2\, \mathbf{I}. \tag{3.48}$$

And the correlation vector is

$$\begin{aligned} \boldsymbol{S} &= E\left[\boldsymbol{X}_d^{*}(t)\boldsymbol{R}(t)\right] \\ \boldsymbol{S} &= E\left[A_d e^{-j\omega_d t}\,\mathrm{Re}^{j\omega_d t}\right] \\ \boldsymbol{S} &= A_d{}^2 U_d^{*} \qquad for \quad A_d = R \end{aligned} \tag{3.49}$$

Setting $\sigma^2 = 0.001$, $SNR = 30dB$, $\theta_d = 0^{\mathrm{O}}$, $\theta_i = -60^{\mathrm{O}}$, $f = 5Ghz$ and a separation distance between elements of $d = \lambda/2$, we can obtain the weight vector using (3.22) as

$$\boldsymbol{W} = \begin{bmatrix} 0.7067 + 0.1509\mathrm{i} \\ 0.7067 - 0.1509\mathrm{i} \end{bmatrix}$$

Here we define radiation pattern using (3.2) and (3.3), as

$$G(\theta) = \left| \sum_{k=0}^{M-1} w_{kopt} \exp\left(j \frac{2\pi k d}{\lambda} \sin\theta \right) \right| \tag{3.50}$$

$$G_{dBi}(\theta) = 10\log\left(\left(G(\theta) \frac{2\pi Max[G]}{\int_0^{2\pi} G(\phi)\, d\phi} \right)^2 \right) \tag{3.51}$$

where M is the number of elements, and varying θ in the interval $[-90,90]$ degrees, as shown in the Figure 3.9.

3.3.2 Maximum Signal-to-Interference Ratio

The weights can be chosen to directly maximize the signal-to-interference ratio (SIR) [13]. Assuming that $\boldsymbol{R}_s = E\{\boldsymbol{s}\boldsymbol{s}^H\}$ and $\boldsymbol{R}_u = E\{\boldsymbol{u}\boldsymbol{u}^H\}$ are known, we may choose to maximize the ratio of the output signal power σ^2_s and the total interfering signal power σ^2_u. The total output signal power may be written as

$$\sigma_s^2 = E\left\{ \left| \boldsymbol{w}^H \boldsymbol{s} \right|^2 \right\} = \boldsymbol{w}^H \boldsymbol{R}_s \boldsymbol{w} \tag{3.52}$$

and the output noise power is

$$\sigma_u^2 = E\left\{ \left| \boldsymbol{w}^H \boldsymbol{u} \right|^2 \right\} = \boldsymbol{w}^H \boldsymbol{R}_u \boldsymbol{w} \tag{3.53}$$

Therefore, the (SIR) is given as

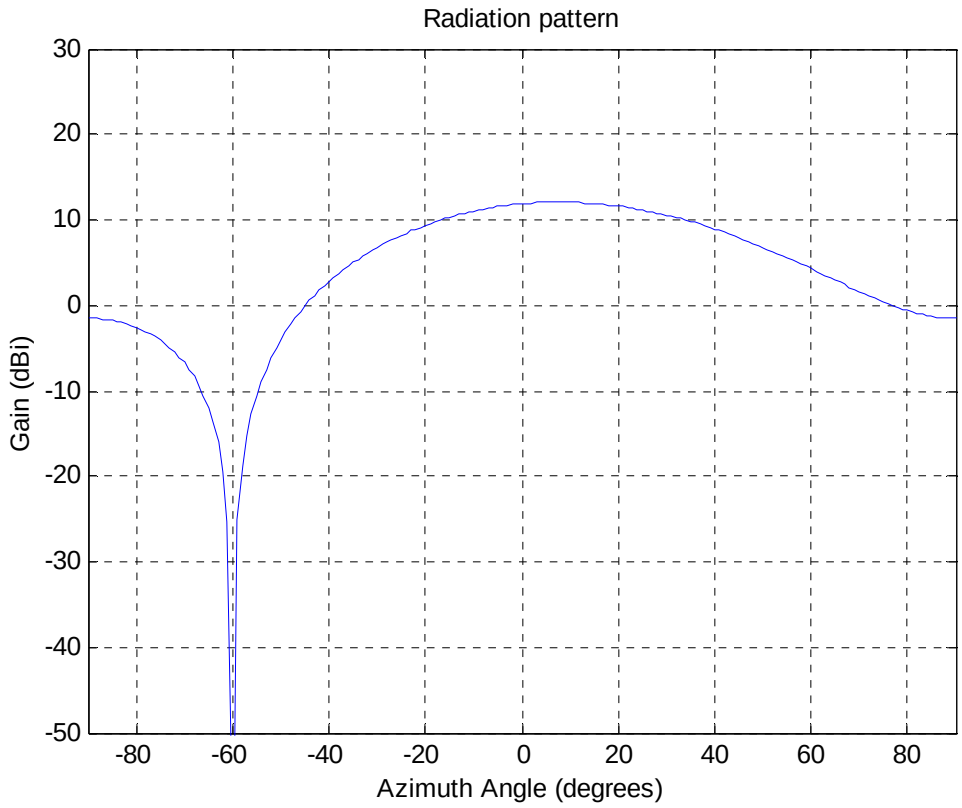

Figure 3.9: Radiation pattern for a two-element array, $\theta_d = 0^{\mathrm{O}}$ and $\theta_i = -60^{\mathrm{O}}$.

$$\mathrm{SIR} = \frac{\sigma_s^2}{\sigma_u^2} = \frac{\boldsymbol{w}^H \boldsymbol{R}_s \boldsymbol{w}}{\boldsymbol{w}^H \boldsymbol{R}_u \boldsymbol{w}} \tag{3.54}$$

Taking the derivative of (3.54) with respect to $\boldsymbol{w}$ and setting it to zero, we obtain

$$\boldsymbol{R}_s \boldsymbol{w} = \frac{\boldsymbol{w}^H \boldsymbol{R}_s \boldsymbol{w}}{\boldsymbol{w}^H \boldsymbol{R}_u \boldsymbol{w}} \boldsymbol{R}_u \boldsymbol{w} \tag{3.55}$$

which appears to be a joint eigenproblem. The value $\frac{\boldsymbol{w}^H \boldsymbol{R}_s \boldsymbol{w}}{\boldsymbol{w}^H \boldsymbol{R}_u \boldsymbol{w}}$ is bounded by the minimum and maximum eigenvalues of the symmetric matrix $\boldsymbol{R}_s^{-1} \boldsymbol{R}_u$. The maximum eigenvalue $\lambda_{\max}$ satisfying

$$\boldsymbol{R}_u^{-1} \boldsymbol{R}_s \boldsymbol{w} = \lambda_{\max} \boldsymbol{w} \tag{3.56}$$

is the optimum value of (SIR); (i.e., SIR = $\lambda_{\max}$). Corresponding to this value, there is a unique eigenvector, $\boldsymbol{w}_{\mathrm{opt}}$, which represents the optimum weights. Therefore,

$$\boldsymbol{R}_s \boldsymbol{w}_{opt} = \text{SIR}\ \boldsymbol{R}_u \boldsymbol{w}_{opt} \tag{3.57}$$

Noting that $\boldsymbol{R}_s = E\{d^2(t)\}\boldsymbol{v}\boldsymbol{v}^H$, we obtain

$$\boldsymbol{w}_{opt} = \beta \boldsymbol{R}_u^{-1} \boldsymbol{v} \tag{3.58}$$

where

$$\beta = \frac{E\{d^2(t)\}}{\text{SIR}} \boldsymbol{v}^H \boldsymbol{w}_{opt} \tag{3.59}$$

That is, the maximum (SIR) criterion can also be expressed in terms of the Wiener solution.

3.3.3 Minimum Variance

If the desired signal and its direction are both unknown, one way of ensuring a good signal reception is to minimize the output noise variance [13]. Recall that the beamformer output is

$$\begin{aligned} y(t) &= \boldsymbol{w}^H \boldsymbol{x} \\ &= \boldsymbol{w}^H \boldsymbol{s} + \boldsymbol{w}^H \boldsymbol{u} \end{aligned} \tag{3.60}$$

To ensure that the desired signal is passed with a specific gain and phase, a constraint may be used so that the response of the beamformer to the desired signal is

$$\boldsymbol{w}^H \boldsymbol{v} = g \tag{3.61}$$

Minimization of contributions to the output due to interference is accomplished by choosing the weights to minimize the variance of the output power

$$\begin{aligned} Var\{y\} &= \boldsymbol{w}^H \boldsymbol{R} \boldsymbol{w} \\ &= \boldsymbol{w}^H \boldsymbol{R}_s \boldsymbol{w} + \boldsymbol{w}^H \boldsymbol{R}_u \boldsymbol{w} \end{aligned} \tag{3.62}$$

subject to the constraint defined in (3.61). This is equivalent to minimizing the quantity $\boldsymbol{w}^H \boldsymbol{R}_u \boldsymbol{w}$. Using the method of Lagrange, we have

$$\nabla \boldsymbol{w} \left(\frac{1}{2} \boldsymbol{w}^H \boldsymbol{R}_u \boldsymbol{w} + \beta[1 - \boldsymbol{w}^H \boldsymbol{v}]\right) = \boldsymbol{R}_u \boldsymbol{w} - \beta \boldsymbol{v} \tag{3.63}$$

so that

$$\boldsymbol{w}_{opt} = \beta \boldsymbol{R}_u^{-1} \boldsymbol{v} \tag{3.64}$$

where

$$\beta = \frac{g}{\boldsymbol{v}^H \boldsymbol{R}_u^{-1} \boldsymbol{v}} \tag{3.65}$$

That is, solution (3.64), which is derived from the minimum variance criterion, is also the Wiener solution. If $g = 1$, the response of the beamformer is often termed the minimum variance distortionless response (MVDR) beamformer.

3.4 Algorithms for Adaptive Beamforming

We have shown in the previous section different optimum criteria. The choice of a particular criterion is not critically important in terms of performance. On the other hand, the choice of adaptive algorithms for deriving the adaptive weights is highly important in that it determines both the speed of convergence and hardware complexity required to implement the algorithm.

The most common adaptive algorithm for continuous adaptation is the least-mean-square (LMS) algorithm, which is based on the steepest-descent method, that recursively computes and updates the weight vector. Continuous adaptation works well when statistic related to the signal environment are stationary. The primary virtue of the LMS algorithm is its simplicity; however, the disadvantage of this method is that convergence can be slow compared with other algorithms [19].

One way to speed up the convergence rate is to employ the direct inversion of the covariance matrix $\boldsymbol{\Phi}$ in (3.22) [20]. Although the direct matrix inversion (DMI) algorithm converges more rapidly that the LMS algorithm, the practical difficulties that are associated with the DMI algorithm are two: the increase of computational complexity, which cannot be easy overcome, and the numerical stability resulting form the use of finite-precision arithmetic and the requirements of inverting large matrixes.

Recursive algorithms [22] perform recursive, rather that direct, approximate computations of the inverse of the input correlation matrix. Recursive algorithms allow to continue update the weight vector, whereas sample-matrix inversion requires the accumulation of n samples of the input vector. Its computational complexity varies also with the square of the number of elements, the same as for the DMI algorithm. Thus the recursive least-square algorithm and DMI algorithms do not differ greatly in computational complexity when the number of weights is large. However, the recursive algorithm avoids the numerical problems of matrix inversion, provides an update weight vector at every sample time and accommodates data weighting.

A different technique than recursively algorithms, is the use of Neural Networks as in [23]. Here the disadvantage is the time spent while training the neural network with the training patterns. Once the network is trained, the time response of the network is relatively short.

3.5 Antenna Arrays

In many applications of antennas, point-to-point communications is of interest [13]. Antennas with enormous directivity are needed for achieving high efficiency, and array antennas are used in order to satisfy this need. The term array, as applied to antennas,

means an assembly of radiating elements in an electrical and geometric arrangement of such a nature that the radiation from these elements adds up to a maximum field intensity in a particular direction or directions and cancels or very nearly cancels others. In the next section we shall see two basic arrays: the linear array and the circular array.

3.5.1 Linear Array

Consider an *N*-element linear array as shown in the Figure 3.10 [21]. Smart antennas use an array of low gain antenna elements which are connected by a combining network [3]. If a plane wave impinges upon the array at an angle θ with respect to the array normal, the wavefront arrives at element 1 sooner than at element 2, since the differential distance along the two ray path is $d\sin\theta$. Here θ is the azimuthal angle and ϕ is the elevation angle of the plane wave incident on the array. For simplicity, we consider $\phi = \pi/2$ represented as the horizon (not shown in the Figure 3.10).

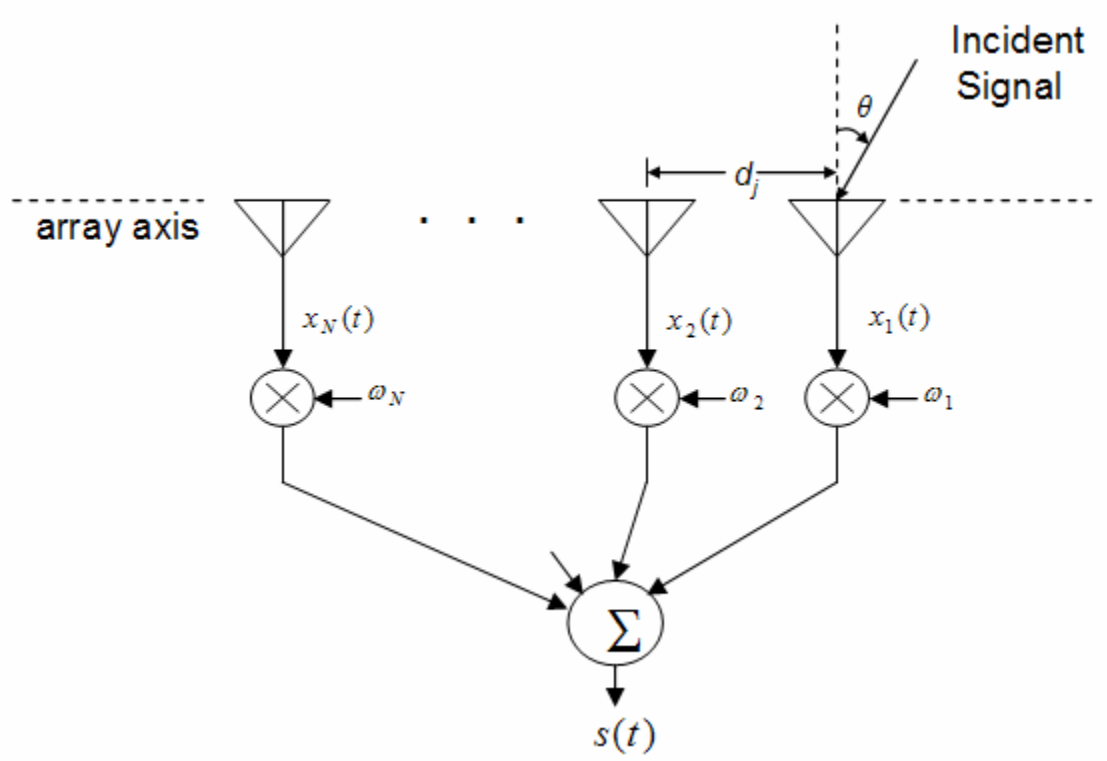

Figure 3.10: An *N*-element linear array.

To simplify the analysis of antenna arrays, we make the following assumptions:

- The spacing between array elements is small enough that there is no amplitude variation between the signals received at different elements.

- There is no mutual coupling between elements.

- All incident fields can be decomposed into a discrete number of plane waves.

That is, there are a finite number of signals.

- The bandwidth of the signal incident on the array is small compared with the carrier frequency.

- The pattern of each element $f_j(\theta) = 1$, ideally for isotropic elements.

- The incoming signal is at frequency ω_0, **X** is given by

$$\mathbf{X} = Ae^{j\omega_0 t}\mathbf{U} \tag{3.66}$$

Where A is the amplitude, $e^{j\omega_0 t}$ is its time dependency, and **U** is a vector containing the interelement phase shifts and the element patterns,

$$\mathbf{U} = [f_1(\theta), f_2(\theta)e^{-j\phi_2(\theta)}, f_3(\theta)e^{-j\phi_3(\theta)}, \cdots, f_N(\theta)e^{-j\phi_N(\theta)}]^T \tag{3.67}$$

with

$$\phi_j = \frac{2\pi}{\lambda}\left[\sum_{k=1}^{j-1} d_k\right]\sin\theta, \qquad j \geq 2. \tag{3.68}$$

For a plane wave incident on the array from the direction (θ), the difference in phase between the signal component incident on adjacent array elements, as shown in Figure 3.11, is:

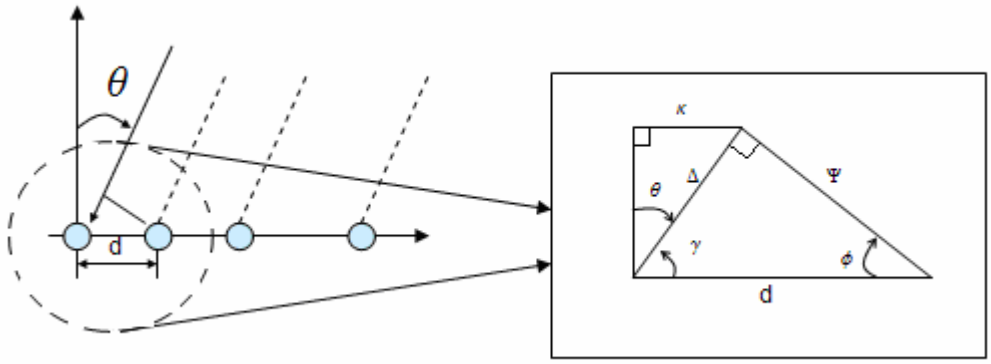

Figure 3.11: The difference in phase between signal adjacent elements.

If

$$\theta + \gamma = \pi/2$$
$$\gamma = \pi/2 - \theta \tag{3.69}$$

Then

$$\pi = \gamma + \phi + \pi/2 \tag{3.70}$$

Substituting (3.69) in (3.70) we have:

$$\begin{aligned} \pi &= \pi/2 - \theta + \phi + \pi/2 \\ \pi &= \pi - \theta + \phi \\ \phi &= \theta \end{aligned} \tag{3.71}$$

Now, with (3.71), we have the delay as:

$$\begin{aligned} \sin\phi &= \frac{\Delta}{d} \\ \Delta &= d\sin\phi \\ \therefore \quad \Delta &= d\sin\theta \end{aligned} \tag{3.72}$$

where Δ is the distance that the signal must be delayed to arrive at the element 2 after it arrives at the element 1. The delay is:

$$\tau = \frac{d\sin\theta}{c} \tag{3.73}$$

where d is the separation distance between adjacent elements of the linear array, and c is the speed of the light, $3\times10^8\ m/s$. By setting the phase of the signal at the origin arbitrarily to zero, the phase lead of the signal at element j relative to that at element 0 is:

$$\phi_j = j\frac{2\pi}{\lambda}d\sin\theta \tag{3.74}$$

where $\lambda = c/f$, and f is the carrier frequency in Hz.

Lets set the $\sigma^2 = 0.001$, $SNR = 30dB$, $f = 5Ghz$, a separation distance between elements of $d = \lambda/2$ and the number of elements to 8, and lets vary θ_d and θ_i in the interval $[-90,90]$ degrees for the equations (3.50) and (3.51). Some results are shown in the next figures:

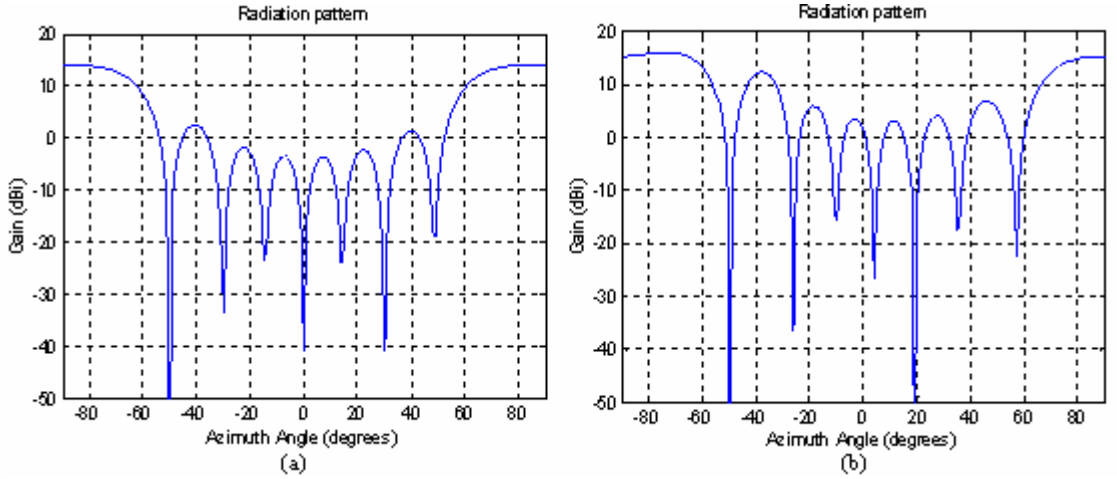

Figure 3.12: 8-element linear array radiation pattern. (a) A user in $\theta_d = -90^{\mathrm{O}}$ and an interferer in $\theta_i = -50^{\mathrm{O}}$. (b) A user in $\theta_d = -60^{\mathrm{O}}$ and an interferer in $\theta_i = -50^{\mathrm{O}}$.

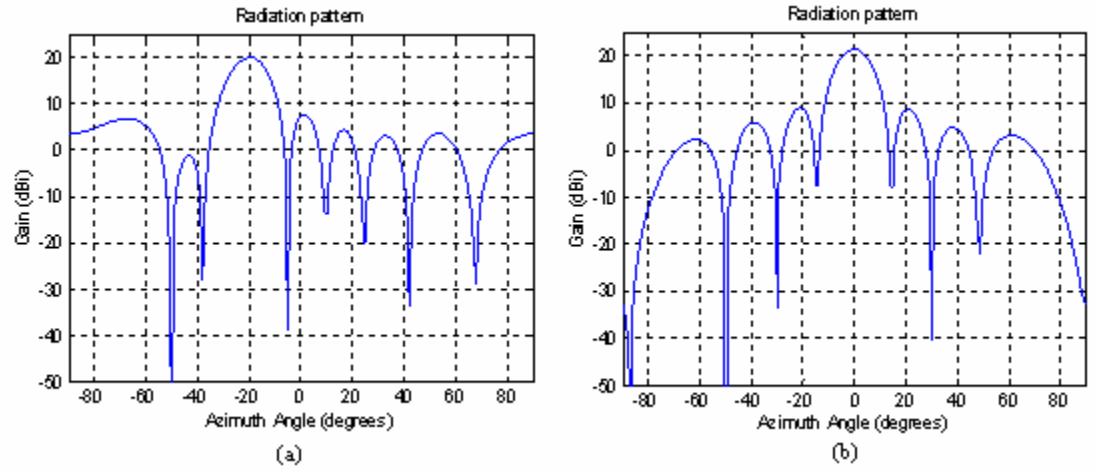

Figure 3.13: 8-element linear array radiation pattern. (a) A user in $\theta_d = -20^{\mathrm{O}}$ and an interferer in $\theta_i = -50^{\mathrm{O}}$. (b) A user in $\theta_d = 0^{\mathrm{O}}$ and an interferer in $\theta_i = -50^{\mathrm{O}}$.

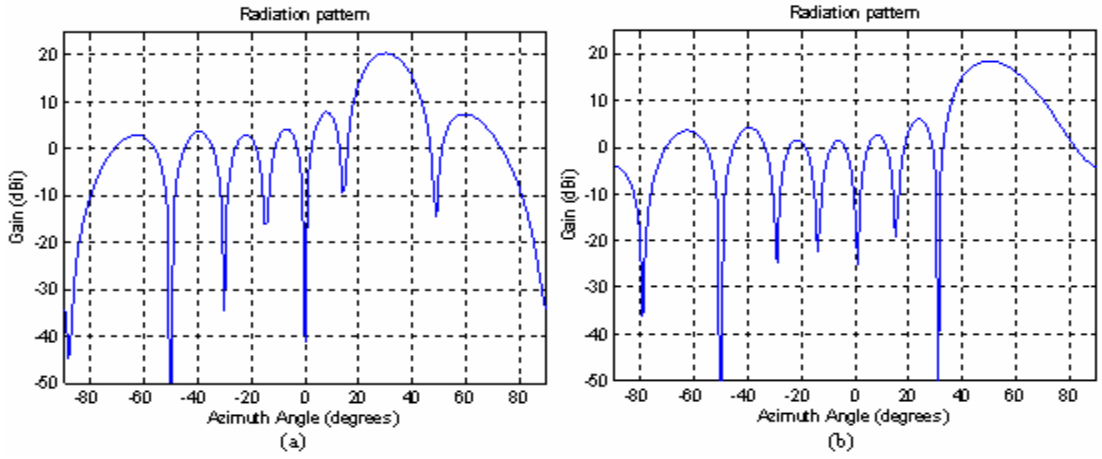

Figure 3.14: 8-element linear array radiation pattern. (a) A user in $\theta_d = 30^{\mathrm{O}}$ and an interferer in $\theta_i = -50^{\mathrm{O}}$. (b) A user in $\theta_d = 50^{\mathrm{O}}$ and an interferer in $\theta_i = -50^{\mathrm{O}}$.

We note that a larger gain in one direction necessarily results in a reduced gain in some other direction. Intuitively, one can think of an adaptive array's pattern as a ball of dough around the antenna. The volume of the ball represents the total power. Replacing this with an adaptive array causes the dough to be "squished" around so that some directions are pulled out (gain higher than 0 dBi) and some are pushed in (gain lower than 0 dBi). But since the power emanating is the same (you only have so much dough), the lobes have to balance each other out, that is, preserve the law of conservation of power [14].

When the distance separation between adjacent elements in the linear array is greatest than $d = \lambda/2$ several main lobes will be formed in visible space on each side of the array plane. The extra main lobes formed with large element spacing are referred to as grating lobes, as shown in the Figure 3.15.

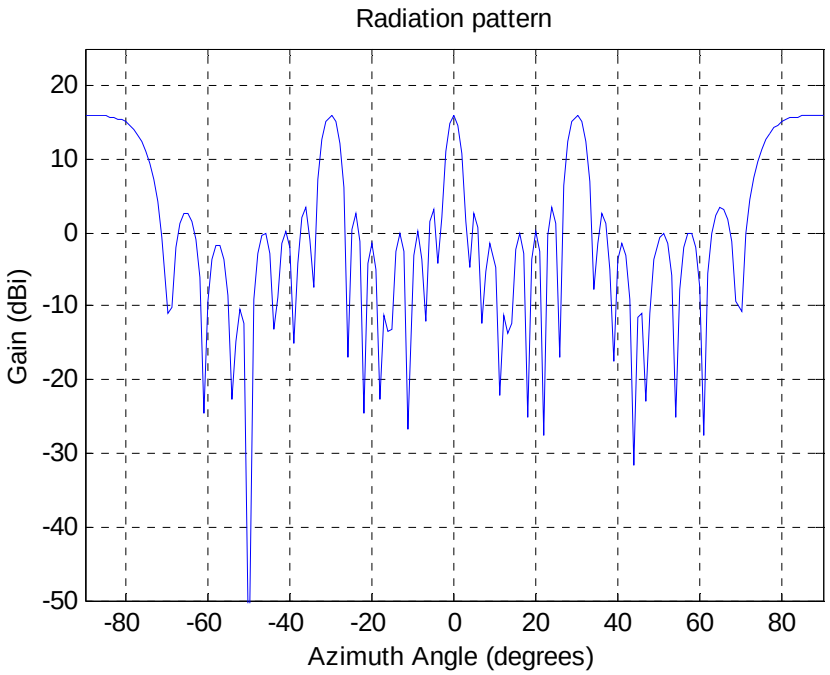

Figure 3.15: Grating lobes radiation pattern for an 8-element linear array. $\theta_d = 0^{\mathrm{O}}$ and $d = 2\lambda$.

The response of an adaptive array pattern to interfering signals depends on the number of interfering signals in relation to the number of degrees of freedom in the array. An *N*-element array has *N*-1 degrees of freedom in its pattern. One degree of freedom is needed to form a pattern maximum on the desired signal. The remaining *N*-2 degrees are available to null interference signals. If *N*-2 or fewer interference signals are incident on the array, the array does not normally null the individual interference signals but instead forms a compromise pattern that minimizes the total interference power at the array output [21]. Then, the main idea of smart antenna concept is steering a high-gain main lobe in the direction of the desired user while placing deep nulls in the direction of the stronger interferers. The number of lobes and nulls an antenna can place in a specific direction is equal to the number of elements minus one.

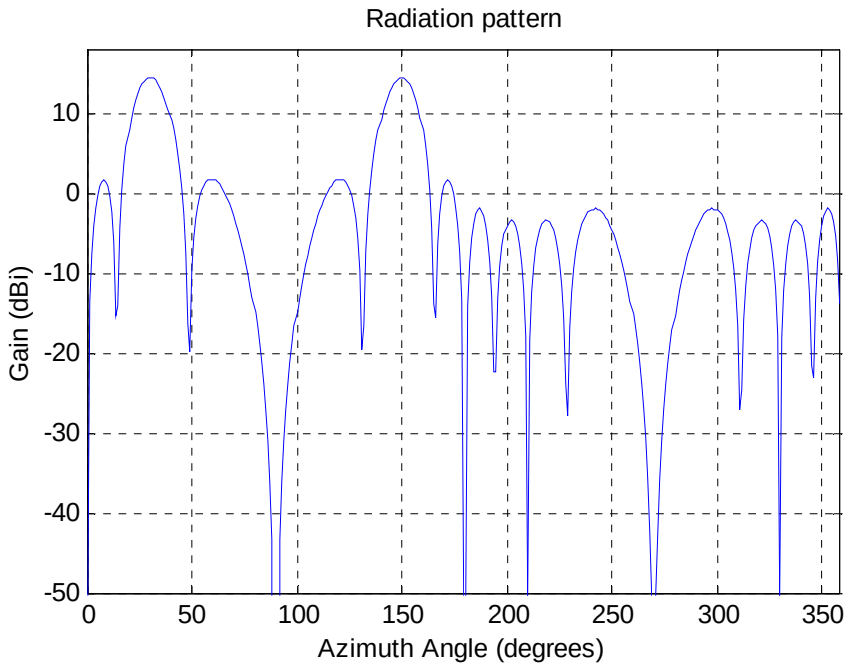

Figure 3.16: Mirror lobe effect in an 8-element linear array. $\theta_d = 30^O$ and $\theta_{mirror} = 150^O$.

The radiation pattern presented here for a linear array is just for 180^O, because the entire radiation pattern (from 0^O to 360^O) looks like a mirror for the next 180^O. This effect is shown in the Figure 3.16 and Figure 3.17, where the linear array acts instead of a mirror along the axis of the linear array.

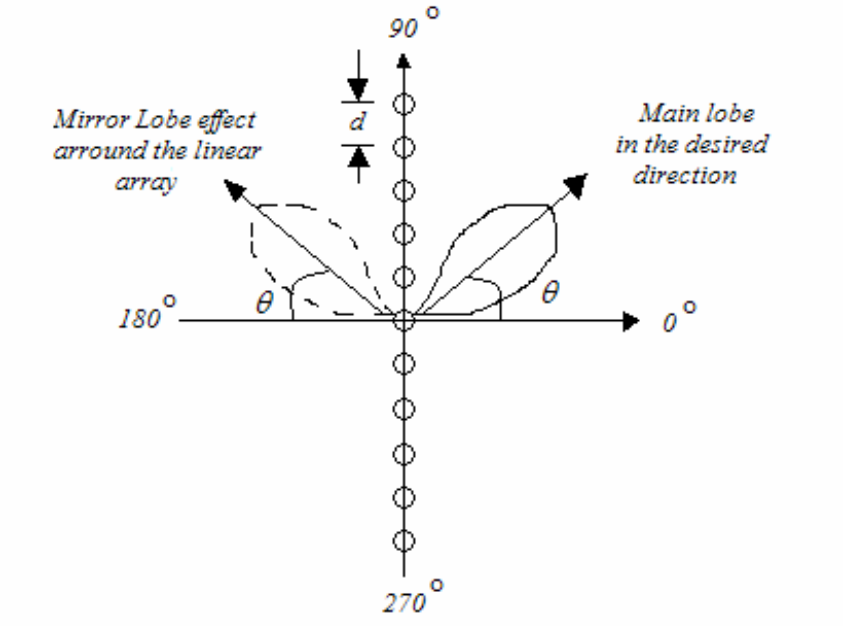

Figure 3.17: Mirror lobe effect in a linear array.

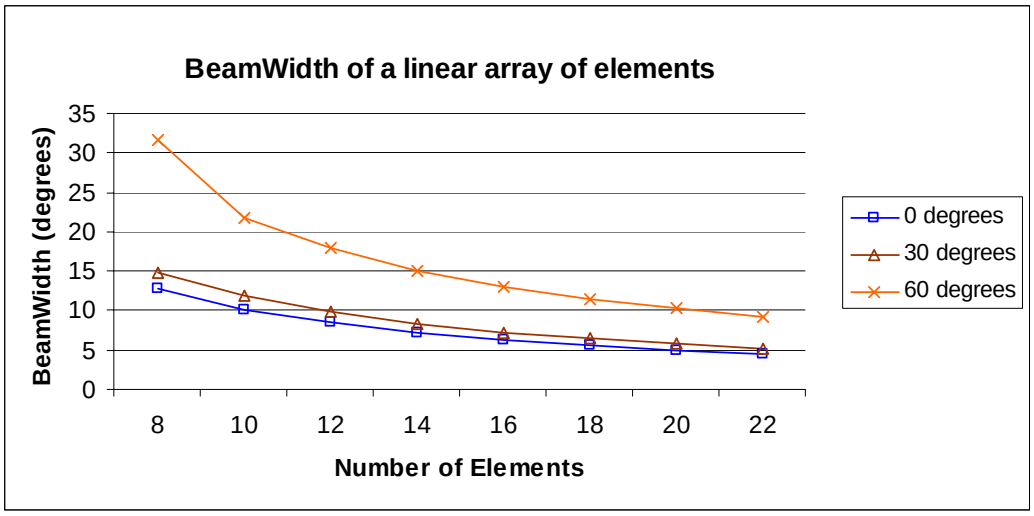

Figure 3.18: Beamwidth behavior of a linear array.

If we point the main lobe toward a desired direction (0, 30 and 60 degrees in this example) and vary the number of elements of the linear array, we will see the beamwidth behavior as shown in the Figure 3.18. The beamwidth, as defined in section 3.1, is the angular width of the main lobe, measured between the points on the main lobe that are 3-dBi below the peak of the main lobe, as shown in the Figure 3.19. With the results shown in the Figure 3.18, we can see that the beamwidth is minimum when the direction of the main lobe is pointed toward the 0^{O} direction (or 180^{O} due to the mirror lobe effect), this is because in the 0^{O} direction, the wavefront signal arrives at the same time to every element of the linear array, as shown in the Figures 3.10 and 3.11. On the counterpart, the bigger beamwidth that we can obtain is when the main lobe is pointed toward the 90^{O} or 270^{O} direction.

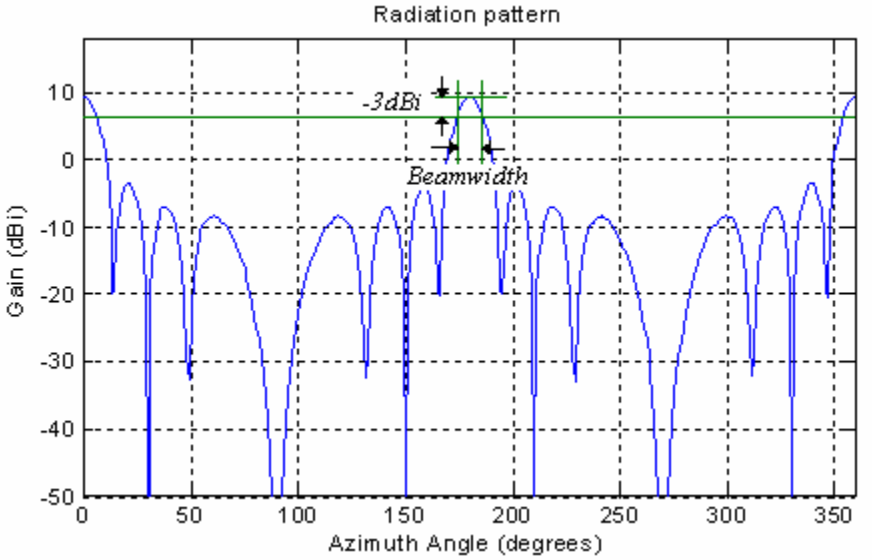

Figure 3.19: Beamwidth on a linear array.

3.5.2 Circular Array

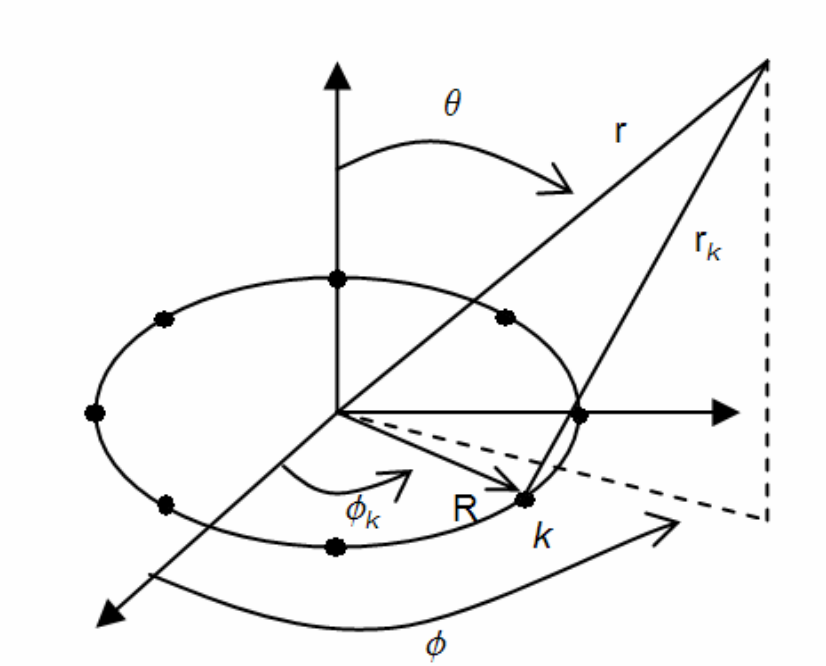

Figure 3.20: A circular array with equally spaced *K* elements.

A circular array [13] consisting of *M* identical elements evenly spaced in a circle of radius *R* is shown in the Figure 3.20. Since the *M* elements are equally spaced around the circle of radius *R*, the azimuth angle of the k^{th} element is given as $\phi_k = k\frac{2\pi}{M}$. If a plane wave impinges upon the array in the direction of (θ,ϕ), as shown in the coordinate system of the Figure 3.21, (where the horizon is represented with $\theta = \pi/2$), the relative phase at the k^{th} element with respect to the center of the array is given by

$$\gamma = \phi - \phi_k$$
$$A = R\cos\gamma$$

and the delay respect to the center of the circle is

$$\tau = \frac{d}{c} = -\frac{R\cos(\phi - \phi_k)}{c} \tag{3.75}$$

the phase lead of the signal at element k relative to that at element center is

$$\psi_k = -\frac{2\pi}{\lambda} R\cos(\phi - \phi_k) \tag{3.76}$$

where $\lambda = c/f$, c the speed of light, $3x10^8\ m/s$ and f is the carrier frequency in Hz. Now the spacing between adjacent elements is given by

$$d = R\sqrt{\sin^2\phi_k + (1-\cos\phi_k)^2}\ . \qquad (3.77)$$

One of the inherent characteristics of a circular array is the presence of high sidelobe levels. For a circular array with equally spaced elements and uniform weighting, the lowest achievable peak sidelobe level is about 8 *dBi* with respect to the main lobe [13].

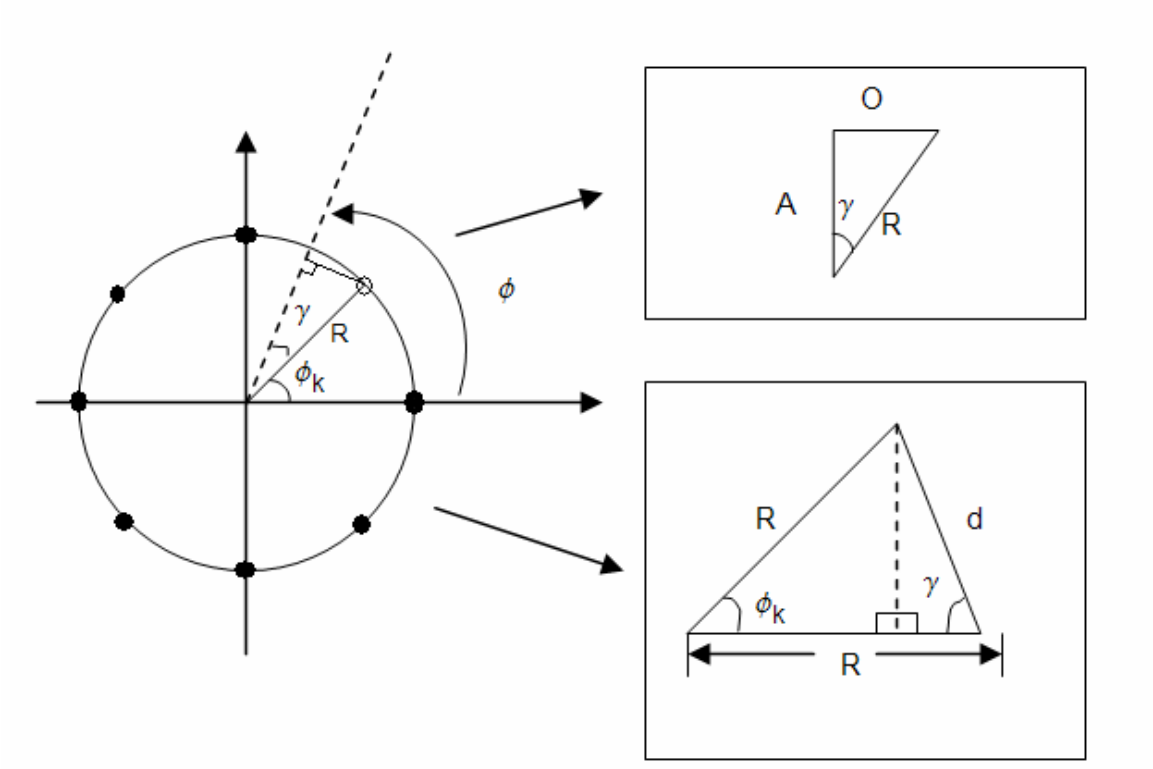

Figure 3.21: A circular array with equally spaced K elements with $\theta = \pi/2$.

Lets set the $\sigma^2 = 0.001$, $SNR = 30dB$, $f = 5Ghz$, a radius of $R = 3\lambda$ and the number of elements to 10, and lets vary θ_d in the interval $[0,360]$ degrees in the equations (3.50) and (3.51). Some results are shown in the next figures:

(a)

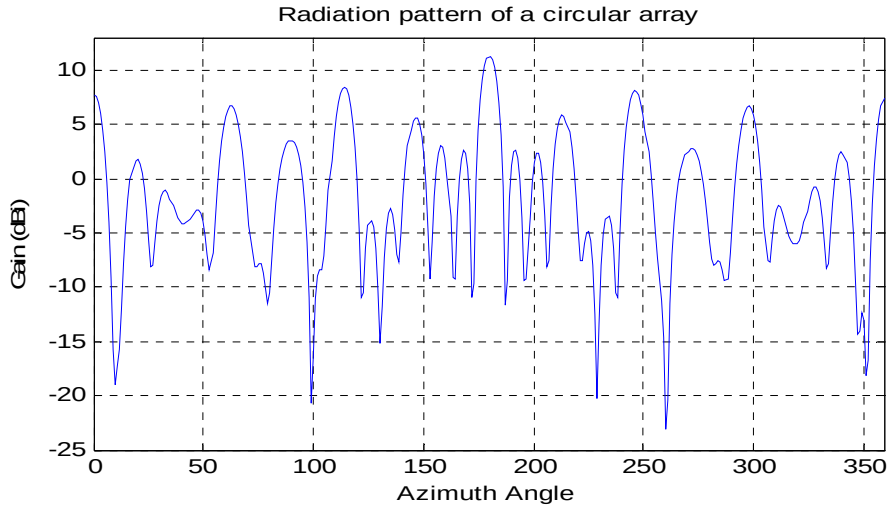

(b)

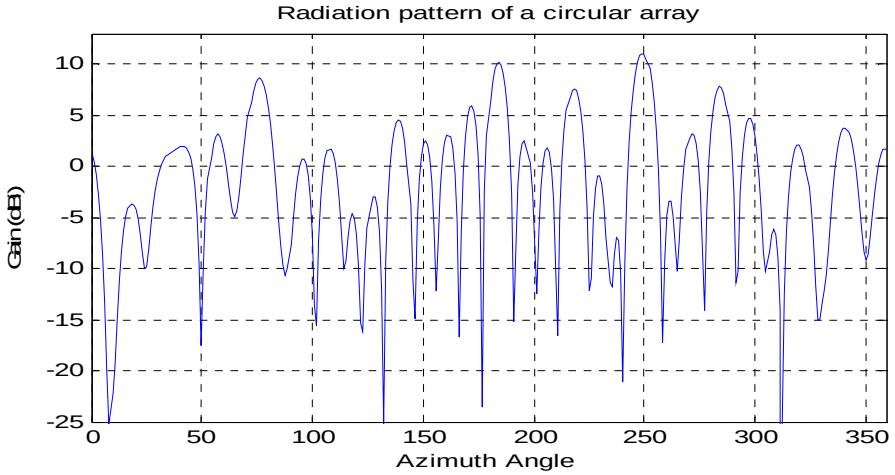

(c)

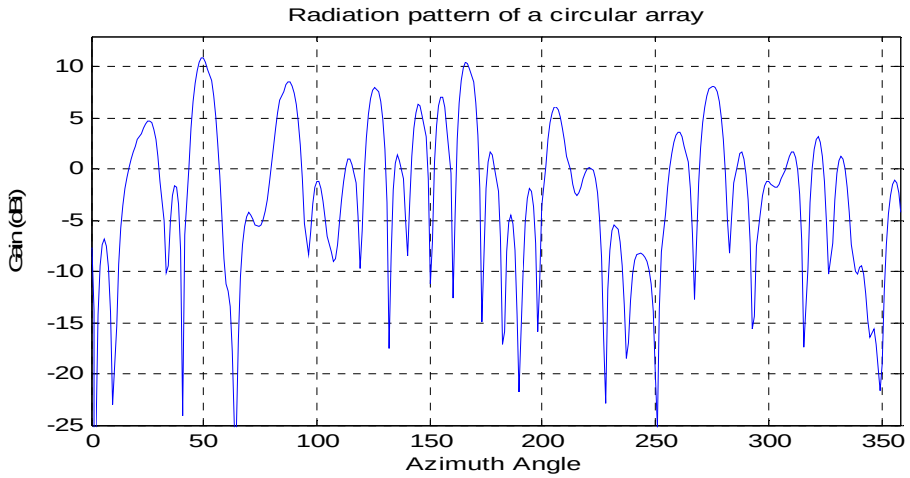

Figure 3.22: 10-element circular array radiation pattern. (a) A user in $\theta_d = 180^{\mathrm{O}}$ and an interferer in $\theta_i = 10^{\mathrm{O}}$; (b) A user in $\theta_d = 250^{\mathrm{O}}$ and an interferer in $\theta_i = 10^{\mathrm{O}}$; (c) A user in $\theta_d = 50^{\mathrm{O}}$ and an interferer in $\theta_i = 10^{\mathrm{O}}$.

3.5.3 Linear Array versus Circular Array

Due to the d = $\lambda/2$ constrain in the linear array, where we can increase the number of elements and the size of the array will increase too, is difficult to increase the number of elements to get more accuracy in the radiation pattern without increasing the size of the linear array. For a f_c=*5Ghz*, and varying the number of elements of a linear array, we can see how the size increase too, as shown in the Figure 3.23.

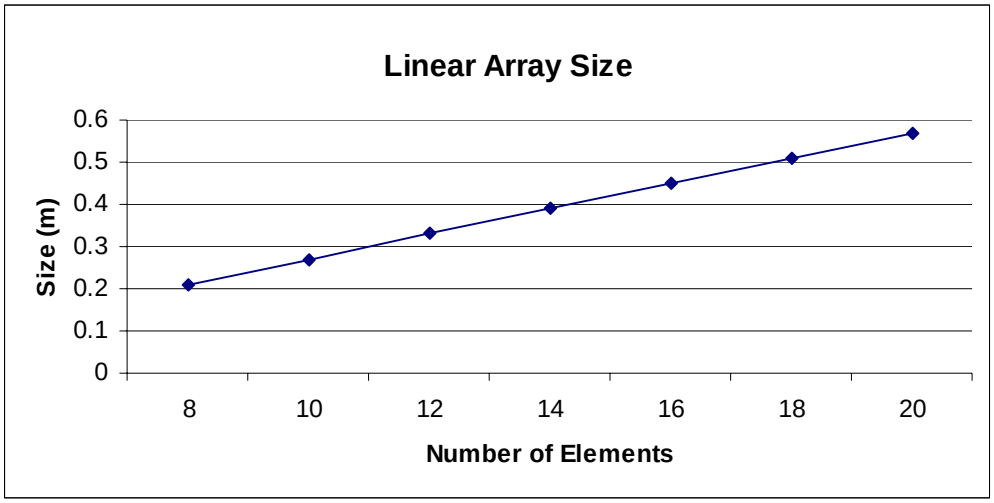

Figure 3.23: Linear array size (m) for different number of elements.

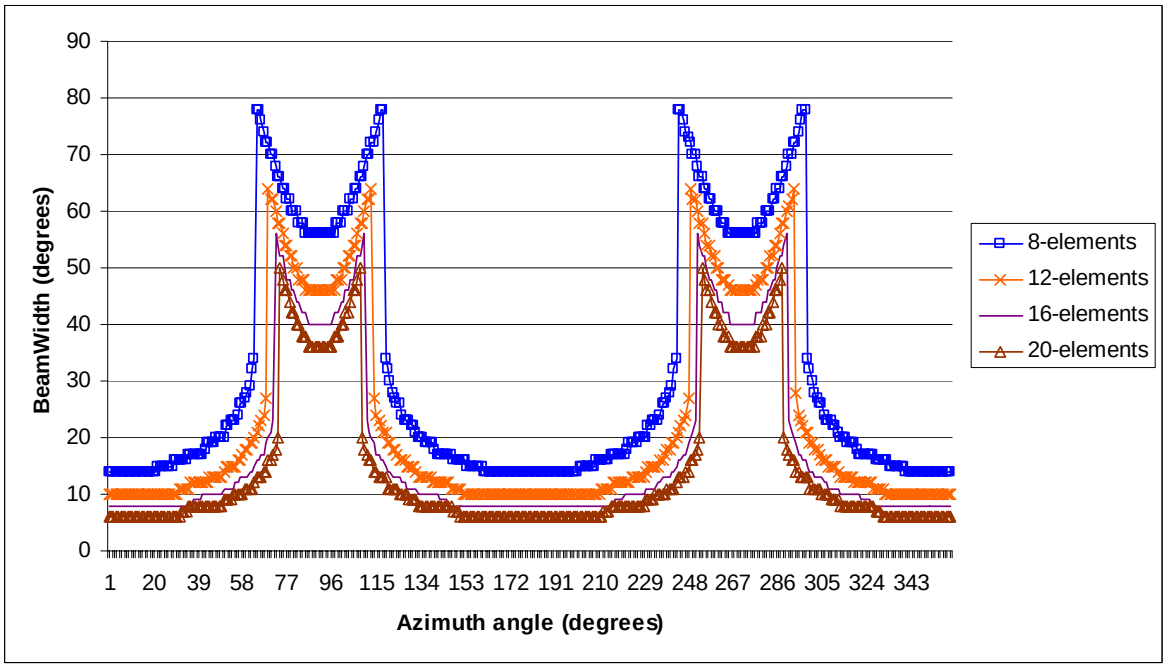

Figure 3.24: Linear array beamwidth for the entire circumference (360^{O}), for the main lobe.

As shown in the Figure 3.18 and the section 3.5.1, the beamwidth of a linear array is varying when we point the main lobe toward different angles. The number of element of the linear array can be varied too. The result is shown in the Figure 3.24. As seen before, the minimum beamwidth for each linear array size, is when the main lobe is pointed toward the 0° or 180° directions.

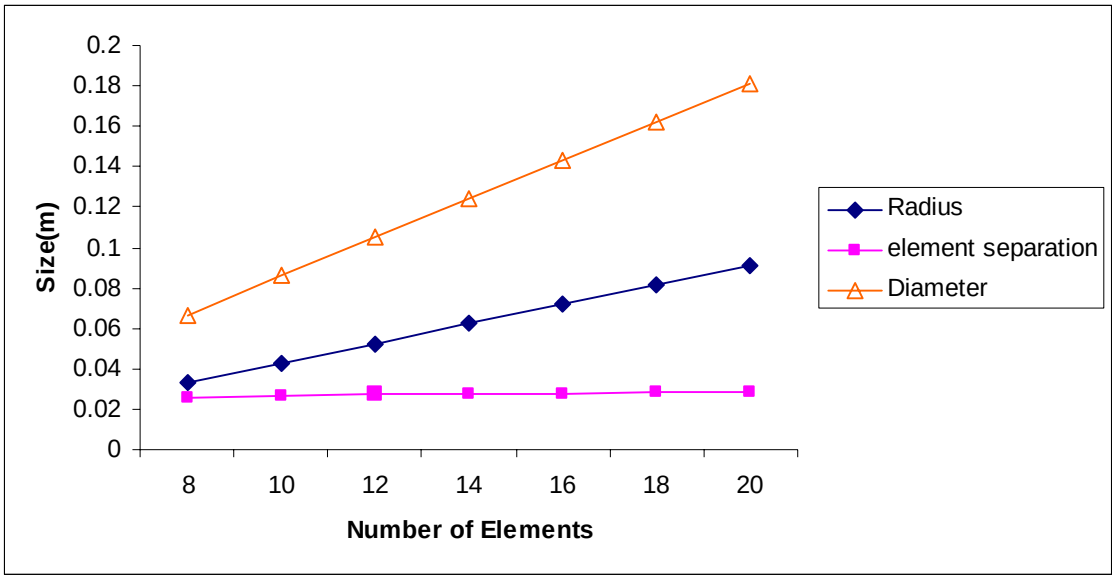

Figure 3.25: Circular array size (m) for different number of elements.

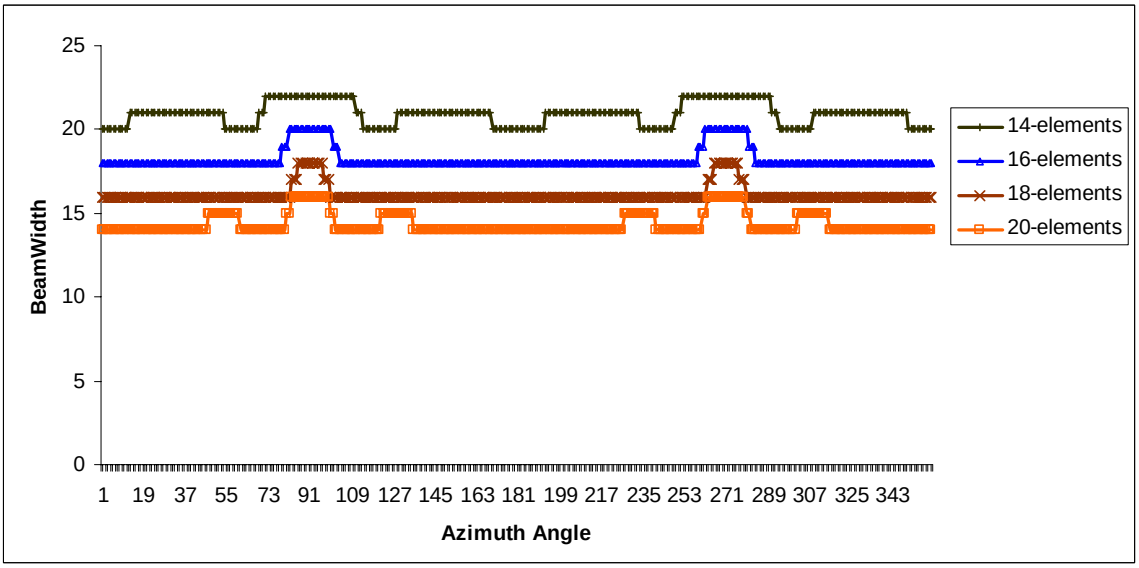

Figure 3.26: Circular array beamwidth for the entire circumference (360^{O}), for the main lobe.

In the Figure 3.25 is shown how can be varied the size of the physical dimension of the circular array, varying the radius of this array. Here we show another parameter of interest, the separation between elements d in the equation (3.77). The resulting beamwidth variation for the arrays of the Figure 3.25, is shown in the Figure 3.26. Here we can see that the maximum beamwidth is reached in the 90° and 270° directions.

In the circular array, we let fix radius of the circle and the number of elements can be varied. Then, if we point toward 90° the main lobe, we will see how the beamwidth reaches a minimum after a threshold in the number of elements is reached. This behavior is shown in the Figure 3.27. This array has a diameter of $D = 0.1814$ meters.

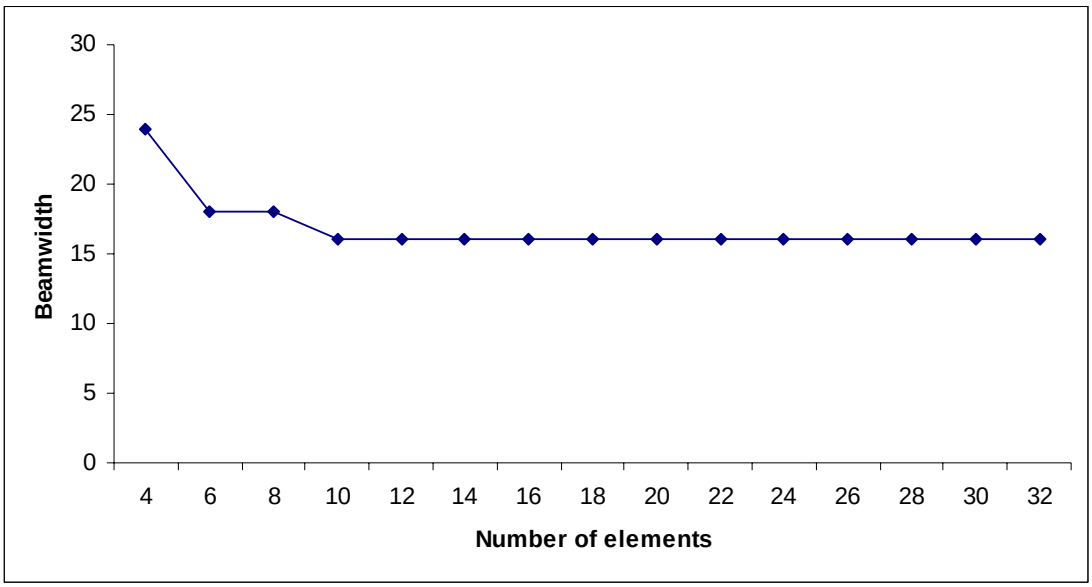

Figure 3.27: Circular array beamwidth.

If we carry out a comparison between the linear array and the circular array, it may be used the number of elements, the size of the array, or the beamwidth of the main lobe. Also, it may be used the radiation pattern to see which one of they two is causing more Not Desired Radiation Pattern (NDRP) than the other one, considering that the array causing less NDRP is the best.

A linear array radiation pattern is shown in the Figure 3.28, and we define the NDRP levels as:

- **High level**. This Not Desired Radiation Pattern (NDRP) is due to the mirror effect of the main lobe. Is the highest NDRP level, because is about the same gain of the main lobe. Is obtained with the average over the beamwidth of the mirror effect lobe.

- **Low level**. This NDRP is due to the side lobes of the radiation pattern that neither belongs to the main lobe nor the mirror effect lobe. This NDRP level is the average about all the side lobes.

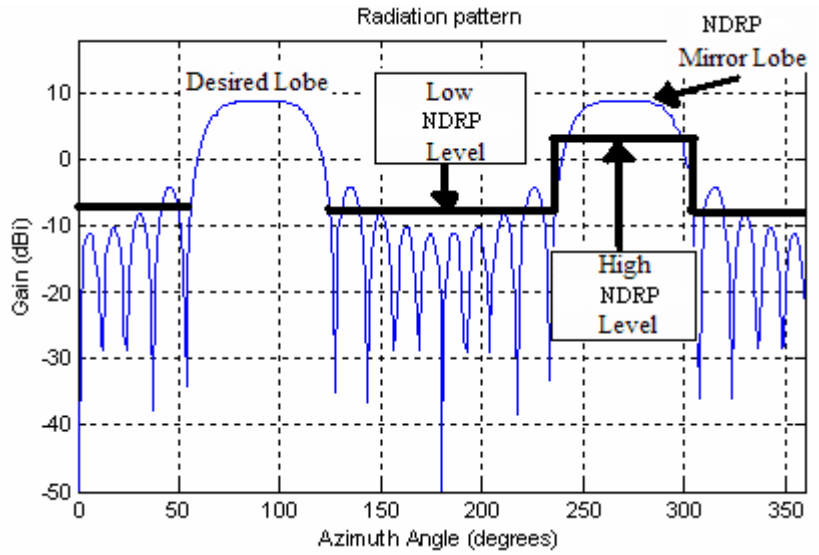

Figure 3.28: Linear array Not Desired Radiation Pattern.

Let Δ be the beamwidth of the mirror effect lobe, in the Figure 3.28, and then is defined the total NDRP as:

$$NDRP_{Total\_Linear} = NDRP_{High} \bullet \Delta + NDRP_{Low} \bullet 2(\pi - \Delta) \qquad (3.78)$$

A circular array radiation pattern is shown in the Figure 3.29, in the circular array case, we only have one NDRP level. This is due to all the side lobes, and this NDRP level is the average about all the side lobes.

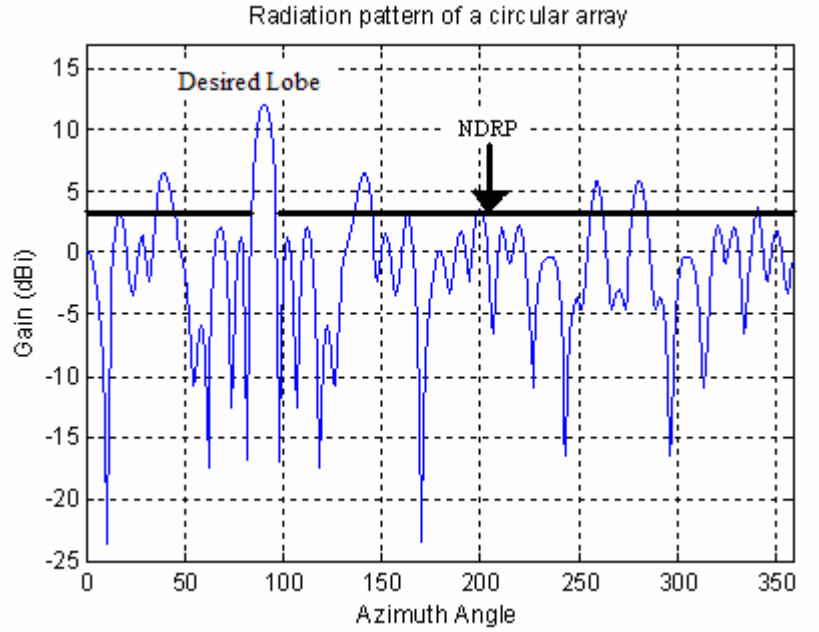

Figure 3.29: Circular array NDRP.

Now, let Δ be the beamwidth of the main lobe, in the Figure 3.29, and then is defined the total NDRP as:

$$NDRP_{Total\_Circular} = Interf \bullet (2\pi - \Delta) \tag{3.79}$$

Let's point toward 90°, 135° and 180° the desired lobe, as typical directions in any array. In the Table 3.1 we have different values for the linear array with 8 and 10 elements, with sizes of *0.21m* and *0.27m* respectively, and for the circular array with 20 and 30 elements, with *0.18m* and *0.21m* of diameters respectively, the total NDRP of (3.78) and (3.79).

If the beamwidth is minimum, the radiation pattern will have less NDRP, due to the small side lobes. With the results shown in the Table 3.1, we conclude that the size of the each array is an important consideration when minimizing the NDRP. We can obtain less NDRP with bigger sizes. And also, with a big number of elements we can obtain less NDRP. The best case, causing less NDRP, is the linear array in the 180°, as we was expecting due to the results shown in the Figure 3.24. This direction causes the smallest beamwidth in the linear array. We exaggerate the number of elements in the circular array cases, to reach the smallest beamwidth able to produce these circular arrays.

	Linear array		**Circular array**	
	10-elements (dBi)	8-elements (dBi)	20-elements (dBi)	30-elements (dBi)
90 degrees	-5.4728e3	-5.0213e3	-5.9822e3	-6.6390e3
135 degrees	-6.6440e3	-6.3036e3	-6.1986e3	-6.2229e3
180 degrees	-8.5797e3	-8.1270e3	-5.6102e3	-6.1298e3

Table 3.1: Total NDRP for different linear and circular array patterns.

3.6 Multibeam Smart Antenna Design

In this part a contribution to the state of the art is made, modifying the criteria of the section 3.3.1 (MMSE), and generating an alternate form by the analysis of the MMSE with multiple reference signals. First we try the analysis with two reference signals, and then we introduce *M* reference signals, in the feedback loop; finally we obtain a general function. This equation will works to obtain the optimum weights vector needed to calculate the radiation pattern with multiple main beams in any array.

3.6.1 Two-Reference Signal MMSE

Now we will see how multiple beams can be formed simultaneously within the same array. Consider the feedback loop of the Figure 3.30.

Here we introduce a second reference signal $R_2(t)$ and then is subtracted from the output array $s(t)$ to obtain the error $\varepsilon_2(t)$. The square total error $\varepsilon^2(t)$ is the sum of the errors as follow:

$$\varepsilon^2(t) = [\varepsilon_1 + \varepsilon_2]^2 = \left[\left(R_1(t) - \sum_{j=1}^{N} w_j x_j(t) \right) + \left(R_2(t) - \sum_{j} w_j x_j(t) \right) \right]^2 \tag{3.80}$$

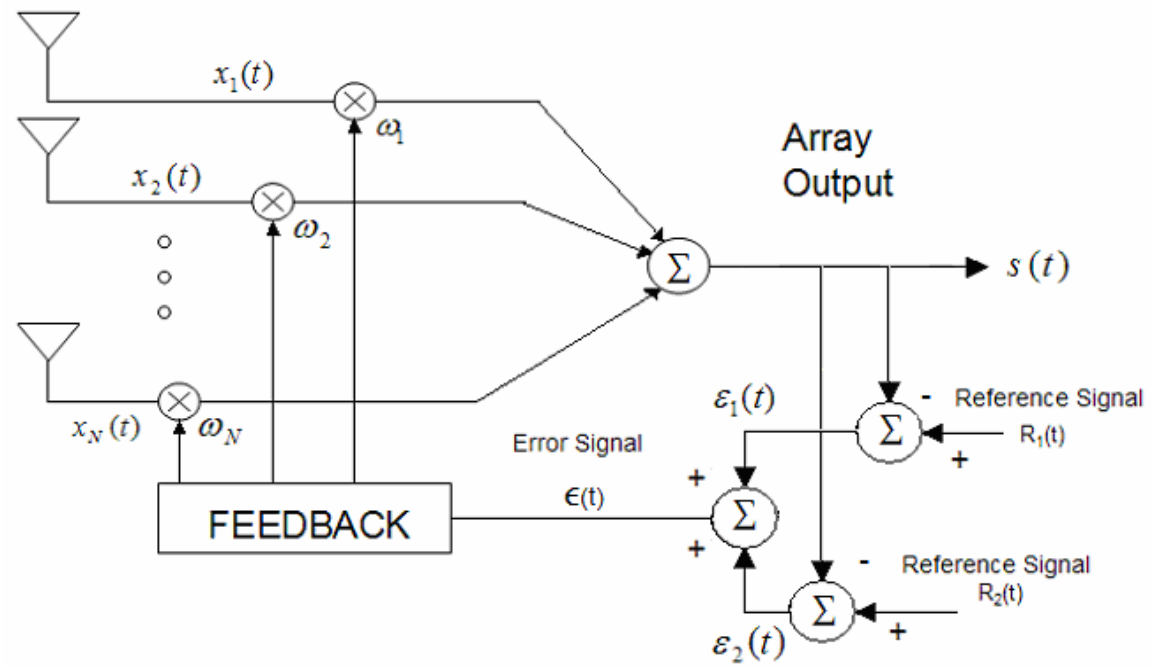

Figure 3.30: The adaptive array for two reference signals.

$$\varepsilon^2(t) = R_1{}^2(t) + R_2{}^2(t) - 4R_1(t)\sum_{j=1}^{N} w_j x_j(t) - 4R_2(t)\sum_{j=1}^{N} w_j x_j(t) + 4\left\{\sum_{j=1}^{N} w_j x_j(t)\right\}^2 + 2R_1(t)R_2(t)$$

and the mean square error is

$$E\left[\varepsilon^2(t)\right] = E\left[R_1{}^2(t) + R_2{}^2(t) + 2R_1(t)R_2(t)\right] - 4\sum_{j=1}^{N} w_j E\left[R_1(t)x_j(t)\right] - 4\sum_{j=1}^{N} w_j E\left[R_2(t)x_j(t)\right] + 4\sum_{i=1}^{N}\sum_{j=1}^{N} w_i w_j E\left[x_i(t)x_j(t)\right]$$

This result may be written more simply by using matrix notation

$$E\left[\varepsilon^2(t)\right] = E\left[R_1{}^2(t) + R_2{}^2(t) + 2R_1(t)R_2(t)\right] - 4\ \boldsymbol{W}\boldsymbol{S}_1 - 4\ \boldsymbol{W}\boldsymbol{S}_2 + 4\boldsymbol{W}^T\boldsymbol{\Phi}\boldsymbol{W} \qquad (3.81)$$

where $\boldsymbol{W}$ and $\boldsymbol{S}$ are column matrices

$$\boldsymbol{W} = [w_1, w_2, w_3, ..., w_N]^T \qquad (3.82)$$

$$\boldsymbol{S}_1 = E\begin{bmatrix} x_1(t)r_1(t) \\ \vdots \\ x_N(t)r_1(t) \end{bmatrix}, \quad \boldsymbol{S}_2 = E\begin{bmatrix} x_1(t)r_2(t) \\ \vdots \\ x_N(t)x_2(t) \end{bmatrix} \qquad (3.83)$$

where (3.83) are the reference correlation vectors , and $\boldsymbol{\Phi}$ is a N x N matrix,

$$\boldsymbol{\Phi} = E\begin{bmatrix} x_1(t)x_1(t) & x_1(t)x_2(t) & x_1(t)x_3(t) & \cdots & x_1(t)x_N(t) \\ x_2(t)x_1(t) & x_2(t)x_2(t) & x_2(t)x_3(t) & \cdots & x_2(t)x_N(t) \\ \vdots & \vdots & \vdots & \ddots & \vdots \\ x_N(t)x_1(t) & x_N(t)x_2(t) & x_N(t)x_3(t) & \cdots & x_N(t)x_N(t) \end{bmatrix} \tag{3.84}$$

where (3.84) is the covariance matrix. Superscript T denotes the transpose.

The weight vector yielding minimum $E[\varepsilon^2(t)]$, which we denote by $\boldsymbol{W}_{opt}$, may be found by setting

$$\nabla_W \{E[\varepsilon^2(t)]\} = 0, \tag{3.85}$$

where ∇_W denotes the gradient with respect to $\boldsymbol{W}$. Since

$$\nabla_W \{E[\varepsilon^2(t)]\} = -4\,\boldsymbol{S}_1 - 4\,\boldsymbol{S}_2 + 8\boldsymbol{\Phi}\boldsymbol{W}, \tag{3.86}$$

we find

$$8\boldsymbol{\Phi}\,\boldsymbol{W}_{opt} = 4\,(\boldsymbol{S}_1 + \boldsymbol{S}_2) \tag{3.87}$$

or

$$\boldsymbol{W}_{opt} = \frac{1}{2}\boldsymbol{\Phi}^{-1}(\boldsymbol{S}_1 + \boldsymbol{S}_2) \tag{3.88}$$

where $\boldsymbol{\Phi}$ is assumed to be nonsingular so its inverse matrix exists.

3.6.2 Multi-Reference Signal MMSE

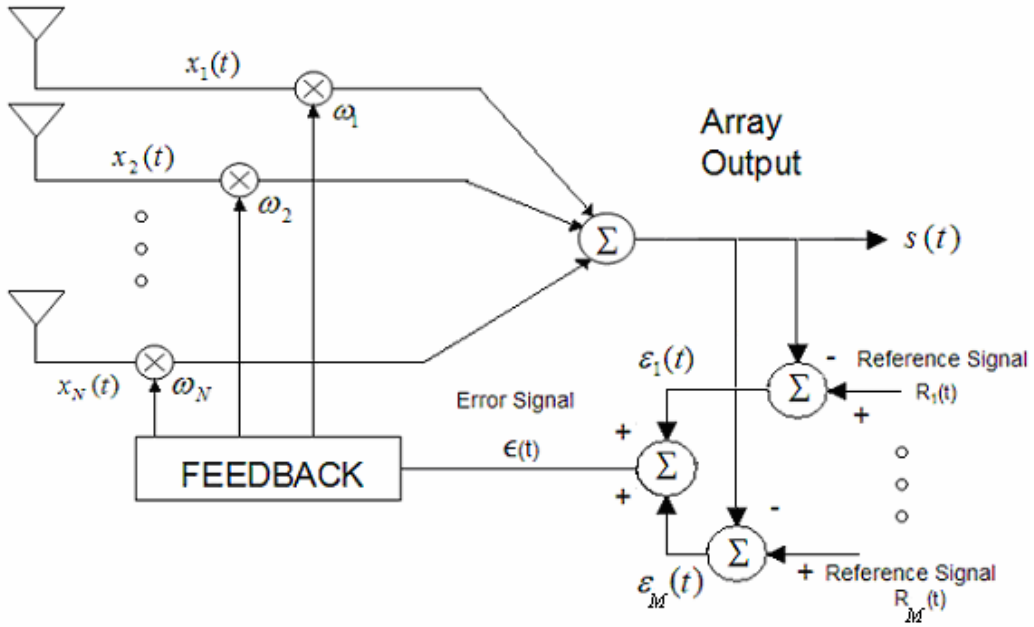

Figure 3.31. The adaptive array for multiple reference signals.

Now if we introduce M reference signals, as shown in the Figure 3.31, and keep the N elements in the adaptive array (where $M < N$), we have,

$$\varepsilon^2(t) = \left(\sum_{i=1}^{M} \varepsilon_i\right)^2 = \sum_{i=1}^{M}\left(R_i(t) - \sum_{k=1}^{N} w_k x_k(t)\right)^2 + 2\sum_{i=1}^{M-1}\sum_{j=i+1}^{M}\left(R_i(t) - \sum_{k=1}^{N} w_k x_k(t)\right)\left(R_j(t) - \sum_{k=1}^{N} w_k x_k(t)\right)$$

$$\varepsilon^2(t) = \sum_{i=1}^{M}\left[R_i^2(t) - 2R_i(t)\sum_{k=1}^{N} w_k x_k(t) + \left(\sum_{k=1}^{N} w_k x_k(t)\right)^2\right] + \tag{3.89}$$

$$2\sum_{i=1}^{M-1}\sum_{j=i+1}^{M}\left[R_i(t)R_j(t) - R_i(t)\sum_{k=1}^{N} w_k x_k(t) - R_j(t)\sum_{k=1}^{N} w_k x_k(t) + \left(\sum_{k=1}^{N} w_k x_k(t)\right)^2\right]$$

$$\varepsilon^2 = \sum_{i=1}^{M} R_i^2(t) - 2\sum_{i=1}^{M} R_i(t)\sum_{k=1}^{N} w_k x_k(t) + \sum_{i=1}^{M}\left(\sum_{k=1}^{N} w_k x_k(t)\right)^2 + 2\sum_{i=1}^{M-1}\sum_{j=i+1}^{M} R_i(t)R_j(t)$$

$$-2\sum_{i=1}^{M-1}\sum_{j=i+1}^{M} R_i(t)\sum_{k=1}^{N} w_k x_k(t) - 2\sum_{i=1}^{M-1}\sum_{j=i+1}^{M} R_j(t)\sum_{k=1}^{N} w_k x_k(t) + 2\sum_{i=1}^{M-1}\sum_{j=i+1}^{N}\left(\sum_{k=1}^{N} w_k x_k(t)\right)^2$$

and the mean square error is

$$E\left[\varepsilon^2\right] = \sum_{i=1}^{M} E\left[R_i^2(t)\right] - 2\sum_{i=1}^{M}\sum_{k=1}^{N} w_k E\left[R_i(t)x_k(t)\right] + \sum_{i=1}^{M}\sum_{k=1}^{N}\sum_{l=1}^{N} w_k w_l E\left[x_k(t)x_l(t)\right] + 2\sum_{i=1}^{M-1}\sum_{j=i+1}^{M} E\left[R_i(t)R_j(t)\right]$$

$$-2\sum_{i=1}^{M-1}\sum_{j=i+1}^{M}\sum_{k=1}^{N} w_k E\left[R_i(t)x_k(t)\right] - 2\sum_{i=1}^{M-1}\sum_{j=i+1}^{M}\sum_{k=1}^{N} w_k E\left[R_j(t)x_k(t)\right] + 2\sum_{i=1}^{M-1}\sum_{j=i+1}^{M}\sum_{k=1}^{N}\sum_{l=1}^{N} w_k w_l E\left[x_k(t)x_l(t)\right]$$

This result may be written more simply by using matrix notation

$$E\left[\varepsilon^2\right] = \sum_{i=1}^{M} E\left[R_i^2(t)\right] - 2\sum_{i=1}^{M} \boldsymbol{W}\boldsymbol{S}_i + \sum_{i=1}^{M} \boldsymbol{W}^T \boldsymbol{\Phi}\boldsymbol{W} + \boldsymbol{2}\sum_{\boldsymbol{i=1}}^{\boldsymbol{M-1}}\sum_{\boldsymbol{j=i+1}}^{\boldsymbol{M}} E\left[R_i(t)R_j(t)\right] - 2\sum_{i=1}^{M-1}\sum_{j=i+1}^{M} \boldsymbol{W}\boldsymbol{S}_i$$

$$-2\sum_{i=1}^{M-1}\sum_{j=i+!}^{M} \boldsymbol{W}\boldsymbol{S}_j + 2\sum_{i=1}^{M-1}\sum_{j=i+1}^{M} \boldsymbol{W}^T \Phi \boldsymbol{W} \tag{3.90}$$

where $\boldsymbol{W}$ and $\boldsymbol{S_M}$ are column matrices

$$\boldsymbol{W} = [w_1, w_2, w_3, ..., w_N]^T \tag{3.91}$$

$$\boldsymbol{S_M} = E\begin{bmatrix} x_1(t)r_N(t) \\ \vdots \\ x_N(t)r_N(t) \end{bmatrix} \tag{3.92}$$

where (3.92) are the reference correlation vectors , and $\boldsymbol{\Phi}$ is a N x N matrix,

$$\boldsymbol{\Phi} = E\begin{bmatrix} x_1(t)x_1(t) & x_1(t)x_2(t) & x_1(t)x_3(t) & \cdots & x_1(t)x_N(t) \\ x_2(t)x_1(t) & x_2(t)x_2(t) & x_2(t)x_3(t) & \cdots & x_2(t)x_N(t) \\ \vdots & \vdots & \vdots & \ddots & \vdots \\ x_N(t)x_1(t) & x_N(t)x_2(t) & x_N(t)x_3(t) & \cdots & x_N(t)x_N(t) \end{bmatrix} \tag{3.93}$$

where (3.93) is the covariance matrix. Superscript T denotes the transpose.

The weight vector yielding minimum $E[\varepsilon^2(t)]$, which we denote by $\boldsymbol{W}_{opt}$, may be found by setting

$$\nabla_{\boldsymbol{W}}\{E[\varepsilon^2(t)]\} = 0 \tag{3.94}$$

where ∇_W denotes the gradient with respect to $\boldsymbol{W}$. Since

$$\nabla_{\boldsymbol{W}}\{E[\varepsilon^2(t)]\} = -2\sum_{i=1}^{M}\boldsymbol{S}_i + 2\sum_{i=1}^{M}\boldsymbol{\Phi}\boldsymbol{W} - 2\sum_{i=1}^{M-1}\sum_{j=i+1}^{M}\boldsymbol{S}_i - 2\sum_{i=1}^{M-1}\sum_{j=i+1}^{M}\boldsymbol{S}_j + 4\sum_{i=1}^{M-1}\sum_{j=i+1}^{M}\boldsymbol{\Phi}\boldsymbol{W} = 0 \tag{3.95}$$

we find

$$2\boldsymbol{\Phi}\boldsymbol{W}\,\mathrm{M} + 4\boldsymbol{\Phi}\boldsymbol{W}\,\mathrm{M}\frac{\mathrm{M}-1}{2} - 2\left[\sum_{i=1}^{M}\boldsymbol{S}_i + \sum_{i=1}^{M-1}\sum_{j=i+1}^{M}\boldsymbol{S}_i + \sum_{i=1}^{M-1}\sum_{j=i+1}^{M}\boldsymbol{S}_j\right] = 0$$

$$2\boldsymbol{\Phi}\boldsymbol{W}\,\mathrm{M}^2 - 2\,\mathrm{M}\sum_{i=1}^{M}\boldsymbol{S}_i = 0$$

$$2\boldsymbol{\Phi}\boldsymbol{W}\,\mathrm{M}^2 = 2\,\mathrm{M}\sum_{i=1}^{M}\boldsymbol{S}_i$$

$$\boldsymbol{W}_{opt} = \frac{1}{\mathrm{M}}\,\boldsymbol{\Phi}^{-1}\sum_{i=1}^{M}\boldsymbol{S}_i \tag{3.96}$$

where $\boldsymbol{\Phi}$ is assumed to be nonsingular so its inverse matrix exists.

Example 2

Now, consider a linear array consisting of 10 isotropic elements. Two desired signals at frequency ω_d and an interference signal propagates into the array from the angles θ_{d1}, θ_{d2} and θ_i respectively, relative to the broadside. Let the elements be one-half wavelength apart of each others at frequency ω_d. Now the elements signal are given by

$$\begin{aligned} x_1(t) &= d_{1,1}(t) + d_{1,2}(t) + i_1(t) + n_1(t) \\ x_2(t) &= d_{2,1}(t) + d_{2,2}(t) + i_2(t) + n_2(t) \\ &\vdots \\ x_{10}(t) &= d_{10,1}(t) + d_{10,2}(t) + i_{10}(t) + n_{10}(t) \end{aligned} \tag{3.97}$$

where $d_j(t)$ and $n(t)$ are the desired signal and thermal noise components, respectively. The desired signal 1 is given by

$$\begin{aligned} d_{1,1} &= A_{d1}e^{j\omega_d t} \\ d_{2,1} &= A_{d1}e^{j(\omega_d t-\phi_{2d1})} \\ &\vdots \\ d_{10,1} &= A_{d1}e^{j(\omega_d t-\phi_{10d1})} \end{aligned} \tag{3.98}$$

and the desired signal 2 is given by

$$\begin{aligned} d_{1,2} &= A_{d2}e^{j\omega_d t} \\ d_{2,2} &= A_{d2}e^{j(\omega_{d2} t-\phi_{2d2})} \\ &\vdots \\ d_{10,2} &= A_{d2}e^{j(\omega_d t-\phi_{10d2})} \end{aligned} \tag{3.99}$$

where A_{d1} and A_{d2} are the desired signal amplitudes, for the desired signal 1 and 2, respectively and ϕ_d is the interelement phase shift for each signal and element. Since the inter-element spacing is one-half wavelength, ϕ_d is given by the equation (3.74).

The interference signal is assumed to be

$$\begin{aligned} i_1 &= A_i e^{j\omega_d t} \\ i_2 &= A_i e^{j(\omega_d t-\phi_{2i})} \\ &\vdots \\ i_{10} &= A_i e^{j(\omega_d t-\phi_{10i})} \end{aligned} \tag{3.100}$$

where A_i is the amplitude, ϕ_i is the interelement phase shift. The thermal noises are assumed to be zero-mean random processes, statistically independent of each other and the desired signal, each power σ^2. Thus,

$$E\{n_i^*(t)n_j(t)\} = \sigma^2\delta_{ij}, \tag{3.101}$$

where δ_{ij} is the Kronecker delta,

$$\delta_{ij} = \begin{cases} 1, & i = j \\ 0, & i \neq j, \end{cases} \tag{3.102}$$

and

$$E\{d_i^*(t)n_j(t)\} = 0. \tag{3.103}$$

Finally we suppose the reference signals are correlated with the desired signals,

$$r_1(t) = R_1 e^{j\omega_d t}$$
$$r_2(t) = R_2 e^{j\omega_d t} \tag{3.104}$$

Thus the input signal-to-noise ratio and interference-to-noise ratio are

$$\xi_{d1} = \frac{A_{d1}^2}{\sigma^2} \tag{3.105}$$
$$\xi_{d2} = \frac{A_{d2}^2}{\sigma^2}$$
$$\xi_i = \frac{A_i^2}{\sigma^2} \tag{3.106}$$

respectively. The signal vector may be written

$$\mathbf{X} = \mathbf{X}_{d1} + \mathbf{X}_{d2} + \mathbf{X}_i + \mathbf{X}_n\,, \tag{3.107}$$

where the desired signal is given by

$$\boldsymbol{X}_{d1} = \begin{bmatrix} d_{1,1}(t) \\ d_{2,1}(t) \\ \vdots \\ d_{10,1}(t) \end{bmatrix} = A_{d1} e^{j\omega_d t} \begin{bmatrix} 1 \\ e^{-j\phi_{2d1}} \\ \vdots \\ e^{-j\phi_{10d1}} \end{bmatrix} = A_{d1} e^{j\omega_d t} \boldsymbol{U}_{d1} \tag{3.108}$$

and

$$\boldsymbol{X}_{d2} = \begin{bmatrix} d_{1,2}(t) \\ d_{2,2}(t) \\ \vdots \\ d_{10,2}(t) \end{bmatrix} = A_{d2} e^{j\omega_d t} \begin{bmatrix} 1 \\ e^{-j\phi_{2d2}} \\ \vdots \\ e^{-j\phi_{10d2}} \end{bmatrix} = A_{d2} e^{j\omega_d t} \boldsymbol{U}_{d2} \tag{3.109}$$

and the interference signal given by

$$\boldsymbol{X}_i = \begin{bmatrix} i_1(t) \\ i_2(t) \\ \vdots \\ i_{10}(t) \end{bmatrix} = A_i e^{j\omega_d t} \begin{bmatrix} 1 \\ e^{-j\phi_{2i}} \\ \vdots \\ e^{-j\phi_{10i}} \end{bmatrix} = A_i e^{j\omega_d t} \boldsymbol{U}_i\,. \tag{3.110}$$

Finally we have

$$\boldsymbol{X}_n = \begin{bmatrix} n_1(t) \\ n_2(t) \\ \vdots \\ n_{10}(t) \end{bmatrix}. \tag{3.111}$$

The covariance matrix, using (3.93), now becomes

$$\mathbf{\Phi} = E\left[\boldsymbol{X}^*(t)\boldsymbol{X}^T(t)\right]$$

$$\mathbf{\Phi} = E(\mathbf{X}_{d1}{}^*\,\mathbf{X}_{d1}{}^T) + E(\mathbf{X}_{d2}{}^*\,\mathbf{X}_{d2}{}^T) + E(\mathbf{X}_i{}^*\,\mathbf{X}_i{}^T) + E(\mathbf{X}_n{}^*\,\mathbf{X}_n{}^T). \quad (3.112)$$

We find that

$$E(\mathbf{X}_{d1}{}^*\,\mathbf{X}_{d1}{}^T) = A_{d1}{}^2\mathbf{U}_{d1}{}^*\,\mathbf{U}_{d1}{}^T \quad (3.113)$$

$$E(\mathbf{X}_{d2}{}^*\,\mathbf{X}_{d2}{}^T) = A_{d2}{}^2\,\mathbf{U}_{d2}{}^*\,\mathbf{U}_{d2}{}^T \quad (3.114)$$

and

$$E(\mathbf{X}_i{}^*\,\mathbf{X}_i{}^T) = A_i{}^2\,\mathbf{U}_i{}^*\,\mathbf{U}_i{}^T \quad (3.115)$$

and

$$E(\mathbf{X}_n{}^*\,\mathbf{X}_n{}^T) = \sigma^2\,\mathbf{I} \quad (3.116)$$

where $\mathbf{I}$ is the identity matrix. Therefore $\mathbf{\Phi}$ is

$$\mathbf{\Phi} = A_{d1}^2\,\mathbf{U}_{d1}{}^*\,\mathbf{U}_{d1}{}^T + A_{d2}^2\,\mathbf{U}_{d2}{}^*\,\mathbf{U}_{d2}{}^T + A_i^2\,\mathbf{U}_i{}^*\,\mathbf{U}_i{}^T + \sigma^2\,\mathbf{I}. \quad (3.117)$$

And the correlation vectors are

$$\begin{aligned} S_1 &= E\left[\boldsymbol{X}_{d1}{}^*(t)\boldsymbol{R}_1(t)\right] \\ S_1 &= E\left[A_{d1}e^{-j\omega_d t}R_1 e^{j\omega_d t}\right] \\ S_1 &= A_{d1}R_1U_d{}^* \end{aligned} \quad (3.118)$$

and

$$\begin{aligned} S_2 &= E\left[\boldsymbol{X}_{d2}{}^*(t)\boldsymbol{R}_2(t)\right] \\ S_2 &= E\left[A_{d2}e^{-j\omega_d t}R_2 e^{j\omega_d t}\right] \\ S_2 &= A_{d2}R_2U_d{}^* \end{aligned} \quad (3.119)$$

Setting $\sigma^2 = 0.001$, $SNR = 30dB$, $\theta_{d1} = -20^{\mathrm{O}}$ and 5dBi grater than the desired signal 2, with $\theta_{d2} = 10^{\mathrm{O}}$ and $\theta_i = -40^{\mathrm{O}}$, $f = 5Ghz$ and a separation distance between elements of $d = \lambda/2$, we can obtain the weight vector using (3.96) as

$$\boldsymbol{W} = \begin{bmatrix} \boldsymbol{0.3515 + 0.0328i} \\ \boldsymbol{0.1684 + 0.0956i} \\ \boldsymbol{-0.0711 + 0.0769i} \\ \boldsymbol{-0.3160 - 0.1084i} \\ \boldsymbol{-0.2238 - 0.3680i} \\ \boldsymbol{0.0994 - 0.2312i} \\ \boldsymbol{0.1253 + 0.1632i} \\ \boldsymbol{-0.0562 + 0.3217i} \\ \boldsymbol{-0.1519 + 0.2775i} \\ \boldsymbol{-0.1858 + 0.0916i} \end{bmatrix}$$

Here we define radiation pattern similar to (3.50) and (3.51), and we will obtain the results shown in the Figure 3.32.

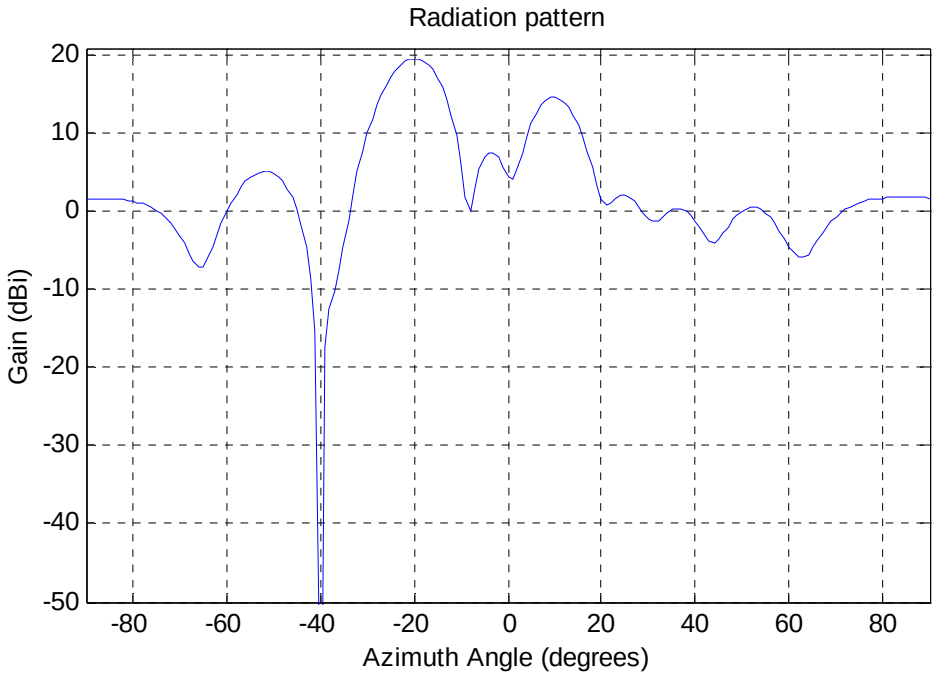

Figure 3.32: 10-element linear array radiation pattern, as a multibeam smart antenna. The reference 1 is in $\theta_{d1} = -20^{O}$ with 5dBi over the reference signal 2, placed to $\theta_{d2} = 10^{O}$ and an interferer in $\theta_i = -40^{O}$.

In the rest of this work we will use the results of this section, equation (3.96), (3.50) and (3.51), to implement ad-hoc networks with the nodes equipped with multibeam smart antennas.

Chapter 4

Model Description

In order to analyze the network performance from the point of view of its capacity and interference in this chapter we have made a simulation to model and analyze the behavior of a wireless CDMA ad-hoc network in which each node is equipped with a Multibeam Smart Antenna. In the following sections we will explain the characteristics considered to model and simulate this ad-hoc network and the propagation model.

4.1 Ad-hoc CDMA Network Modeling

We have considered, for the analysis proposed in this work, the following points:

- An ad-hoc network that uses a CDMA as the access method is analyzed, in which each node can transmit to the neighbors simultaneously, using different codes for each node.

- We consider that each node is equipped with a Multibeam Smart Antenna, and on the average, each node will have no more than 4 neighbors (links). This means that each radiation patter will calculate no more than 4 main lobes with the equation 3.96.

- Perfect power control is considered in the sense that this power is the lowest possible and is about -100 dBm, which will be considered the minimum received signal level.

- We have chosen a point for the interference analysis. This point will be addressed in the center of the scenario (circular region), a point at which the interference conditions will have bigger or crucial repercussions; this point will receive interference for the all direction with the same gain, with an isotropic antenna (0

dBi). And the interference analysis will be done considering the worse case; this is, when all nodes are transmitting simultaneously at the same time.

- Nodes position follow a Poisson distribution, with the Homogeneous Poisson process method, and the nodes are distributed independently of each other.

- Neighbor discovery is assumed, therefore once the network is generated, all the nodes know the position of their neighbors.

- In this work all interference measures will be done before considering the cross-correlation factor of each code.

4.2 Proposed Model: Spatial Point Processes

A spatial point pattern is a set of point locations $\mathbf{s}_1, \ldots, \mathbf{s}_n$ in a study region $\boldsymbol{R}$. Each point location $\mathbf{s}_i$ is a vector containing the coordinates of the i-th event [24],

$$\boldsymbol{s}_i = \begin{bmatrix} s_{i1} \\ s_{i2} \end{bmatrix}. \tag{4.1}$$

The term ***event*** can refer to any spatial phenomenon that occurs at point location. For example, events can be locations of trees growing in a forest, positions of cells in tissue or the incident of disease at locations in a community. Note that this scale of our study affects the reasonableness of the assumption that the events occur at point locations.

In our analysis of spatial point patters, we might have to refer to other locations in the study region $\boldsymbol{R}$, where the phenomenon was not observed. We need a way to distinguish them from the locations where observations were taken, so we refer to these other locations as ***points*** in the region.

One way we can think of spatial point patterns is in terms of the number of events occurring in an arbitrary sub-region of $\boldsymbol{R}$. We denote the number of events in a sub-region $\boldsymbol{A}$ as $\gamma(\boldsymbol{A})$. The spatial process in then represented by the random variables $\gamma(\boldsymbol{A})$, $\boldsymbol{A} \subset \boldsymbol{R}$. Since we have a random process, we can look at the behavior in terms of the first-order and second-order properties. The mean and the covariance of $\gamma(\boldsymbol{A})$ depend on the number of events in arbitrary sub-regions $\boldsymbol{A}$, and they depend on the size of the areas and the study region $\boldsymbol{R}$. Thus, it is more useful to look at the first and second-order properties in terms of the limiting behavior per unit area.

The first-order property is described by the intensity $\lambda(\mathbf{s})$. The ***intensity*** is defined as the mean number of events per unit area at the point **s.** Mathematically, the intensity is given by [24]

$$\lambda(\boldsymbol{s}) = \lim_{\mathrm{ds} \to 0} \left\{ \frac{E[\gamma(\boldsymbol{ds})]}{\mathrm{d}\,s} \right\}, \tag{4.2}$$

where **ds** is a small region around the points **s**, and ds is its area. If it is a ***stationary point process*** then equation (4.2) is a constant over the study region. We can then write the intensity as

$$E[\gamma(A)] = \lambda A, \tag{4.3}$$

where A is the area of the sub-region, and λ is the value of the intensity.

To understand the second-order properties of a spatial point process, we need to look at the number of events in pairs of sub-regions of ***R***. The second order property reflects the spatial dependence in the process. We describe this using the second-order intensity $\gamma(\mathbf{s}_i, \mathbf{s}_j)$. As with the intensity, this is defined using the events per unit area, as follows [24],

$$\gamma(s_i, \mathbf{s}_j) = \lim_{ds_i, ds_j \to 0} \left\{ \frac{E[\gamma(ds_i)\gamma(ds_j)]}{ds_i, ds_j} \right\} \tag{4.4}$$

If the process is stationary, then $\gamma(\mathbf{s}_i, \mathbf{s}_j) = \gamma(\mathbf{s}_i - \mathbf{s}_j)$. This means that the second-order intensity depends only on the vector difference of the two points. The process is said to be ***second-order*** and ***isotropic*** in the second-order intensity depends only on the distance between $\mathbf{s}_i$ and $\mathbf{s}_j$. In other words, it does not depend on the direction.

4.2.1 Homogeneous Poisson Process

Here we present a method for simulating homogeneous Poisson process with no condition imposed on the number of events n [24]. Unconditionally, a homogeneous Poisson process depends on the intensity λ. Therefore, in this case the number of events n changes in each simulated pattern.

We follow the fanning out procedure given in [25] to generate such a process for a circular region. This technique can be though of as fanning out from the origin to a radius r. The successive radii where events are encountered are simulated by using the fact the additional area one needs to travel to encounter another event is exponentially distributed with rate λ. The steps are outlined below.

1. Generate independent exponential variates $X_1, X_2, \ldots$, with rate λ, stopping when

$$N = \min\{n : X_1 + \ldots + X_n > \pi r^2\}. \tag{4.5}$$

2. If $N = 1$, then stop, because there are no events in the circular region.
3. If $N > 1$, then for $i = 1, \ldots, N\text{-}1$, find

$$R_i = \sqrt{\frac{X_1 + \ldots + X_i}{\pi}}. \tag{4.6}$$

4. Generate N-1 uniform (0,1) variates, $U_1, \ldots, U_{N-1}$.
5. In polar coordinates, the events are given by $(R_i, 2\pi U_i)$.

In [25] is described a procedure where the region can be somewhat arbitrary. For example, in cartesian coordinates, the region would be defined between *x* axis and a nonnegative function *f(x)*, starting at $x = 0$. A rectangular region with the lower left corner at the origin is an example where this can be applied.

Lets consider a circular region with radius of 100 meters, and with an intensity of λ=0.0064 points/m^2, this is 200 points in an area of $\pi(100)^2$.

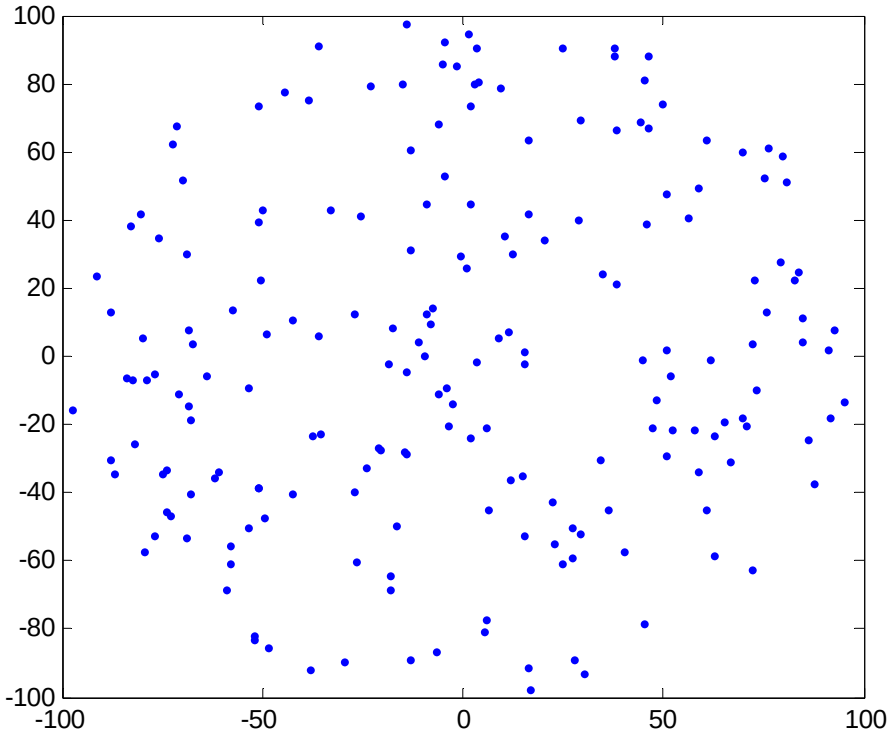

Figure 4.1: Homogeneous Poison Process with λ=0.0064 points/m^2, for a radius of 100m.

The results of the Homogeneous Poisson Process with these characteristics are shown in the Figure 4.1. This method of Homogeneous Poisson Process is used in the rest of this work in order to simulate the nodes in an ad-hoc network. If each point in the region of the Figure 4.1 is a node in an ad-hoc network, we will be able to connect the network with links for each pair of nodes that are in the range of connectivity of each other.

Now consider a region of 1 km^2, of radius of 564.18 m, with an average of 100 nodes in this area, that is $\lambda = 100 nodes / 1 km^2$. Each node will be connected to all the nodes that are in a radius of 100m of the reach of this node. The ad-hoc network with these characteristics is shown in the Figure 4.2, in which we can see that the network is divided into groups called clusters, as shown in the section 2.2.1. Increasing the range of connectivity we may put all the nodes together into the same cluster.

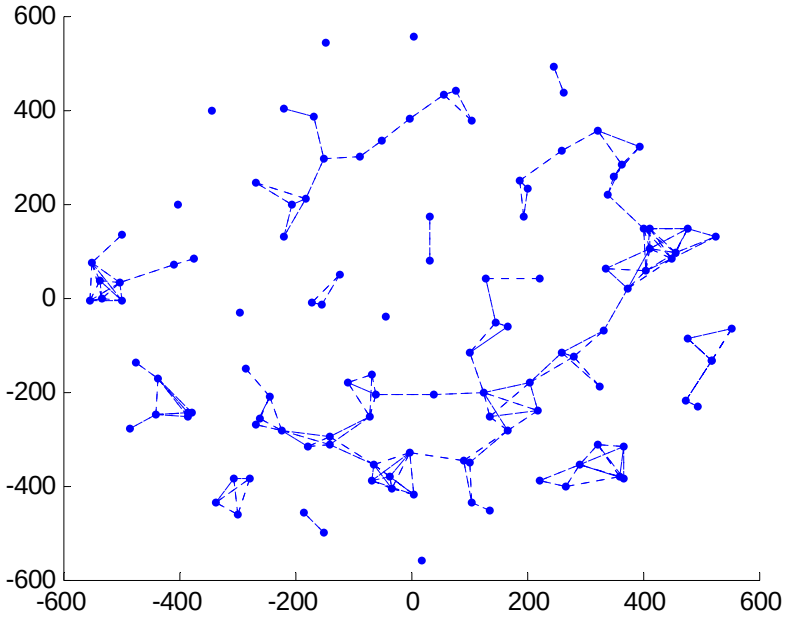

Figure 4.2: Ad-hoc network with $\lambda = 100 nodes / 1 km^2$ and a range of connectivity=100m.

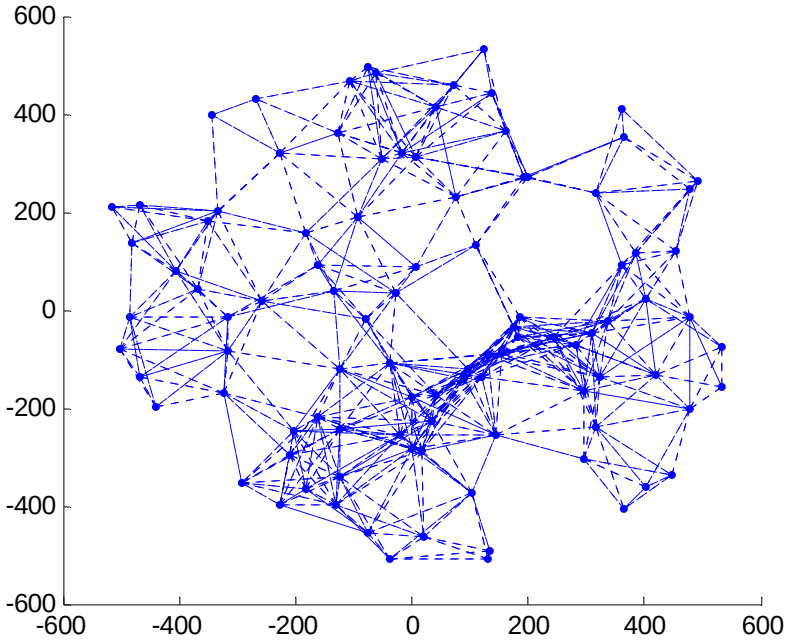

Figure 4.3: Ad-hoc network with $\lambda = 100 nodes / 1 km^2$ and a range of connectivity=200m.

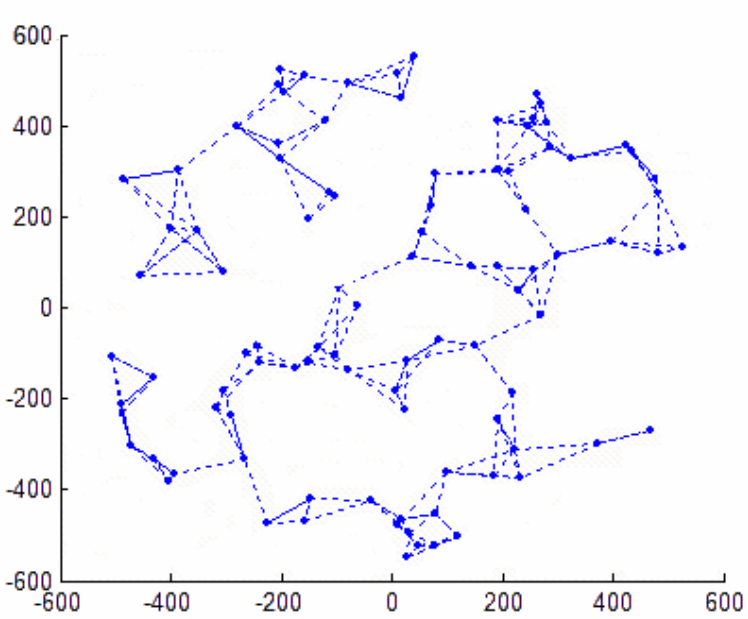

Figure 4.4: Ad-hoc network with $\lambda = 100 nodes / 1km^2$ divided in two clusters.

The result is a network with a lot of unnecessary or redundant links, as the network shown in the Figure 4.3. This redundant links make the nodes to have a lot of neighbors, and consequently to have a lot of main beams to radiate within the same smart antenna. With constrain of *degrees of freedom* we are not allowed to radiate any number of main beams, as shown in the section 3.6. If we are constrained to *n* links per node, on the average, letting the connectivity range to be increased if necessary to reach the *n* closets neighbors, we will obtain the ad-hoc network shown in the Figure 4.4.

Again we have the network divided into clusters. Here are just two clusters, one with the 38.5% of the nodes and the other one with the 61.5% of the rest of the nodes. We have, on the average, 114.7 m and 3.2 links, of connectivity range and links per node respectively.

We wish to have the 100% of the nodes in the same cluster, but we need to keep constant the average of links per node to avoid redundant links. As a result we need to know the connectivity range per node, on the average, to reach the 100% of the nodes in the same cluster. The CDF shown in the Figure 4.5 consist of 300 realizations of generated scenarios; here is shown that if we have 242 m in the connectivity range for each node, we will be able to put 100% of nodes together in one cluster, with a mean of 157.9 m in the connectivity range. The Figure 4.6 is for an intensity of $\lambda = 130 nodes / 1km^2$, and here we need 216 m in the range of connectivity to guaranty 100%, with a mean of 141.8 m of connectivity range. The CDFs for intensities of $\lambda = 160 nodes / 1km^2$ and $\lambda = 200 nodes / 1km^2$, are shown in the Figure 4.7 and Figure 4.8, respectively. As the number of users increases in the same area, the intensity of user per square unit area increases too, this causes the nodes to be nearest to each others and they reach the own neighbors with a smaller connectivity range.

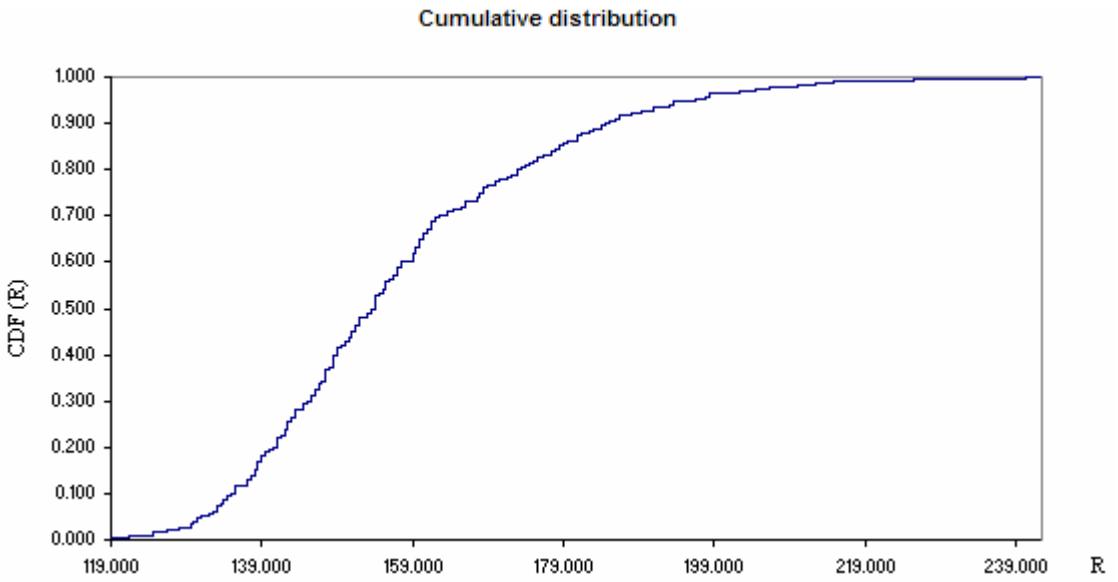

Figure 4.5: CDF connectivity range for an ad-hoc network with $\lambda = 100 nodes / 1 km^2$, to have de 100% of the nodes in one cluster.

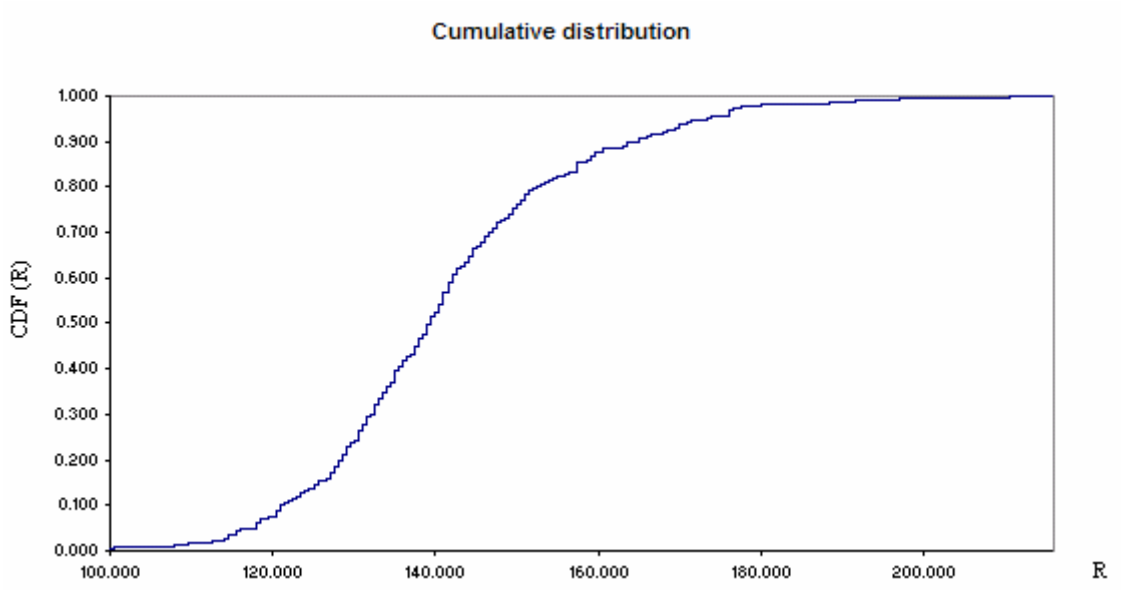

Figure 4.6: CDF connectivity range for an ad-hoc network with $\lambda = 130 nodes / 1 km^2$, to have de 100% of the nodes in one cluster.

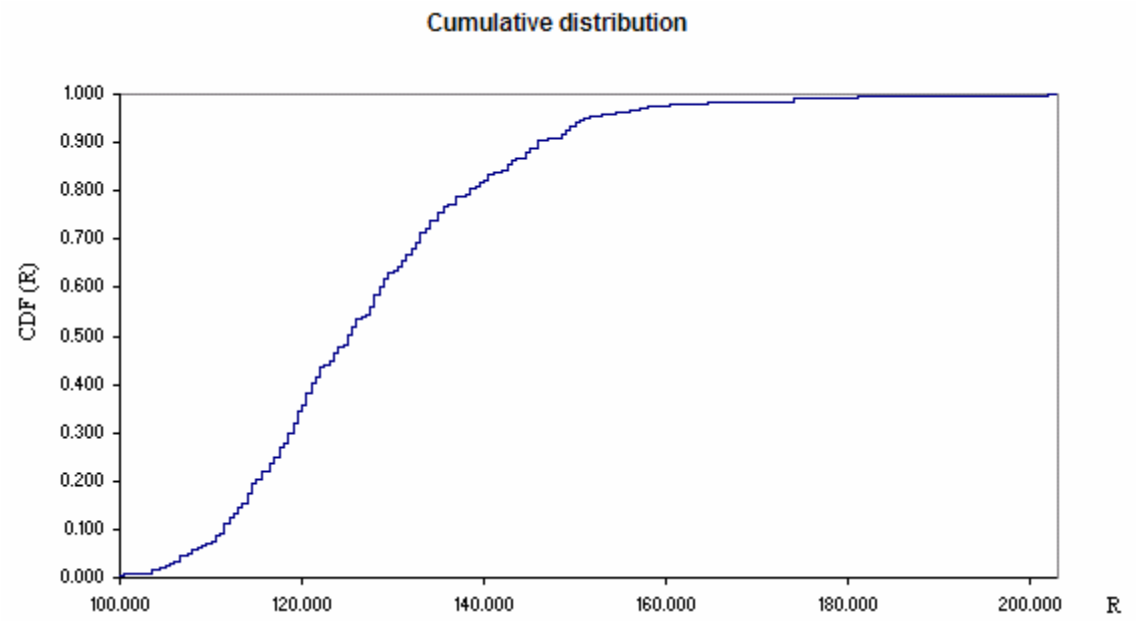

Figure 4.7: CDF connectivity range for an ad-hoc network with $\lambda = 160 nodes / 1km^2$, to have de 100% of the nodes in one cluster.

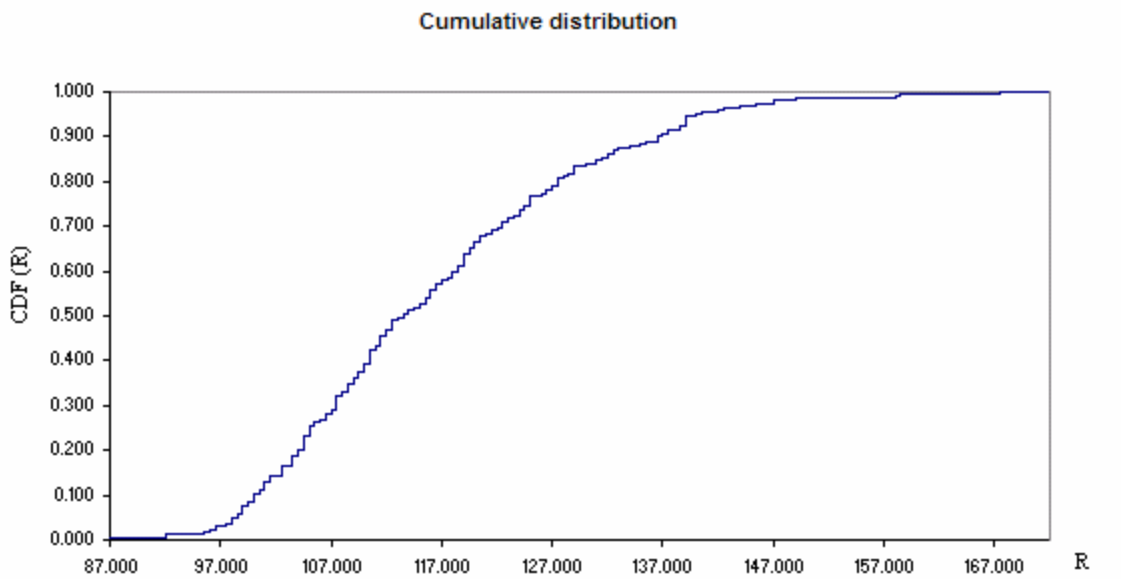

Figure 4.8: CDF connectivity range for an ad-hoc network with $\lambda = 200 nodes / 1km^2$, to have de 100% of the nodes in one cluster.

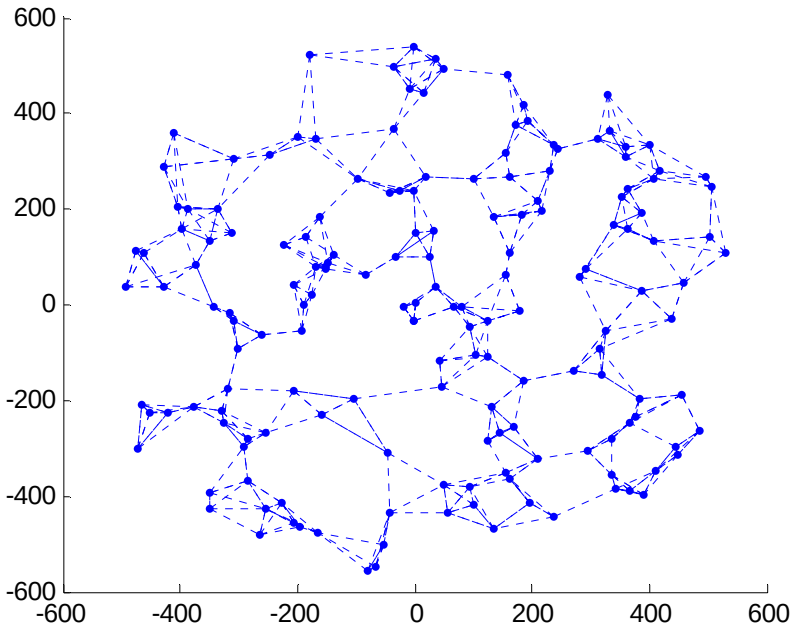

Figure 4.9: Ad-hoc network with $\lambda = 160 nodes / 1km^2$ and a range of connectivity=210m.

An example of an ad-hoc network with 100% of the nodes connected in one cluster and constrained to *n* number of links per node is shown in the Figure 4.9. This network is obtained by using the values of the Figure 4.7 with $\lambda = 160 nodes / 1km^2$, with a range of connectivity of 210 m, with mean connectivity range resulting of 92.83 m and 3.4 links per node, on the average. In the Figure 4.10, we present some values for different percentages of the nodes in the bigger cluster, with different connectivity ranges. As shown in the Figure 4.10 if the intensity of user in the same are increases, the distances between neighbors will be reduced.

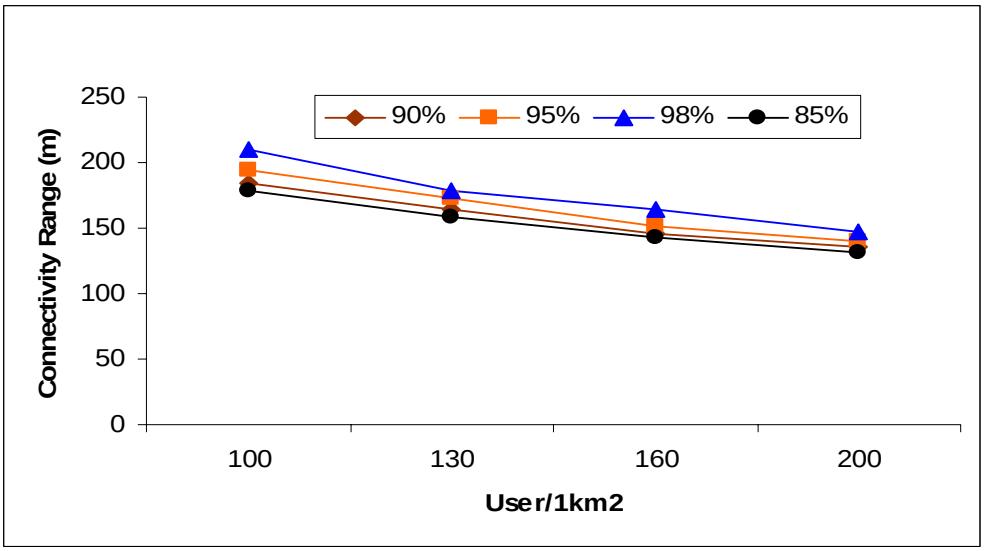

Figure 4.10: Connectivity ranges for various intensities λ.

4.3 Propagation Model

The mobile radio channel places fundamental limitations on the performance of wireless communications systems. The transmission path between the transmitter and the receiver varies from simple line-of-sight to one that is severely obstructed by buildings, mountains, and foliage. Unlike wired channels that are stationary and predictable, radio channels are extremely random and do not offer easy analysis. Even the speed of motion impacts how rapidly the signal level fades as a mobile terminal moves in space. Modeling the radio channel has historically been one of the most difficult parts of radio systems design, and is typically done in a statistical fashion, based on measurements made specifically for an intended communication system or spectrum allocation [1].

The mechanism behind electromagnetic wave propagation are diverse, but can generally be attributed to reflection, diffraction, and scattering. Most cellular radio systems operate in urban areas where there is no direct line-of-sight path between the transmitter and the receiver, and where the presence of high-rise buildings causes severe diffraction loss. Due to the multiple reflections from various objects, the electromagnetic waves travel along different paths of varying lengths. The interaction between these waves causes multipath fading at a specific location, and the strengths of the waves decrease as the distance between the transmitter and receiver increases.

Propagation models have traditionally focused on predicting the average received signal strength at a given distance from the transmitter, as well as the variability of the signal strength in close spatial proximity to a particular location. Propagation models that predict the mean signal strength for an arbitrary transmitter-receiver (T-R) separation distance are useful in estimating the radio coverage area of a transmitter and are called *large-scale* propagation models, since they characterize signal strength over large T-R separation distances (several hundreds or thousands of meters). On the other hand, propagation models that characterize the rapid fluctuations of the received signal strength over very short travel distance (a few wavelengths) or short time durations (on the order of seconds) are called *small-scale* or *fading* models.

4.3.1 Free Space Propagation Model

The free space propagation model is used to predict received signal strength when the transmitter and receiver have a clear, unobstructed line-of-sight path between them. Satellite communication systems and microwaves line-of-sight radio links typically undergo free space propagation. As with most large-scale radio wave propagation model, the free space model predicts that received power decays as a function of the T-R separation distance raised to some power. The free space power received by a receiver antenna which is separated from a radiating transmitter antenna by a distance *d*, is given by the Friis free space equation [1],

$$P_r = \frac{P_t G_t G_r \lambda^2}{(4\pi)^2 d^2} \tag{4.7}$$

where P_t is the transmitted power, P_r is the received power which is a function of the T-R separation, G_t is the transmitter antenna gain, G_r is the receiver antenna gain, d is the T-R separation distance in meters, and λ is the wavelength in meters, and is related to the carrier frequency by

$$\lambda = \frac{c}{f} = \frac{2\pi c}{\omega_c} \tag{4.8}$$

where f is the carrier frequency in Hertz, ω_c is the carrier frequency in radians per second, and c is the speed of light given in meters/s.

The *path loss*, which represents signal attenuation as a positive quantity measured in dB, is defined as the difference (in dB), between the effective transmitted power and the received power, and may or may not include the effect of the antenna gains. The path loss for the free space model when antenna gains are included is given by

$$PL(dB) = 10\log\frac{P_t}{P_r} = -10\log\left[\frac{G_t G_r \lambda^2}{(4\pi)^2 d^2}\right] \tag{4.9}$$

Then, P_t and the P_r are obtained by the equations (4.7) and (4.9) , where these quantities are measured in dBm, meaning that power is measured in milliwatts, where -30 dB is equivalent to 0 dBm. The P_t and the P_r, are given by,

$$P_r = \frac{P_t G_t G_r}{d^2}\left(\frac{\lambda}{4\pi}\right)^2 \qquad or$$

$$P_{r\_dBm} = P_{t\_dBm} + G_{t\_dBi} + G_{r\_dBi} - 20\log(d) + 20\log\left(\frac{\lambda}{4\pi}\right) \tag{4.10}$$

and

$$Pt = \frac{P_r d^2}{G_t G_r}\left(\frac{4\pi}{\lambda}\right)^2 \qquad or$$

$$P_{t\_dBm} = P_{r\_dBm} + 20\log(d) - G_{t\_dBi} - G_{r\_dBi} + 20\log\left(\frac{4\pi}{\lambda}\right) \tag{4.11}$$

respectively. These two equations are used in this work; the equation (4.11) is used to compute the power to be transmitted in each node to reach their neighbors at the controlled power level, as shown in sections 2.3.2 and 2.3.3; in the counterpart, the equation (4.10) is used to calculate the received power at a certain network position (in this work we measure the power in the center of each scenario, as will be shown in the next chapter).

We have seen how the nodes follow a Poisson distribution and the behavior of the ranges of connectivity probabilistically. With this in mind we would think in a cost

function to determine the capacity of the ad-hoc network using multibeam smart antennas, and minimize that function until it reaches a threshold necessary to guarantee a QoS.

This function would establish the position of each node in the scenario, that is, the distance and the angular position to the center of the scenario. In other words, we would need a probabilistic equation to obtain the distance to the center of the scenario, and this equation should consider the distance to the neighbor nodes too, necessary to calculate the probabilistic number of neighbors in each node to obtain the radiation pattern of each node. Finally, once the cost function is obtained considering all the above, λ could be varied to obtain the capacity of the network in each intensity of nodes.

Constrained to the limit of time and due to the goal of this work is just to know and to demonstrate that smart antennas in the ad-hoc network improves the capacity over omnidirectional antennas, we left the calculation of this cost function to future works.

In this work we use simulation results, instead of a cost function to calculate the scenarios, to obtain the Poisson processes and the due to that, we calculate the average of several number of realizations for each value of λ, with the effort to obtain statistical results closet to the reality. The simulations follow the next algorithm:

1. An scenario with the desired λ is created.
2. For each node, it looks for the *n* neighbors that are in the range of connectivity, necessarily to create only and only one cluster.
   2.1 If there are *n>4* neighbors to connect, are chosen the closest as the neighbors of this node.
3. If there are more than one cluster in the network:
   3.1 Go to step 1.
   3.2 Else, continue.

4 For each node, are calculated the distances to the own *j-th* neighbors, and with the equation 3.96, 3.50 and 3.51, are calculated the radiation pattern for this node, making the longest distance being reached with the bigger main beam. The rest of the *j-1* distances, are G_j dBi below the bigger main beam, dependently of the distance below the longest one.

5 For each node, are calculated the power to transmit, necessarily to reach the farthest neighbor to a power of $P_r = -100dBm$. With radiation patter calculated in the step 4, the nearest neighbors will receive at last -100dBm too.

6 From the center of the network, are calculated the distance and the angular position to each node. Then, with the radiation patter, the distance, the position and the power transmitted from each node, are calculated with the equation 4.10 the received power from each node, with a $G_r = 0\ dBi$. The sum of each individual power will be the interference on the center of this ad-hoc network.

Chapter 5

Numerical Results and Conclusions

In this chapter, are presented the numerical results for the scenarios proposed in the chapter 4, using the results of section 3.6 for multibeam smart antennas. First we shall present the analysis of the interference of a CDMA ad-hoc network for the omnidirectional case, as a point of reference as the comparison between linear array and circular array. We continue analyzing the interference to find the system's capacity necessary to guarantee a QoS required, named *threshold*.

5.1 Interference Analysis and System Capacity

As we shown in section 2.3.3 and in equation (2.6), the signal-to-noise ratio and the ratio of the transmitted bandwidth W to bit rate R are related in the energy per bit ratio E_b / N_0. For a CDMA ad-hoc network, we have made that each node needs to communicate with their own neighbors simultaneously, just by spreading the signal with the codes for each intended receiver. The signal of each node needs to reach the farthest neighbor at the minimum power controlled level of -100dBm. Consequently the neighbors that are inside the circumference of the circle described by the longest distance, as the radius, will receive a higher level of power, as shown in the Figure 5.1 for the omnidirectional antenna case.

In the Figure 5.1, the center of the area under analysis will receive different levels of power. The total interference received in the center will be the sum of the individual received power of each node, as the worse case. The equation (2.6) becomes:

$$\frac{E_b}{N_0} = \frac{P_{r0}}{\sum_{i=1}^{N} P_{ri}} \frac{W}{R} \qquad (5.1)$$

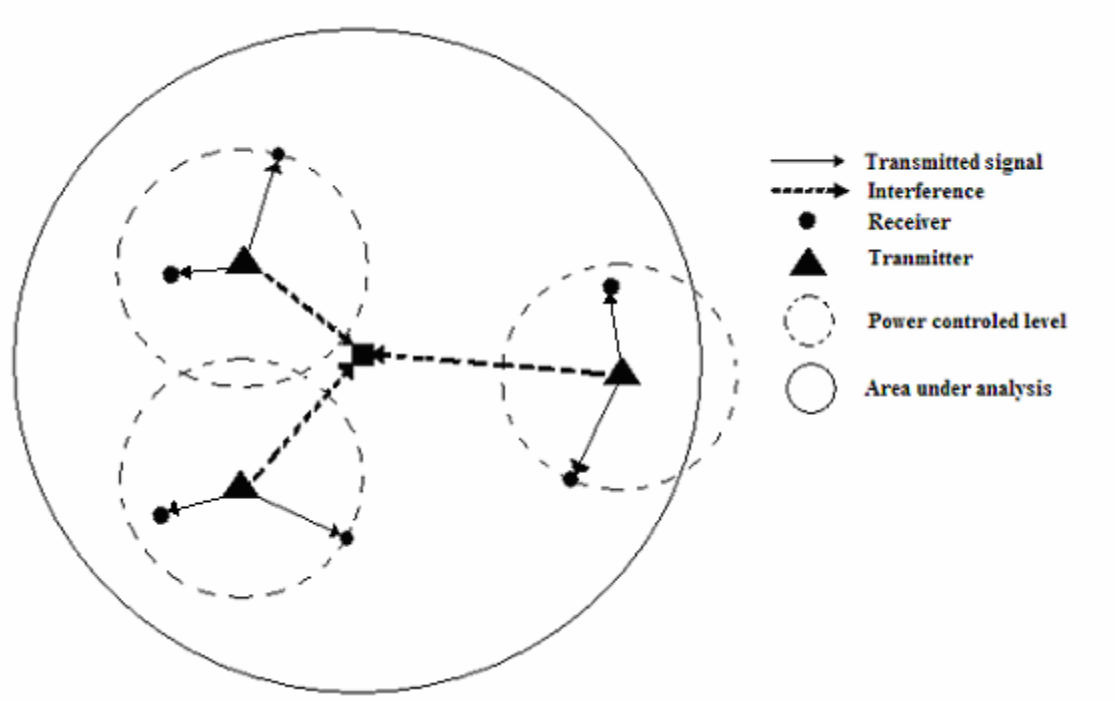

Figure 5.1: Omnidirectional antennas case for CDMA simultaneous transmission.

where E_b/N_0 is the energy per bit ratio, P_{r0} is the minimum power controlled level, fixed to -100dBm, P_{ri} is the power received from each node in the center of the area under

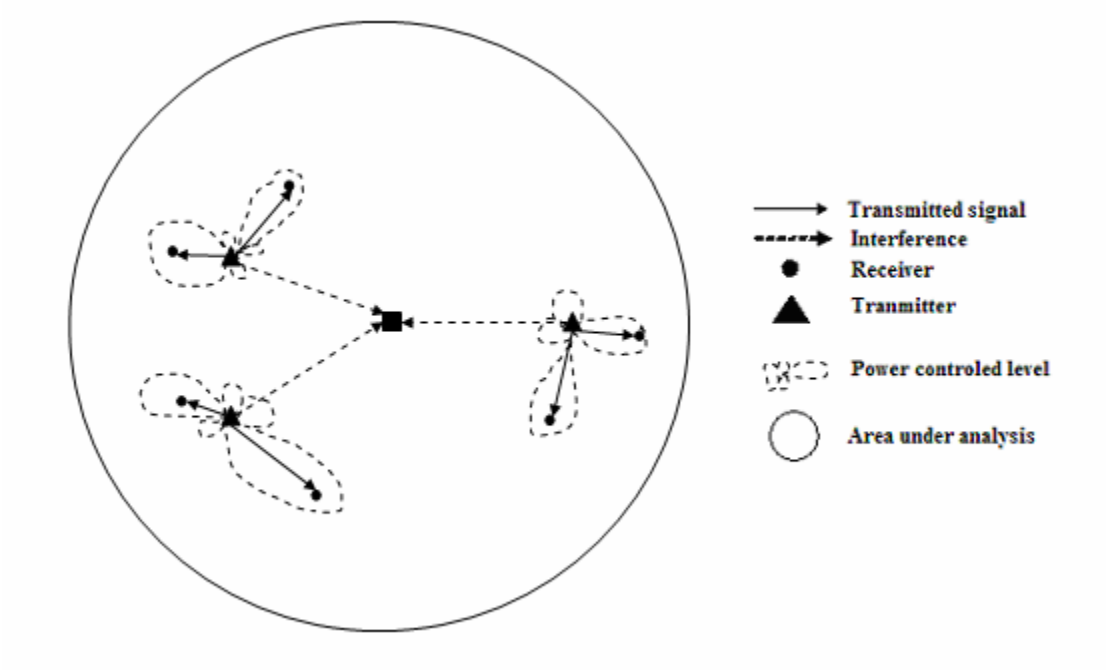

Figure 5.2: Smart antennas case for CDMA simultaneous transmission.

analysis obtained with the equation (4.10), W is the bandwidth and R the bit rate. Now, we have the same ad-hoc network with their nodes equipped with smart antennas, where the interference scenario is shown in the Figure 5.2. Here each neighbor will receive the perfect power controlled level fixed to -100 dBm, due to the multibeam smart antenna radiation pattern. The total interference for the equation (5.1) is

$$I_T = \sum_{i=1}^{N} P_{ri} = \sum_{i=1}^{N} \frac{P_{ti} G_{ti}(1)}{d_i^2} \left(\frac{\lambda}{4\pi} \right)^2 \quad . \tag{5.2}$$

where N is the number of nodes in the ad-hoc network, and the $G_r = 1$ because we are receiving with an isotropic antenna in the center of the scenario.

First we will analyze the scenario with omnidirectional antennas as the reference case. Due to the need to communicate with the same radiation pattern with the neighbors, in the omnidirectional antenna case we may consider one of the three proposed radius for the distance to radiate the power, as shown in the Figure 5.3.

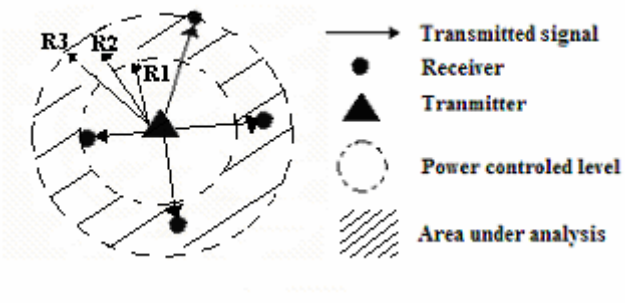

Figure 5.3: Omnidirectional antenna radius.

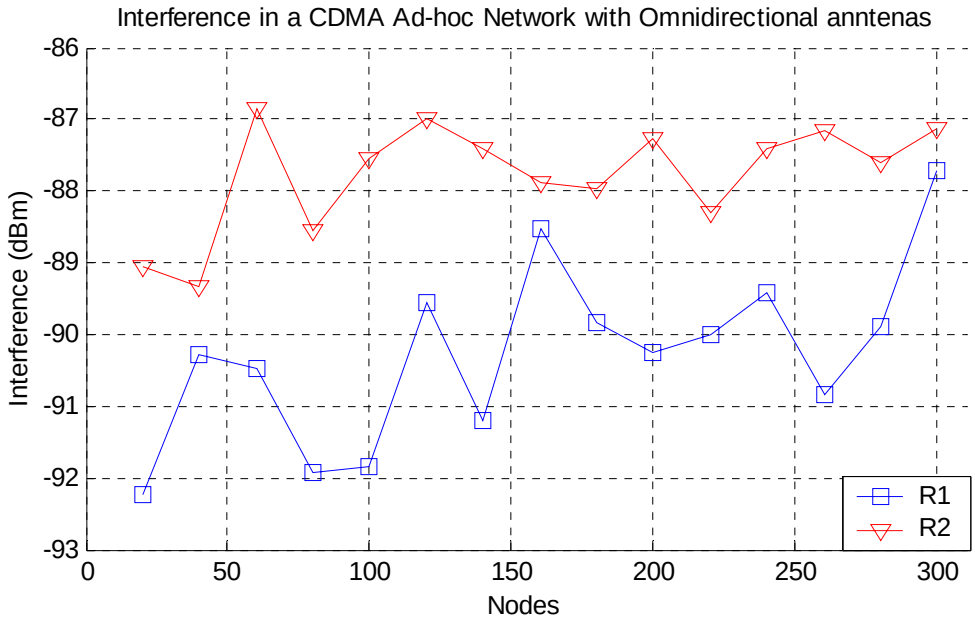

Figure 5.4: Interference with two difference distance in the omnidirectional case.

In the Figure 5.3 we have an area between two concentric circles, one described by the R1 radius and the other one by the R3 radius. The R2 radius is the middle of R1 and R3. Inside the area under analysis of the Figure 5.3, all the nodes are the neighbors of this node. The worse case of interference will be when R3 is considered as the distance *d* in the equation (4.11). Due to the transmission of the same power in all directions, any of this radius as the distance *d* in the equation (4.11) will produce greater interference than any array in the smart antenna cases. Consequently we analyze the R1 and R2 radius as the distance *d* and the interference analysis for values of λ from 20 to 300 nodes in 1km^2. The interference for this two cases is shown in the Figure 5.4, with the longest distance, R2, producing a greater interference. This procedure is done instead the step 5 of the algorithm employed shown in the last section of the previous chapter. The curves of the Figure 5.4, are the assembling average of various realizations with the same parameters for each λ. We refer by realization as one run of the algorithm of the last section in chapter 4.

If we draw a line as the expected value along the values of λ, we will see the predicted values of interference in the network, as shown in the Figure 5.5. This is done with the interference of the values from the Figure 5.4.

Bandwidth	20MHz
Tx Rate	512kbps
E_b/N_0	7 dB
P_{r0}	-100 dBm

Table 5.1: Experimental parameters in CDMA ad-hoc network.

Using the values of the table 5.1 for experimental CDMA ad-hoc network, in the equation (5.1), we have that it will work with acceptable QoS (E_b/N_0 = 7 dB), as in cellular CDMA systems [12]. This value of I_T = -91.07 dBm, and systems with values of interference above this value, will be rejected as systems with acceptable QoS.

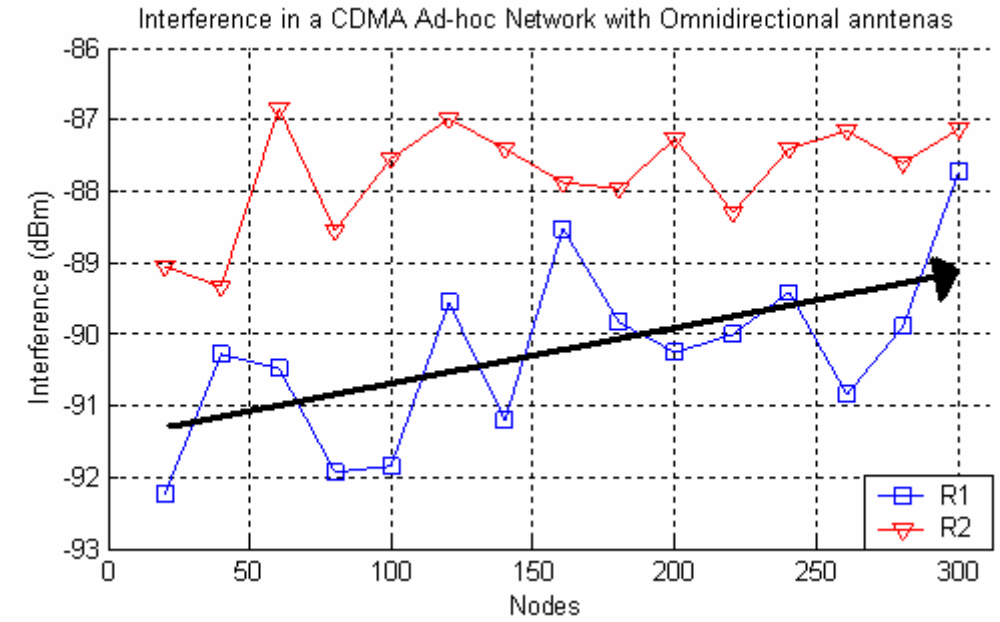

Figure 5.5: Interference in the omnidirectional case and prediction line.

In the Figure 5.5 only the result for R1, the smallest radius, is below the threshold of -91.07 dBm. We wish to know the capacity for the network with this radius, by obtaining the tendency lines as the assembling average over a large number of realizations with the same parameter for each λ. In the Figure 5.6 is shown the tendency line for the interference in an ad-hoc network with omnidirectional antenna with radius R1, where it intersects the threshold line of -91.07 dBm in λ = 46.125 users approximately.

Now we will show the results for the CDMA ad-hoc network with the nodes equipped with smart antennas. First we will consider the linear array as the smart antenna.

Using the same parameters of the Table 5.1, the interference results for this CDMA ad-hoc network is shown in the Figure 5.7, for various values of user intensity λ and an assembling average over a considerable number of realizations, with 6, 9, 12 and 15 elements in the linear array. Again, the interference presents variation along the values of λ, however we can see how the result shows a logarithmic tendency like in Figure 5.6 for the omnidirectional case. Even then, we wish to know the capacity of this network, and we carry out the assembling average over a large number of realizations for this network in each value of λ, than before. The results for the CDMA ad-hoc network interference for nodes quipped with linear array smart antennas with 6, 9, 12 and 15 elements, are shown in the Figure 5.8. The results of the Figure 5.8 show that the linear array smart antenna with the bigger number of elements, 18, takes more hops over λ to reach the desired threshold for the QoS of I_T = -91.07 dBm. That is, the slope for the smaller arrays line are bigger than the 15-elemets line, and consequently the smaller array line reaches the threshold line of I_T before than the bigger array line.

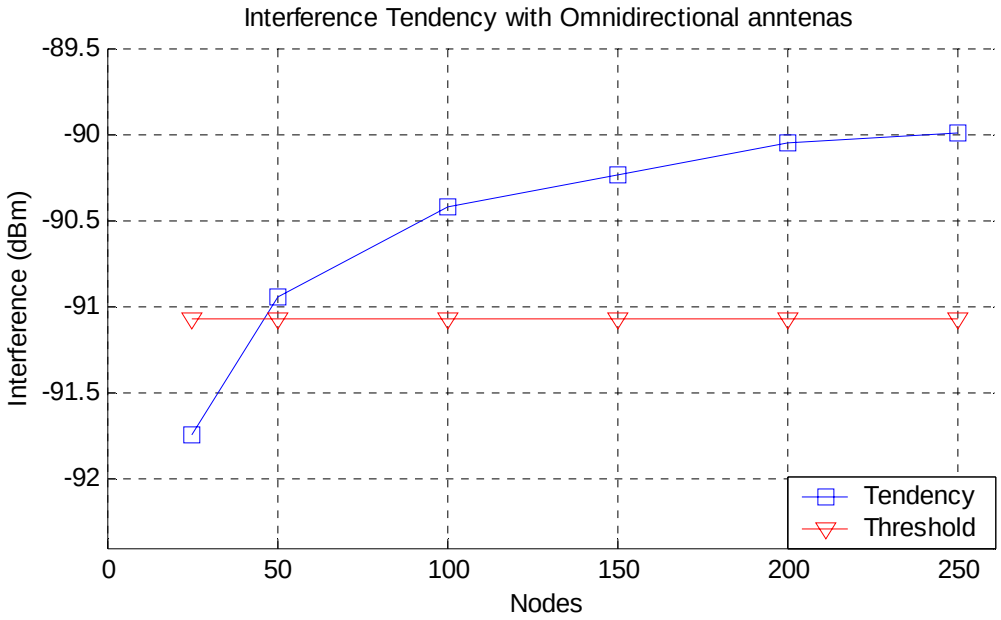

Figure 5.6: Interference tendency for omnidirectional antenna in the R1 case.

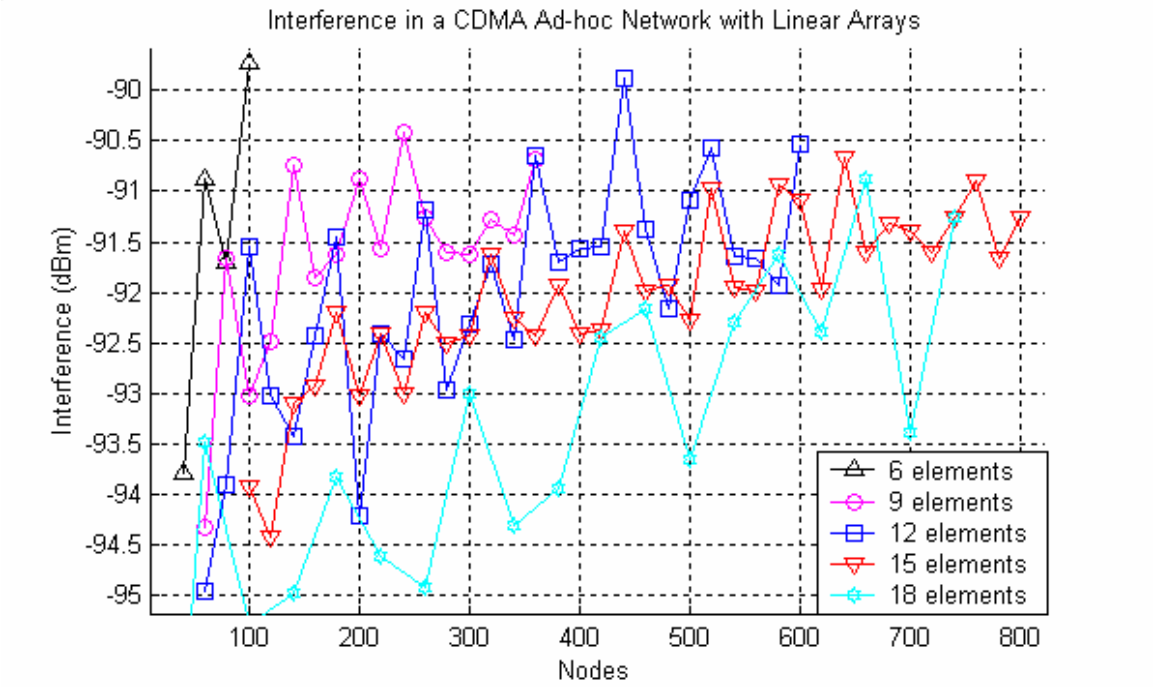

Figure 5.7: Interference for the Linear Array case.

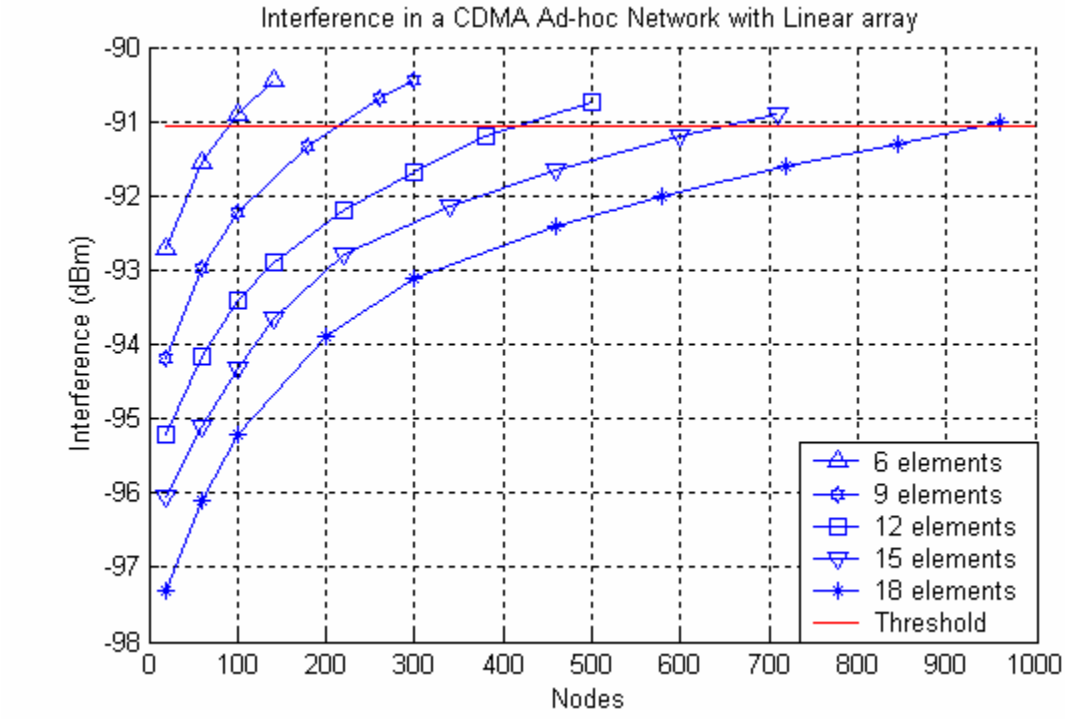

Figure 5.8: Interference tendency for the Linear Array case.

Now we present some results for the circular smart antenna case, used in each node for the CDMA ad-hoc network. First are presented the interference as the assembling average over a small number of realizations to see the fluctuation in the interference due to the variation in the distribution and position of the nodes in the area of the scenario for each realization. The result is shown in the Figure 5.9 for various circular smart antennas with 6, 9, 12, 15, 18 and 21 elements respectively. As in the linear smart antenna, the interference presents a lot of variation and is difficult to determine the capacity with these results. As we were expecting, according to the results of the section 3.5.3, the interference with a larger array (i.e. 21 elements), is small for each value of λ, compared with a smaller array (i.e. 12 elements array).

Again, we made an assembling average over a greater number of realizations than for the Figure 5.9. Notice that every point in the tendency Figures, is the assembling average over a large number of realization, in other words, is the expected value for each value of λ, and not the exactly capacity value for each λ. In the Figure 5.10 is shown the interference tendency (the expected value) for each λ, and the threshold line set to -91.07 dBm, for the circular smart antenna case, and noticing when the network may support the QoS required. From the Figure 5.10 is shown that the capacity is about 900 nodes approximately, for the 21 elements circular smart antennas.

In the Table 5.2 are shown the results for the network capacities for the different smart antenna types, compared with the omnidirectional reference case. Comparing the results shown in the section 3.5.3, where we use a larger number of elements in the circular array, here we use no more than 21 elements, that is, a smaller array size. Considering in the better case that the omnidirectional antenna in the CDMA ad-hoc network allows 50 nodes, using 12 elements with a linear smart antenna we have an improvement over 800%.

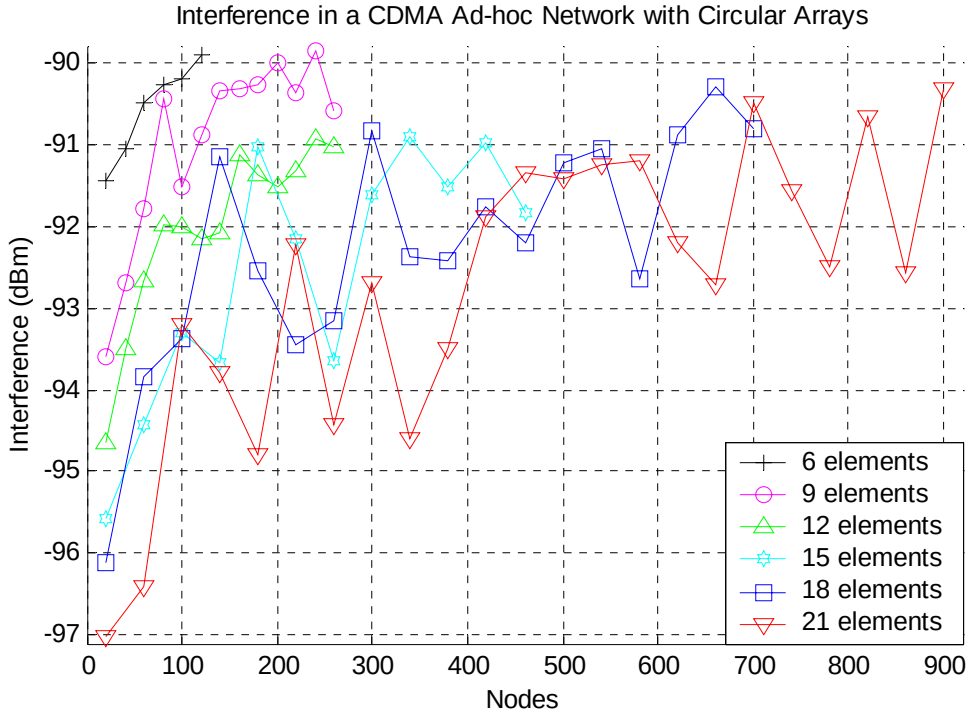

Figure 5.9: Interference for the Circular Array case.

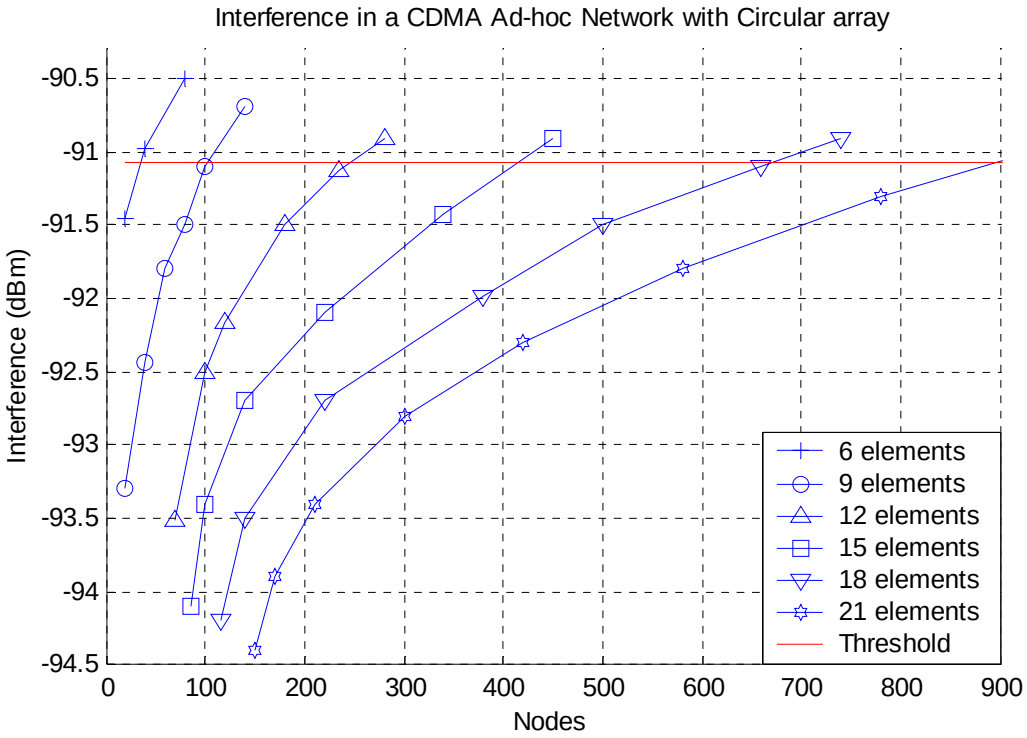

Figure 5.10: Interference tendency for the Circular Array case.

When we use circular smart antennas in the CDMA ad-hoc network with 12 elements we have an improvement of 490% and if is increased the number of elements to 21, we will have an improvement over 1800%. An important characteristic is the diameter of these arrays, because is about the half of the respective linear array size.

Antenna Type	**Length (m) / Diameter (m)**	**Number of elements**	**Network Capacity (nodes)**	**Average BeamWidth (degrees)**
Omnidirectional	--------	1	< 50	360
Linear Smart antenna	0.15	6	≅ 89	40
	0.24	9	≅ 213	29.31
	0.33	12	≅ 414	22.77
	0.42	15	≅ 647	18.88
	0.51	18	≅ 933	16.17
Circular Smart antenna	0.0477	6	≅ 36	49.10
	0.0764	9	≅ 102	33.09
	0.1050	12	≅ 245	24.58
	0.1337	15	≅ 420	19.58
	0.1623	18	≅ 670	16.15
	0.1910	21	≅ 900	13.95

Table 5.2: Experimental capacity results for a CDMA ad-hoc network

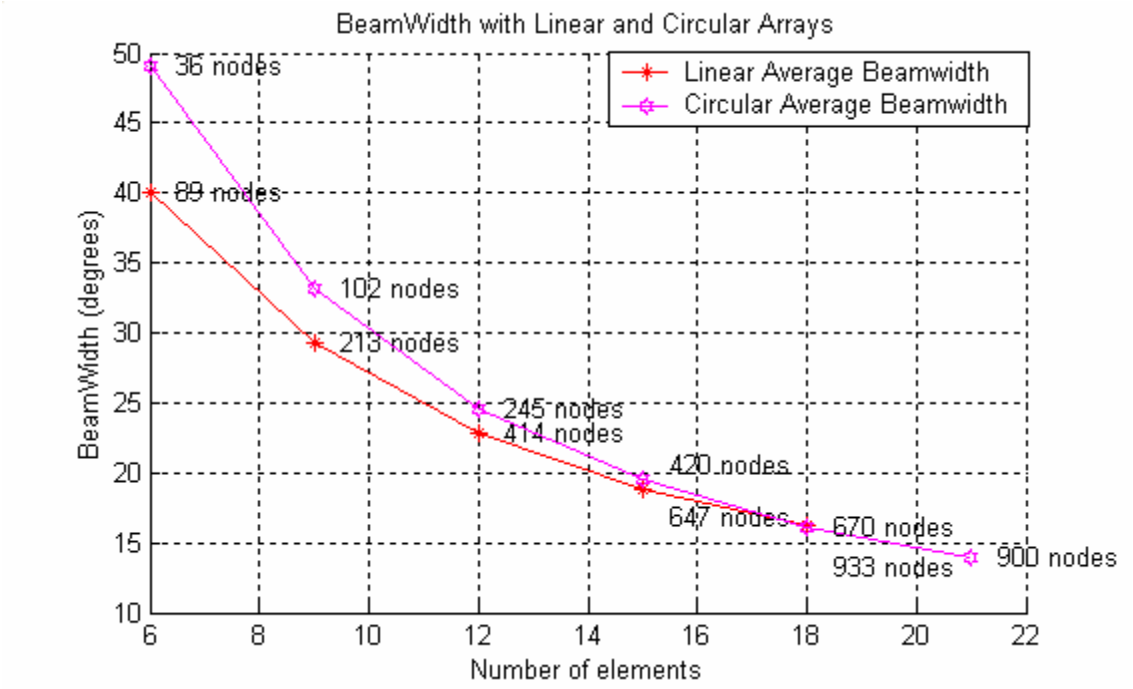

Figure 5.11: Beamwidth against number of elements, shown the network capacities.

Figures 5.11 and 5.12 are different ways to graphically show the result of the table 5.2.

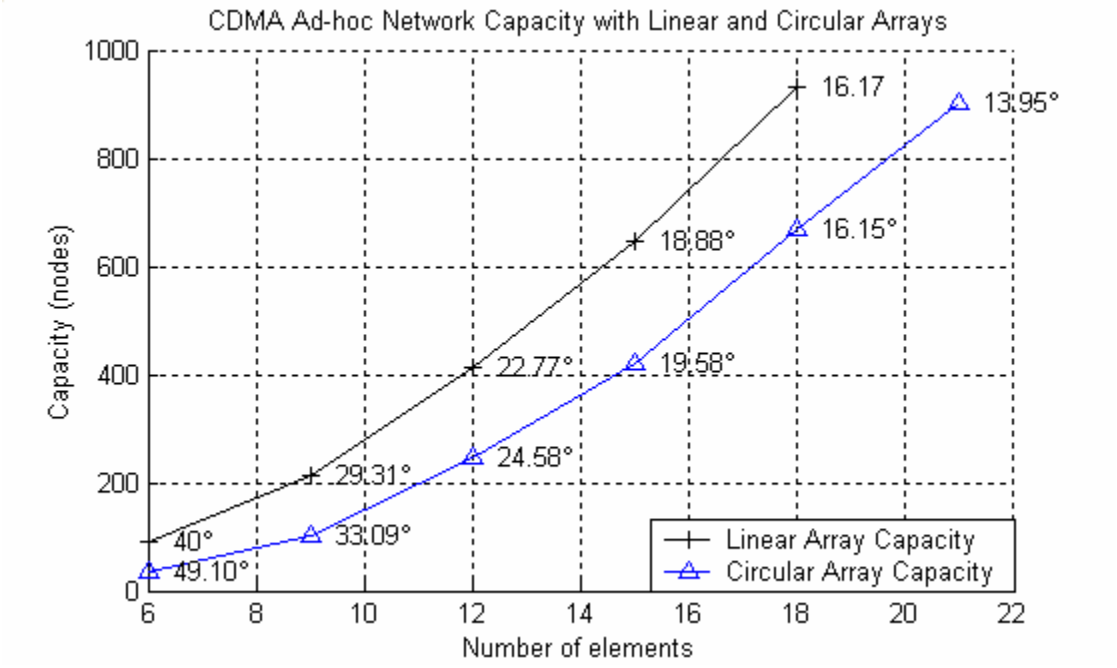

Figure 5.12: Capacity against number of elements, shown the beamwidths.

5.2 Conclusions

In the section 3.5.3 we compared just the radiation pattern of an insolated smart antenna and found that, on the average, the linear array would preset less interference than the circular array smart antenna. When we have the CDMA ad-hoc network with the nodes equipped with smart antennas, we founded that the linear array is better, having a capacity improvement over the circular array. But we have to take into account different characteristics. An important characteristic is the size of the array considered. From the results of the Table 5.2 and the section 3.5.3, we can see that the number of elements can be increased in the circular array with the radius fixed to one size and have improvement, when in the linear array we are not able to do it without increasing the size of the array, if are considering the size, then the circular array will be the best. We may obtain better capacity improvements with bigger sizes of the arrays and also, with a big number of elements. According to the scenario, the propagation model and the network modeling of this thesis, the circular array produces better capacity, with smaller array sizes, in order of 1800% over the omnidirectional case, than the linear smart antenna, with bigger array sizes. One can choose a metric to consider an array in particular, such as the number of elements, the beamwidth or the physical size of the array; any of the smart antennas improves the capacity over the omnidirectional antennas case.

We conclude that the results shown logarithmic tendencies instead of linear tendencies, for bigger values in the number of elements, due to the closets nodes in the networks with larger λ, in the same area. In other words, small values of λ makes the nodes needing to reach their neighbors using a large amount of power. As the network becomes dense the nodes have their neighbors closest and consequently they use less amount of power than before to reach them with the minimum power controlled level. That is the reason why is seen in the interference behavior of all the scenarios, when using bigger values of number of elements, how the interference increases with short hops of λ, when the λ were small; in the counterpart, with larger values of λ the interference value increase not much in each hop of λ.

For the algorithm shown in the last section of the chapter 4, we make a variation in the step 2. When the intensity of nodes λ increases to larger quantities, more than 700 users/1km^2, as in the linear and circular smart antenna cases, we need 5 links per node on the average, to obtain just one cluster for the entire network, instead of 4 links as shown in the algorithm of the chapter 4. This effect is due to density of the network, when the nodes have their neighbors closer than when the density is less, multiple cluster are formed, due to the constraint of the maximum number of links, and we need extra links to allow the cluster reaches another neighbor clusters and so on, until we have just one cluster at the end for each CDMA ad-hoc network realization.

Even though it was not the purpose, we propose the multibeam smart antennas as a solution to the *hidden terminal* problem, the *exposed terminal* problem and the *deafness* as seen in [14]. Due to the ability to listen/talk more than one node at the same time, or to receive/transmit more than one signal at the same time directionality.

Finally, we conclude that the implementation of smart antennas instead of omnidirectional antennas in an Ad-Hoc network using the CDMA as the access technique produces larger capacity improvements compared to the case when we use

omnidirectional antennas, due to the capability of point toward any direction the desired beams and avoiding interference to the neighbors.

5.3 Future Work

According to the work done in this thesis, for the future research are suggested the following ideas.

- Use smart antennas considering the elevation angle, that is, array patterns in three dimensional space.

- Instead of a planar scenario in just two dimensional space, consider more realistic scenarios with buildings or mountains in a three dimensional scenario, and nodes placed to different heights.

- Consider in the propagation model effects like the scattering, reflection and diffraction.

- Would be interesting to use some techniques like genetic algorithm or neural network in the algorithm for the adaptive beamforming and to obtain a faster response when calculating the radiation patterns.

- What would be the in interference and the capacity in the scenarios used in this work if planar arrays where used?

- Consider different transmission rates, bandwidth and power controlled level according to a defined protocol.

- Build a cost function instead of simulation, as seen in the last part of the section 4.3.1, to calculate the probability of outage, the interference and the capacity.

Bibliography

[1] Theodore S. Rappaport, *WIRELESS COMMUNICATIONS principles and practice.* Prentice Hall, 2002.

[2] Charles E. Perkins, *AD HOC NETWORKING*, Addison-Weley, 2001

[3] Joshep C. Liberti, Jr. and Theodore S. Rappaport. *SMART ANTENNAS FOR WIRELESS COMMUNICATIONS: IS-95 and Third Generation CDMA Applications.* Upper Saddle River, 1999.

[4] Amitava Mukherjee, Somprakash Banyopadhyay and Debashis Saha. *LOCATION MANAGEMENT AND ROUTING IN MOBILE WIRELESS NETWORKS.* Artech House, 2003.

[5] David B. Johnson, Computer Science Department, Carnegie Mellow University. *Routing in Ad Hoc Networks of Mobile Hosts.* Mobile Computing Systems and Applications, 1994. Proceedings, Workshop on 8-9 Dec. 1994 Page(s): 158-163.

[6] M. Scott Corson, Joshep Macker and Stephen G. Batsell. *Architectural Considerations for Mobile Mesh Networking.* Military Communications Conference, 1996. MILCOM '96, Conference Proceeding, IEEE. Volume 1, 21-24 Otc.

[7] Elizabeth M. Roger, University of California, Santa Barbara and Chai-Keong Toh, Georgia Institute of Technology. *A Review of Current Routing Protocols for Ad Hoc Mobile Wireless Networks.* Personal Communications, IEEE. Volume 6, Issue 2 April 1999 Page(s): 46-55.

[8] Zygmunt J. Hass, Siamak Tabrizi. *On Some Challenges and Design Choices in Ad-Hoc Communications.* IEEE MILCOM '98, Bedford, MA. Oct. 18-21, 1998.

[9] Baker, D.J., and A. Ephremides. *The Organization of a Mobile Radio Network Via Distributed Algorithm.* IEEE Trans. Commun. Vol. COM-29, 1981.

[10] Lin, R., and Mario Gerla. *Adeptive Clustering for Mobile Wireless Networks.* IEEE Journal on Selected Areas in Communications. Vol. 15, No. 7, Sept. 1997.

[11] Samuel C. Yang. *CDMA RF System Engineering.* Artech House 1998.

[12] Klein S. Gilhousen, Senior Member, IEEE, Irwin M. Jacobs, Fellow, IEEE, Roberto

Padovani, Senior Member, IEEE, Andrew J. Viterbi, Fellow, IEEE, Lindsay A. Weaver, Jr., and Charles E. Wheatley III, Senior Member, IEEE. *On The Capacity Of a Cellular CDMA System.* IEEE TRANSACTION ON VEHICULAR TEHCNOLOGY, VOL. 40, NO. 2, MAY 1991.

[13] John Litva and Titus Kwok-Yeung Lo. *DIGITAL BEAMFORMING IN WIRELESS COMMUNICATIONS.* Artech House Publishers, 1996.

[14] Stefano Basagni, Marco Conti, Silvia Giordano, and Ivan Stojmenović. *MOBILE AD HOC NETWORKING*. Wiley, 2004.

[15] http://www.iec.org/online/tutorials/smart_ant/topic03.html. International Engineering Consortium.

[16] J.C. Liberti. *Analysis of CDMA Cellular Radio Systems Employing Adaptive Antennas*. Ph. D. Dissertation MPRG-TR-95-17, Mobile & Portable Radio Research Group. Virginia Tech, Blackburg, VA, Sep. 1995.

[17] J.C Liberti and T.S. Rappaport. *Reverse Channel Performance Improvement in CDMA Cellular System Employing Smart Antennas*. IEEE Vehicular Technology Conf., pp. 884-848. Apr. 1996.

[18] R. T. Compton Jr. *ADAPTIVE ANTENNAS*. Prentice Hall, 1988.

[19] S. Haykin. *ADAPTIVE FILTER THEORY*. Prentice Hall, Englewood Cliffs, NJ, 1991.

[20] I. S. Reed, J. D. Mallet, and L. E. Brennen. *Rapid convergence rate in adaptive arrays.* IEEE Trans. Aerosp. Electron. Syst., VOL. AES-10, pp. 853-863, Nov. 1974

[21] Carl A. Olen, member, IEEE, and R. T. Compton Jr., Fellow, IEEE. *A Numerical Pattern Synthesis Algorithm for Arrays.* IEEE TRANSACTION ON ANTENNA AND PROPAGATION, VOL. 38, NO. 10, OCTOBER 1990.

[22] Don J. Torreri. *PRINCIPLES OF SECURE COMMUNICATIONS SYSTEMS*. Artech House, second edition, 1992.

[23] Vladimir Z. Rivera. "Estimación de la Dirección de Arribo y de los Coeficientes Óptimos en un Sistema de Antenas Inteligentes Usando Redes Neuronales". Thesis of M.C. in Telecommunications, ITESM. Monterrey, N.L. May 2003

[24] Wendy L. Martinez and Angel R. Martinez. COMPUTATIONAL STATISTICS HANDBOOK WITH MATLAB. CRC Press, 2001.

[25] Sheldon Ross. SIMULATED. Academic Press, second edition. New York, 1997.